JOURNAL OF
EMERGING
INVESTIGATORS

VOLUME 4, ISSUE 3 | MARCH 2021
emerginginvestigators.org

Anemone microbiomes

How stress and other effects can change this species' bacterial populations

Watching paint dry

How environmental effects and colors impact paint properties

Wind mitigation

How roof designs could help protect buildings from bad weather

Bahamian biodiversity

Analyzing wildlife along a tropical mangrove

COVID-19 and pollution

Did stay-at-home orders improve air and water quality in California?

JOURNAL OF EMERGING INVESTIGATORS

The Journal of Emerging Investigators is an open-access journal that publishes original research in the biological and physical sciences that is written by middle and high school students. JEI provides students, under the guidance of a teacher or advisor, the opportunity to submit and gain feedback on original research and to publish their findings in a peer-reviewed scientific journal. Because grade-school students often lack access to formal research institutions, we expect that the work submitted by students may come from classroom-based projects, science fair projects, or other forms of mentor-supervised research.

JEI is a non-profit group run and operated by graduate students, postdoctoral fellows, and professors across the United States.

Contents

VOLUME 4, ISSUE 3 | MARCH 2021

JOURNAL OF
EMERGING INVESTIGATORS

Article

Effects of Various Environmental Factors on Stomatal Density, Area, and Potential Conductance Index

Lina Kim[1]*, Sonia Balani[1]*, Martin Edelberg[1], Natalie Macke[1]
[1] Pascack Hills High School, Montvale, New Jersey
* Authors made the same contribution to the manuscript

SUMMARY

Stomata, microscopic pores on a leaf flanked with flexible guard cells that open and close the stomatal opening, account for 95% of terrestrial movement of water vapor and carbon essential to the survival of plants. The climate crisis is challenging plants with elevated CO_2, drought, varying soil salinity, varying soil acidity, and increasing temperature. While research has been done on how stomata respond to elevated CO_2 alone, markedly less research has been done on the effect of elevated CO_2 in combination with other environmental factors. Thus, the purpose of this study was to determine the effects of elevated CO_2 in combination with other environmental factors on stomatal density, size, and conductance in radish, barley, tomato, and buckwheat. A controlled experiment with these plants and six conditions (Control, Elevated CO_2, Elevated CO_2 + Salinity, Elevated CO_2 + Acidity, Elevated CO_2 + Temperature, and Elevated CO_2 + Drought) was conducted, and data was collected. The results trend towards a decrease in stomatal density, stomatal area, and potential conductance index (PCI) in the elevated CO_2 conditions compared to the control conditions. Additionally, our results suggest that the other four conditions do not amplify the effect of elevated CO_2 levels alone. Overall, results showed variation in data among the tested plants, suggesting that making generalizations about the impact of CO_2in combination with other environmental factors is risky. Thus, further research on the effects of multiple environmental conditions on stomatal characteristics is warranted to determine the impact on agriculture adaptation and water management strategies.

INTRODUCTION

Climate change, resulting from the ongoing rise of heat-trapping gases such as CO_2 within Earth's atmosphere, is a pressing issue in the world today. The effects on agriculture include reduced crop yield from an increase in temperature, reduced soil moisture from a lack of precipitation, and higher net photosynthetic rates from an excess of CO_2 (1). Furthermore, the effect of climate change will vary throughout the world. Changes in rainfall patterns, temperature, and CO_2 levels may have significant effects on global agriculture, which are causing suitable land for key crops to undergo geographic shifts. Thus, in low-income populations that base their survival on isolated agricultural systems (systems in which the population creates and distributes their own food supply), climate change poses a major threat to their quality of life and economic stance (2).

Stomata, tiny pore-like structures on the leaf, play an integral role in gas exchange that drive photosynthesis (3). They are an essential part of important hydrological cycles and overall plant growth, because they regulate a majority of terrestrial movement of gases in plants (4). Stomata consist of kidney-shaped cells, also known as guard cells, that have an arrangement of microfibrils that allow the stomatal aperture to open and close. The opening and closing of these pores depend on external factors, such as concentrations of CO_2 and water supply. For instance, stomata tend to stay closed if water is scarce and open if water is available (3). Stomatal density is used to measure this response, which then reveals survival mechanisms that the plant develops based on its conditions. Oftentimes, higher stomatal density suggests more CO_2 uptake and water loss, whereas lower levels suggest the opposite (5). In fact, Arabidopsis plants that are genetically modified to have reductions in stomatal density have shown increased water-use efficiency, as fewer overall stomata are transporting water and gas in and out the leaf, leading to more water retention (6). In the same regard, stomatal area is another effective metric used to indicate how the individual stomata of a plant responds to its environment. For instance, larger stomatal sizes often indicate slower responses and guard cell movement, whereas smaller stomatal sizes indicate the opposite (7). If a plant were to have slower stomatal responses, this may negatively affect how quickly a plant may adapt, deterring plant growth and development.

However, the response of stomatal development to elevated CO_2 conditions is still unclear (8). Research has found both significant decreases in herbarium specimens and increases in stomatal densities of woody, herbaceous, and annual species of plants after exposure to elevated CO_2 concentrations (9, 10). Further, another study reported no stomatal response to CO_2 enrichment for non-vascular plants and some moss sporophytes. (11). As for stomatal area, elevated CO_2 may cause guard cells to induce stomatal closure, often resulting in a lower stomatal area. (12). Conversely, according to a study, elevated CO_2 may alleviate the impact of drought on barley by lowering stomatal conductance and area, which would improve water status (13). These stomatal trends may be used to create novel, more-efficient crop management appliances to regulate plants in the midst of an increasingly variable climate.

Thus, we investigated how stomatal density, stomatal area, and PCI are affected in common agricultural plants such as *Hordeum vulgare* (barley), *Raphanus sativus* (radish), *Solanum lycopersicum* (beefsteak tomato), and *Fagopyrum esculentum* (buckwheat) when exposed to elevated CO_2

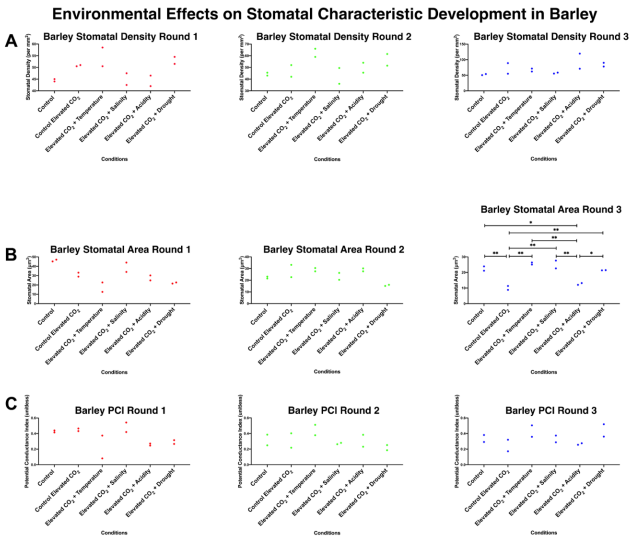

Figure 1: Stomatal density (A), stomatal area (B), and PCI (C) data collected over three rounds in barley plants. Each round of data was collected every two weeks over a total of six weeks, with two leaves of each plant being measured for every condition. The statistical analysis conducted on the round three data is presented with brackets connecting the groups with statistically significant differences. Statistically significant differences are marked with asterisks to denote *p*-values (* *p*-value < 0.05, ** *p*-value < 0.01).

levels alone and elevated CO_2 levels in combination with increased soil temperature, soil acidity, soil salinity, and drought stress. Stomatal density is a measurement describing the stomata present per square millimeter. Stomatal area is a calculation describing the general size of each stomata. PCI is a calculated value that describes the rate of gas exchange depending on stomatal density and guard cell length (14).

We hypothesized that elevated carbon dioxide conditions will decrease stomatal density, size, and PCI in radish, tomato, barley, and buckwheat plants as a result of increased gas exchange. Because a major function of the stomata is water regulation, environmental conditions that require the plant to retain water will limit the size, density, and PCI. Therefore, conditions such as increased salinity, increased temperature, increased acidity, and drought stress will further decrease stomatal characteristics, and thus amplify the impact of elevated CO_2 levels. Our results show varied data, which does not create any conspicuous trends across the plants, simply suggesting that different plants react differently to their conditions.

RESULTS

To study the effect of elevated CO_2 in addition to other environmental factors on stomata, six groups were created — a standard control in normal growing conditions (C group), a control with elevated CO_2 conditions (E group), and four groups with elevated CO_2 combined with one of the following factors: increased temperature (ET group), increased soil salinity (ES group), increased soil acidification (EA group), or drought stress (ED group). The testing conditions were determined based on projections for the developing natural environment, currently being impacted by climate change. For instance, elevated CO_2 conditions were kept at over 700 ppm compared to normal CO_2 conditions, which was kept at around 400 ppm (15). Increased temperature values were kept at the highest end of optimal growing temperatures relative to each plant (these specific temperatures can be found in the Methods section). Soil salinity was increased to a 5% saline concentration (slightly saline), which is compared to the control condition of a 0-3% concentration (non-saline) (16). Soil acidity was increased to a pH of 5-5.5 (strongly acidic), which is compared to the control conditions with a pH of 6-6.5 (slightly acidic) (17). Drought stress was induced by watering with 50% of the normal 46 mL per pot. Stomatal density and stomatal size were measured every two weeks for a total of three times throughout the six-week experiment. PCI was calculated from stomatal density and guard cell length. The data was observed in two ways. First, for each plant, we examined the development of stomatal characteristics over time in each of the six testing conditions by looking at the correlation between time and stomatal density, stomatal area, or PCI. Second, we examined the notable correlations among conditions by comparing two groups and looking at that difference across all four plants.

Barley

Stomatal Density: The ET, ES, and ED groups showed a positive correlation between time and stomatal density for barley plants. The C, E, and EA groups showed no trend in stomatal density for barley plants (**Figure 1A**).

Stomatal Area: The E group displayed a negative correlation between time and stomatal area for barley plants. The C, ET, ES, EA, and ED groups displayed no trend in stomatal area for barley plants (**Figure 1B**).

PCI: The E and ES groups both had a negative correlation between time and PCI for barley plants. The other conditions — the C, ET, EA, and ED groups — showed no trend in PCI for barley plants (**Figure 1C**).

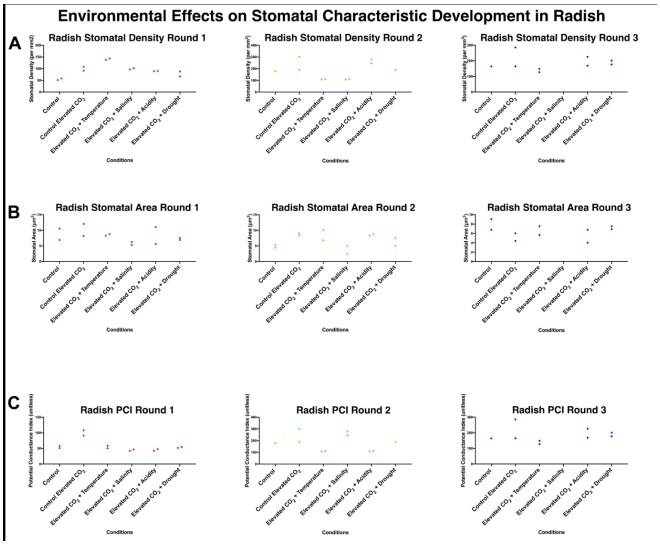

Figure 2: Stomatal density (A), stomatal area (B), and PCI (C) data collected over three rounds in radish plants. Each round of data was collected every two weeks over a total of six weeks, with two leaves of each plant being measured for every condition. The statistical analysis conducted on the round three data is presented with brackets connecting the groups with statistically significant differences. Statistically significant differences are marked with asterisks to denote *p*-values (* *p*-value < 0.05, ** *p*-value < 0.01).

Radish

Stomatal Density: The EA group showed a positive correlation between time and stomatal density for radish plants. The C, E, ET, and ED groups showed no trend in stomatal density for radish. Additionally, there was no data collected for the third round of the ES group for stomatal density in radish plants, so a meaningful trend cannot be determined (**Figure 2A**).

Stomatal Area: The E and ET groups displayed a negative correlation between time and stomatal area for radish plants. The C, EA, and ED groups displayed no trend in stomatal area for radish plants. Again, there was no data collected for the third round of the ES group for stomatal area in radish plants, so a meaningful trend cannot be determined (**Figure 2B**).

PCI: The C, EA, and ED groups all showed a positive correlation between time and PCI for radish plants. The E and ET groups showed no trend in PCI for radish plants. Like in stomatal density and stomatal area, a meaningful trend for PCI was not determined due to lack of data for the ES group (**Figure 2C**).

Tomato

Stomatal Density: The E group had a negative correlation between time and stomatal density for tomato plants, whereas the ED group had a positive correlation. The C, ET, ES, and EA groups had no trend in stomatal density for tomato plants (**Figure 3A**).

Stomatal Area: The EA and ED groups both had positive correlations between time and stomatal area for tomato plants. The C, E, ET, and EA groups had no trend in stomatal density for tomato plants (**Figure 3B**).

PCI: The C and ET groups had a negative correlation between time and PCI for tomato plants, whereas the EA and ES groups had a positive correlation. The C, E, and ED groups had no trend in PCI for tomato plants (**Figure 3C**).

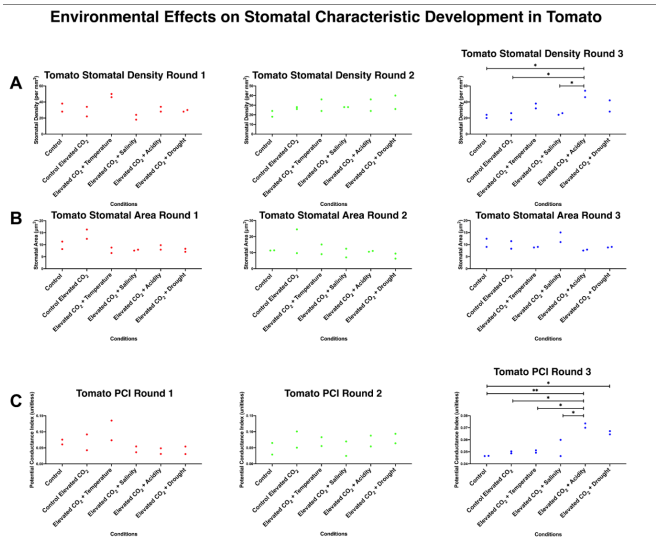

Figure 3: Stomatal density (A), stomatal area (B), and PCI (C) data collected over three rounds in tomato plants. Each round of data was collected every two weeks over a total of six weeks, with two leaves of each plant being measured for every condition. The statistical analysis conducted on the round three data is presented with brackets connecting the groups with statistically significant differences. Statistically significant differences are marked with asterisks to denote *p*-values (* *p*-value < 0.05, ** *p*-value < 0.01).

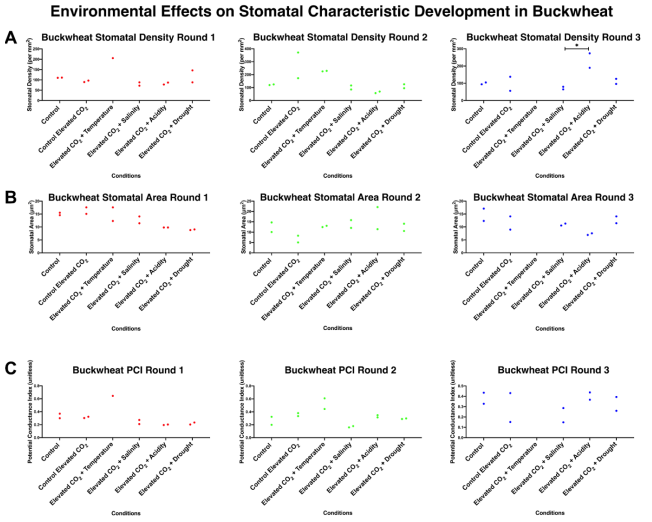

Figure 4: Stomatal density (A), stomatal area (B), and PCI (C) data collected over three rounds in buckwheat plants. Each round of data was collected every two weeks over a total of six weeks, with two leaves of each plant being measured for every condition. The statistical analysis conducted on the round three data is presented with brackets connecting the groups with statistically significant differences. Statistically significant differences are marked with asterisks to denote *p*-values (* *p*-value < 0.05, ** *p*-value < 0.01).

Buckwheat

Stomatal Density: The EA group had a positive correlation between time and stomatal density for buckwheat plants. The C, E, ED, and ES groups had no trend in stomatal density for buckwheat plants. The ET group did not have any data collected for round three, so a meaningful trend cannot be determined (**Figure 4A**).

Stomatal Area: The ED group had a positive correlation between time and stomatal area for buckwheat plants. The C, E, EA, and ES groups all no trend in stomatal area for buckwheat plants. The third round of data in the ET group was not collected, so a meaningful trend cannot be determined (**Figure 4B**).

PCI: The ED and EA groups both had positive correlations between time and PCI for buckwheat plants. The C, E, and ES groups had no trend in PCI for buckwheat plants. Similar to the stomatal density and stomatal area of buckwheat plants, the third round of data in the ET group was not collected, so a meaningful trend with PCI cannot be determined (**Figure 4C**).

Notable Correlations Among Conditions

Apart from the trends over time that occurred in individual conditions for each plant, trends based on comparisons between testing groups were also analyzed. Essentially, we analyzed and compared the differences between the round three values of stomatal density, stomatal area, and PCI between all six testing groups. Statistical analysis was performed exclusively on this interpretation of the data. There were some trends that were consistent throughout all plants in these comparisons, but after performing a One-way ANOVA with post-hoc Tukey HSD Test, only a few values

had a statistically significant difference. We found a decrease in stomatal area between the C group and the EA group in barley, buckwheat, radish, and tomato (**Figure 1B**, **Figure 2B**, **Figure 3B**, **Figure 4B**). Barley had a statistically significant decrease in stomatal area ($p < 0.05$, ANOVA test) (**Figure 1B**). We found an increase in stomatal density across all four plants in the EA group compared to the C and E groups (**Figure 1A**, **Figure 2A**, **Figure 3A**, **Figure 4A**) Tomato had a statistically significant increase in stomatal density ($p < 0.05$, ANOVA test) (**Figure 3A**). Finally, when comparing the E group to the EA group for PCI, there was also an increase among all four plants (**Figure 1C**, **Figure 2C**, **Figure 3C**, **Figure 4C**). Tomato had a statistically significant increase in stomatal density ($p < 0.01$, ANOVA test) (**Figure 3C**).

DISCUSSION

All three stomatal characteristics studied (stomatal density, stomatal area, and PCI) showed major variation in each of the four plants. These variations suggest that plants respond differently to their given environments based on their needs for survival. For example, barley tends to thrive in cool, dry, mild winters in droughty soil and can tolerate more alkaline and salty soils. (18). Radish tends to thrive in cool, moist weather with well-drained and slightly acidic soil, but it is not as tolerant to saline (19, 20). Tomato tends to thrive in very warm temperatures with well-drained, slightly acidic soils and is somewhat tolerant to saline (21). Buckwheat tends to thrive in warmer temperatures with airy, moist, slightly acidic soils and is less tolerant to drought stress but more tolerant to saline. (22, 23). Over the 6-week growth period, each plant responded to a certain condition in different ways. For instance, for the stomatal density measurement in the ES group, barley and tomato had no trend over time, whereas radish and buckwheat had a positive trend over time. Likewise, for the stomatal area measurement in the E group, barley and radish had a negative trend over time, whereas tomato and buckwheat had no trend over time. These are some of the many examples that indicate that there was never an instance where all four plants had the same type of trend in a certain condition for a specific measurement. Thus, the variation of results could emerge not only from the environmental condition, but the type of plant as well, which is a key theme throughout our data.

Additionally, to address our initial hypotheses, we observed how the testing groups compared between conditions in the last round of measurements for each plant. The majority (66.7%) of the data collected for the plants trended towards a decrease in stomatal characteristics for elevated carbon dioxide conditions as compared to the control conditions. However, much of this data was statistically insignificant. Nonetheless, it still suggests that, in some cases, elevated carbon dioxide decreases stomatal density, stomatal area, and PCI. The second hypothesis stated that environmental conditions requiring plants to retain water combined with the stress of elevated carbon dioxide will further decrease the stomatal density, stomatal area, and PCI in the four plants. However, a majority of the data suggests that the four conditions — the ES, EA, ET, ED groups — did not further amplify the effect of elevated carbon dioxide levels alone.

As mentioned before, there was a lack of statistically significant data, and this could be because we did not test a large enough sample size due to the limited time that we had to conduct the experiment. Only allowing six weeks for plant growth could also have led to a restricted, incomprehensive representation of stomatal development in these plants. Due to limited time and resources, we were unable to set up an additional control group of normal CO_2 concentrations and the environmental conditions, which, if conducted, would have provided more data that would help develop better analyses and conclusions about the effects of elevated CO_2 and the environmental factors. However, we were able to use previously published findings of these specific conditions to add to our analyses later on. If there were opposite effects between the elevated CO_2 control groups and environmental factor control groups, this could lead to more questions about individual and combined effects of CO_2 levels and changing environments in certain plants. Additionally, another possible error could be miscounting some of our data. We could not utilize the available computer program, ImageJ, to count the stomata, as the images taken from the light microscope were not compatible with the program. This led to manual counting of stomata and performing calculations, which lengthened the overall time for data collection and calculation and could have provided a possibility for human error. Lastly, carbon dioxide production was manually regulated with daily reactions of baking soda and vinegar. This reaction created carbon dioxide as well as a byproduct of water vapor. Water vapor, like the environmental factors, could have influenced the stomatal characteristics of the plants. It could have also impacted the results in the drought condition as it was adding back some water into the environment. The hand-crafted system we created may have presented inconsistencies with CO_2 levels in the plants' growing chambers. For future experimentation, prepared sources of CO_2 like carbon dioxide tanks could be used to eliminate problems with byproducts from CO_2 synthesis. There are also other inexpensive, homemade options that can create a pure source of CO_2. Additionally, sustained mechanisms can be used to automatically regulate CO_2 levels, which would alleviate issues of CO_2 level inconsistencies.

Aside from the main hypotheses, there were some other statistically supported findings that appeared in the data. These findings agree with prior research and warrant further study. For example, we found a statistically significant difference between the stomatal area of barley in the C group and the E group, 22.62 μm^2 and 10.02 μm^2 respectively ($p < 0.01$, ANOVA test). Similarly, Yamamoto *et al*. suggested that elevated CO_2 causes enhanced anion channel activity in guard cells which induce stomatal closure, often resulting in a lower stomatal area (12). Our data supports these findings. In the barley plants, the stomatal area in the E group was notably lower than the stomatal area in the C group.

Additionally, the stomatal density and area of barley increased from the E group to the ED group. Barley had a statistically significant difference between the stomatal area in the E group and the ED group ($p < 0.01$, ANOVA test). This evidence refutes previous studies which concluded that elevated CO_2 promotes plant water retention in drought conditions via stomatal closure and lower stomatal densities, leading to less water loss (13).

Based on the instances where our data refuted previous findings, further research can be conducted with more intensive focus on specific environmental conditions and stomatal characteristics in regard to the inconsistencies we saw within our own experiment. For example, the stomatal

area of barley decreased when comparing the E group to the ED group in rounds one and two. However, in round three, the stomatal area of barley increased. This was a contradiction to the established idea that the stomatal area would be generally smaller in conditions where retaining limited water is vital. Additionally, the stomatal density of barley showed a consistent increasing trend between the E group and the ED group condition. Considering the previous conclusion that stomatal density would decrease in order to limit water loss in a drought environment, the trend observed in our data is contradictory. This brings about the question of whether these trends in barley are real or just anomalies in our data. More studies specifically focusing on the individual and combined effect of drought and elevated CO_2 on stomata would confirm or deny the trends visualized in our data as well as previous studies.

Similar inconsistencies arose when looking at the effects of other environmental factors on plants. For instance, previous findings have generally shown that stomatal conductance decreases with elevated CO_2 and increases with rising temperature (24, 25). With a few exceptional cases, stomatal conductance generally decreases in the presence of both increased temperature and elevated CO_2 concentrations (8). However, some of our data refutes this statement. When comparing the E group to the ET group in round three data, the tomato plant had shown hardly any increase or decrease in PCI in the third round. But barley had shown an increase in PCI in the third round, following the previously established trend in past research. This could be due to the fact that the two plants have very different thresholds for optimal temperature ranges. Tomato, which has a higher temperature range of 21-32°C, is more heat tolerant than barley, which has a lower temperature range of 10-20°C (26, 27). Thus, their distinct ideal growing conditions could be the reason why the trends between tomato and barley differed.

Furthermore, increased salinity has also shown to have the same effect. According to previous findings, stomatal conductance generally decreases in elevated CO_2 concentrations and decreases in increased soil salinity (24, 28). In combination, increased soil salinity and elevated CO_2 concentrations have shown to decrease stomatal conductance (8). When comparing the E group to the ES group in round three data, although barley and tomato increased in PCI, buckwheat had decreased and radish had no data available. These variances could be related to each plant's individual salt tolerances and/or reactions to elevated CO_2.

Markedly less research has been done on the effect of soil acidification on stomatal characteristics. Nonetheless, similar to the other environmental factors, all four plants did not unanimously exhibit the same trend in round three data. For the few studies that have been done, stomatal conductance has been found to decrease when soil acidity increases (29). When comparing the E group to the EA group, barley, tomato, and buckwheat showed an increase in PCI, whereas radish showed a decrease in PCI. This variation in the results reverts back to the specific ideal growing conditions of each plant. The four plants have their own soil and environmental needs for optimal growth, meaning that they develop their own tolerances to acid levels in soil.

With these variances observed, more experimentation with environmental factors and elevated CO_2 could further contribute to this project and add clarifications regarding stomatal response to changing environmental conditions. Overall, this experiment emphasizes the importance of studying the impact of changing environmental conditions on crops, which is essential to agricultural productivity. Thus, the conclusions from this type of data can be used to develop novel technology, crop management, and adaptation strategies in order to continue to grow the plants optimally and efficiently.

METHODS

The plants used in this experiment were H*ordeum vulgare* (barley), *Raphanus sativus* (radish), *Solanum lycopersicum* (beefsteak tomato), and *Fagopyrum esculentum* (buckwheat). Beefsteak tomato seeds were purchased from Seed of Change on Amazon, and buckwheat seeds were purchased from Old Cobblers Farm on Amazon. Both barley and buckwheat seeds were purchased from Carolina Biological. Seeds were first potted in 3.5-inch diameter pots in potting soil from Carolina Biological as per the sowing instructions for each type of seed. These pots were transferred to fish tanks which would serve as the growing chambers for each plant. A total of 14 covered, 2.5-gallon betta fish tanks were used to simulate the six growing conditions. Two tanks containing pots of all four plant types were the baseline control. Since there were two types of plants per tank, plants were divided by cardboard dividers in the tanks. Each section of the tank had two pots of the same plant. These plants were grown according to their normal instructions. They were grown under natural light and LED/fluorescent plant lights. Plants in the temperature conditions received the LED plant lamps along with natural light because they helped raise the temperature, and all other plants had fluorescent light along with natural light. All plants were watered with 46 mL of tap water and kept in a room with a baseline temperature between 20–22°C. Reusable ice packs were placed under the pots of radish and barley plants to cool the soil because their average growing temperature was under the room's average temperature. Barley plants were grown at 15°C (25); radish plants were grown at 18°C (28); tomato plants were grown at 29°C (26); buckwheat plants were grown at 27°C (29). The soil temperatures for all the plants were monitored by thermometers in the soil.

The remaining 12 tanks all required elevated levels of carbon dioxide. To achieve this, individual apparatuses were created to synthesize carbon dioxide. A system of gallon milk jugs, water bottles, and tubing was fixed together, and daily reactions of approximately 1/6 gallon of vinegar and 2 tablespoons baking soda yielded the amount of carbon dioxide gas needed to keep the carbon dioxide level above the predetermined amount of 700 parts per million in the 12 tanks (**Figure 5**). Carbon dioxide levels were measured with a Pasco sensor. This method to create carbon dioxide gas for the chambers could be done with other alternatives such as carbon dioxide gas tanks or CO_2 synthesis through yeast. Of these 12 carbon dioxide tanks, 2 were part of the second control group: the E group. This group was grown the same way as the control group, but with the addition of an increased amount of carbon dioxide in the growing chambers.

The remaining 10 tanks would represent the 4 specific environmental factors chosen to be studied along with an elevated carbon dioxide setting. Four of these 10 tanks would be used to represent the ET group. Each of the four tanks would have one of the four plants, and heating pads and growing lights were used to bring the tank temperatures up to

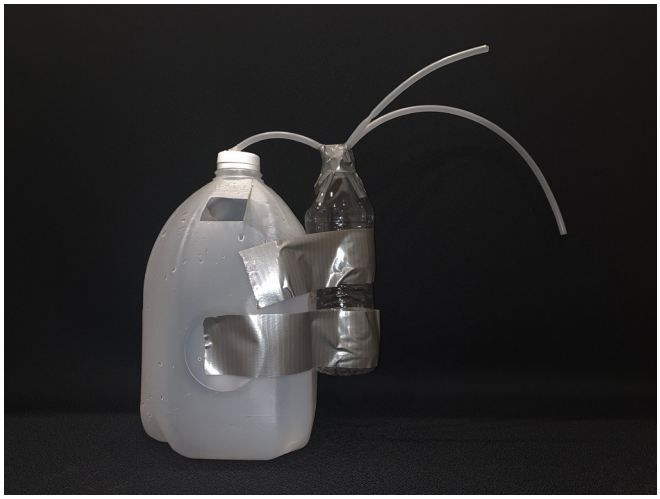

Figure 5: Experimental apparatus used to elevate CO_2 conditions. A milk gallon jug is fastened to a water bottle. A sealable opening in the gallon jug is where vinegar and baking soda would be added in to cause a reaction which produces CO_2 gas. The gas and any excess liquid that overflowed from the strong reaction would pass through the tube connecting the milk jug and the water bottle. Excess liquid would collect in the water bottle, and gas would flow through the remaining two tubes into the growing chambers. Each of the two tubes would be attached to each of the two sections of a growing chamber. The baking soda and vinegar would be replenished regularly to maintain CO_2 levels of 700 ppm or greater.

the highest temperature in the specific plant's growing range. Radish and barley were grown without ice because the room temperature represented the highest temperature in their growing range. Radish was grown at 21°C and barley was grown at 20°C (30, 26). Buckwheat and tomato were heated to their highest temperatures with heating pads. Buckwheat was grown at 37°C and tomato was grown at 32°C (31, 27). Two more tanks were the EA group, in which an acidic mixture of 1 cup vinegar and 1 gallon of water was tested and determined to drop the soil pH from the normal soil pH, 6-6.5, to about 5, which was checked with pH paper to make sure the acidity levels were maintained (17). Two tanks simulated the salinity and elevated carbon dioxide condition, in which a 100 mM solution of 5.844 grams Kosher salt and 1 Liter of water was used to water the plants. The final two tanks were the ED group, in which the amount of water used to water the plants was halved from 46 mL to 32 mL to put a stress on the ability of water retention of the plants. All plants were grown with natural light and LED/fluorescent plant lights, and they were watered twice a week with the water that each condition called for. Plants were subjected to their conditions at the point where the cotyledon emerged during germination.

Data collection started when plants started growing. The plants grew over the course of six weeks, and approximately at every two-week interval, two leaves from each of the four plants in each of the six conditions were collected for stomatal analysis. Two of the most developed, matured leaves were selected for a leaf imprint. Leaf size is a factor in stomatal density and area, which was kept in mind during the experiment. Leaves of similar sizes from each type of plant were used for leaf impressions. Even though the values of stomatal density and area were different by plant, they were recorded nonetheless. This is because, in our analysis, we were focusing on the differences and trends over time among testing groups, not necessarily the numerical values themselves. Thus, these differences and trends over time revealed whether or not our plants adapted to their environments throughout the experiment.

The underside of the leaf was painted in Sally Hansen brand clear top coat nail polish so that light could pass through for analysis under a compound light microscope. Once dry, the layer of nail varnish was peeled off, put on a microscope slide, and labeled for analysis under a Swift brand light microscope with an ocular micrometer as well as any compound light microscope with a one square millimeter viewing range. Stomatal density is a measurement describing the stomata present per square millimeter. Stomatal density was measured once on each leaf by creating a one millimeter by one millimeter viewing window out of a piece of tape and sticking it on the slide being analyzed. Stomata were counted in that square millimeter field and the number was recorded. Alternatively, this process could be done using a program designed for stomatal analysis like ImageJ and a microscope that could directly view leaf tissue, eliminating the need for a clear leaf impression. Stomatal area is a calculation describing the general size of each stomata. Stomatal area was calculated by measuring the length and width of the stomata in micrometers with the Swift microscope and then using an ellipse area formula to calculate the stomatal area ($A = \pi ab$). One stoma was measured on each of the two leaf samples. PCI is a calculated value that describes the rate of gas exchange depending on stomatal density and guard cell length. PCI was calculated by squaring the stomatal length, multiplying it by the stomatal density for that leaf, and then multiplying that by 10^{-4} ($PCI = (\text{guard cell length})^2 \times \text{stomatal density} \times 10^{-4}$). This leaf impression and data collection process was done three times throughout the 6-week time period. Once the third round of measurements and calculations were collected, data analysis along with statistical analyses were performed. One-way Analysis of Variance (ANOVA) tests with a post-hoc Tukey Honestly Significant Difference (HSD) tests were conducted to see if there was significant difference between any of the test groups across all plants and conditions (32). Raw data for each plant and condition were inputted into the website's calculator, and the results of the test were analyzed.

ACKNOWLEDGEMENTS

We would like to thank the Ask-A-Scientist Program, our mentor Claire Meaders, the scientific reviewers, and Harvard's Journal of Emerging Investigators editors for their guidance, help, and support while working on this project.

Received: July 18, 2020
Accepted: November 30, 2020
Published: February 1, 2021

REFERENCES

1. Adams, Richard M., *et al*. "Effects of Global Climate Change on Agriculture: An Interpretative Review." *Climate Research*, vol. 11, no. 1, Dec. 1998, pp. 19–30. *www.int-res.com*, doi:10.3354/cr011019.
2. Aydinalp, Cumhur, and Malcolm S. Cresser. "The effects of global climate change on agriculture." *American-Eurasian Journal of Agricultural & Environmental Sciences* 3.5 (2008): 672-676.

3. Le, Arve, *et al*. "Stomatal Responses to Drought Stress and Air Humidity." Abiotic Stress in Plants - Mechanisms and Adaptations, Sept. 2011. www.intechopen.com, doi:10.5772/24661.
4. Matthews, Jack S. A., and Tracy Lawson. "Climate Change and Stomatal Physiology." *Annual Plant Reviews Online*, American Cancer Society, 2019, pp. 713–52. *Wiley Online Library*, doi:10.1002/9781119312994.apr0667.
5. *Environmental Correlates of Leaf Stomata Density (Description)*. https://www.esa.org/tiee/vol/v1/experiments/stomata/stomata_description.html#:~:text=The%20more%20stomata%20per%20unit,rate%20and%20CO2%20uptake. Accessed 6 Nov. 2020.
6. Bertolino, Lígia T., *et al*. "Impact of Stomatal Density and Morphology on Water-Use Efficiency in a Changing World." *Frontiers in Plant Science*, vol. 10, 2019. *Frontiers*, doi:10.3389/fpls.2019.00225.
7. Lawson, Tracy, and Michael R. Blatt. "Stomatal Size, Speed, and Responsiveness Impact on Photosynthesis and Water Use Efficiency." *Plant Physiology*, vol. 164, no. 4, Apr. 2014, pp. 1556–70. DOI.org (Crossref), doi:10.1104/pp.114.237107.
8. Xu, Zhenzhu, *et al*. "Elevated-CO2 Response of Stomata and Its Dependence on Environmental Factors." *Frontiers in Plant Science*, vol. 7, May 2016. *PubMed Central*, doi:10.3389/fpls.2016.00657.
9. Woodward, F. I. "Stomatal Numbers Are Sensitive to Increases in CO 2 from Pre-Industrial Levels." *Nature*, vol. 327, no. 6123, June 1987, pp. 617–18. *www.nature.com*, doi:10.1038/327617a0.
10. Reid, Chantal D., *et al*. "On the Relationship between Stomatal Characters and Atmospheric CO2." *Geophysical Research Letters*, vol. 30, no. 19, 2003. *Wiley Online Library*, doi:10.1029/2003GL017775.
11. Field, Katie J., *et al*. "Stomatal Density and Aperture in Non-Vascular Land Plants Are Non-Responsive to above-Ambient Atmospheric CO 2 Concentrations." *Annals of Botany*, vol. 115, no. 6, May 2015, pp. 915–22. *DOI.org (Crossref),* doi:10.1093/aob/mcv021.
12. Yamamoto, Yoshiko, *et al*. "The Transmembrane Region of Guard Cell SLAC1 Channels Perceives CO2 Signals via an ABA-Independent Pathway in Arabidopsis." *The Plant Cell*, vol. 28, no. 2, Feb. 2016, pp. 557–67. *PubMed Central*, doi:10.1105/tpc.15.00583.
13. Robredo, Anabel, *et al*. "Elevated CO2 Alleviates the Impact of Drought on Barley Improving Water Status by Lowering Stomatal Conductance and Delaying Its Effects on Photosynthesis." *Environmental and Experimental Botany*, vol. 59, no. 3, Apr. 2007, pp. 252–63. ScienceDirect, doi:10.1016/j.envexpbot.2006.01.001.
14. Holland, Nicholas, and Andrew D. Richardson. "Stomatal Length Correlates with Elevation of Growth in Four Temperate Species†." *Journal of Sustainable Forestry*, vol. 28, no. 1–2, Feb. 2009, pp. 63–73. *Taylor and Francis+NEJM*, doi:10.1080/10549810802626142.
15. Reidmiller, David, *et al*. "Fourth national climate assessment." *Volume II: Impacts, Risks, and Adaptation in the United States*, *Report-in-Brief* (2017).
16. Brouwer, C., A. Goffeau, and M. Heibloem. "Irrigation water management: training manual no. 1-introduction to irrigation." *Food and Agriculture Organization of the United Nations, Rome, Italy* (1985): 102-103.
17. Soil Quality Indicator Sheets | NRCS Soils. https://www.nrcs.usda.gov/wps/portal/nrcs/detail/soils/health/assessment/?cid=stelprdb1237387. Accessed 3 Nov. 2019.
18. Corporation, Grains Research and Development. "Barley Northern Region - GrowNotesTM." Grains Research and Development Corporation, https://grdc.com.au/resources-and-publications/grownotes/crop-agronomy/northern-barleygrownotes. Accessed 15 Nov. 2019.
19. *Explore Cornell - Home Gardening - Vegetable Growing Guides - Growing Guide*. http://www.gardening.cornell.edu/homegardening/scene341b.html. Accessed 16 Nov. 2019.
20. Shannon, M. C., and C. M. Grieve. "Tolerance of vegetable crops to salinity." *Scientia horticulturae* 78.1-4 (1998): 5-38.
21. *Explore Cornell - Home Gardening - Vegetable Growing Guides - Growing Guide*. http://www.gardening.cornell.edu/homegardening/sceneea10.html. Accessed 16 Nov. 2019.
22. *Buckwheat Information*. http://www.hort.cornell.edu/bjorkman/lab/buck/guide/sowingwhen.php. Accessed 17 Nov. 2019.
23. Matsuura, Hiroyuki, *et al*. "Differences in the Vegetative Growth between Common and Tartary Buckwheat in Saline Hydroponic Culture." *Plant Production Science*, vol. 8, no. 5, Jan. 2005, pp. 533–38. *DOI.org (Crossref),* doi:10.1626/pps.8.533.
24. Kelly, Gilor, *et al*. "Hexokinase Mediates Stomatal Closure." *The Plant Journal*, vol. 75, no. 6, 2013, pp. 977–88. *Wiley Online Library*, doi:https://doi.org/10.1111/tpj.12258.
25. Urban, Josef, *et al*. "Stomatal Conductance Increases with Rising Temperature." *Plant Signaling & Behavior*, vol. 12, no. 8, Aug. 2017, p. e1356534. *DOI.org (Crossref),* doi:10.1080/15592324.2017.1356534.
26. *Seeding Strategies*. http://growbarley.com/production/seeding. Accessed 20 Nov. 2019.
27. "Organic Beefsteak Tomato | Seeds of Change." *SeedsOfChange-Us*, https://www.seedsofchange.com/seeds/vegetables/organic-beefsteak-tomato-seeds. Accessed 20 Nov. 2019.
28. Ruiz-Vera, Ursula M., *et al*. "Global Warming Can Negate the Expected CO2 Stimulation in Photosynthesis and Productivity for Soybean Grown in the Midwestern United States." *Plant Physiology*, vol. 162, no. 1, May 2013, pp. 410–23. *www.plantphysiol.org*, doi:10.1104/pp.112.211938.
29. Anugoolprasert, Ornprapa, *et al*. "Effect of Low PH on the Growth, Physiological Characteristics and Nutrient Absorption of Sago Palm in a Hydroponic System." *Plant Production Science*, vol. 15, no. 2, Jan. 2012, pp. 125–31. *DOI.org (Crossref),* doi:10.1626/pps.15.125.
30. Masabni, Joseph. *Easy Gardening: Radishes*. Apr. 2009. *oaktrust.library.tamu.edu*, https://oaktrust.library.tamu.edu/handle/1969.1/87577.
31. *Buckwheat Production — Publications*. https://www.ag.ndsu.edu/publications/crops/buckwheat-production. Accessed 21 Nov. 2019.
32. Vasavada, N. "One-way ANOVA (ANalysis Of VAriance) with post-hoc Tukey HSD (Honestly Significant Difference) test calculator for comparing multiple treatments." *OneWay_Anova_with_TukeyHSD/_get_data* (2016).

JOURNAL OF
EMERGING INVESTIGATORS

Article

Phytochemical analysis of *Annona Reticulata* extract and an *in-vitro* study on its anti-proliferative effects

Rishi Tadiparti[1], Pooja Kasture[2], Ankita Umrao[2], Jyothsna Rao[2], Gururaj Rao[2]

[1] The International School Bangalore, NAFL Valley, Whitefield – Sarjapur Road, Bangalore, KA, India, 562125

[2] iCREST-International Stem Cell Services Limited, 9/1, Mission Road, Bangalore

SUMMARY

***Annona Reticulata* (Ramphal or custard apple) has been a plant of interest in the traditional medicinal system for the prevention and treatment of various inflammatory disease conditions, including cancer. But there has always been a requirement of continuous efforts for the efficient extraction of potential secondary metabolites that are used for treatment. This study is concerned with the anti-cancerous secondary metabolites present in the leaves of the *Annona Reticulata* plant (RL) and its anti-proliferative properties. Many extracts were tested on HeLa cells using a variety of solvents. The anti-proliferative effect of the combination of methanol dry extract and wet extract in acetone was observed to contain the greatest range of dissolved secondary metabolites. At concentrations over 2.5%, weight over volume, a sharp decrease in viability of below 50% for both 24 hours and 48 hour time duration. This result suggests that the leaves may have potent anti-proliferative and possibly anti-cancer properties.**

INTRODUCTION

In Ayurveda, the Ramphal or custard apple plant was often used to treat stomach ailments, fever, parasitic infections, hypertension and rheumatism (1). Other studies in the past have demonstrated that the Annona family has anti-carcinogenic effects (2). Thus this plant was chosen because it has been suggested to have anti-cancerous properties and it is present throughout the Indian subcontinent.

Secondary metabolites are organic compounds produced by bacteria, fungi, or plants which are not directly involved in the healthy growth, development, or reproduction but aid in the plants' long term survival (3). The metabolites were screened for following phytochemicals: saponins, polyphenols, flavonoids, alkaloids and tannins. Saponins are a group of plant glycosides, characterized by their strong foam-forming properties in aqueous solution; they are known to induce apoptotic pathways in cancer cells (4). Polyphenols are mildly acidic and used in chemical manufacture, and its dilute form as a disinfectant. They are also often found in spices and fruit, which are reported to have antioxidant, anti-inflammatory, spasmolytic, antidiarrheal, antimicrobial, and anti-carcinogenic activity (5). Flavonoids are a group of plant metabolites thought to provide health benefits through cell signalling pathways and antioxidant effects; they are demonstrated as anti-cancer agents, and have shown great potential as cytotoxic anti-cancer agents promoting apoptosis in cancer cells (6). Alkaloids are a class of nitrogenous organic compounds, including many drugs and poisons that affect cancer cells and prevent successful cellular divisions (7). Tannins are bitter-tasting natural substances present in some galls, barks, and other plant tissues, consisting of derivatives of gallic acid. They show powerful antioxidant properties and also show promise for the cancer chemoprevention (8). This study aims to understand how the possible the anti-proliferative property of *Annona Reticulata* leaves affect cancerous cells.

The plant, *Annona Reticulata*, is one that's found in abundance throughout the Indian Subcontinent, the birthplace of Ayurveda, a traditional Hindu system of medicine based on the principles of balance between bodily functions, incorporating diet, herbal treatment, and yogic breathing. This plant, even from ancient times, has always been held in high regard because of its inherent medicinal properties, and in India was named after the God Rama "Ramphal." Many studies have shown that the leaves of the plant contain anti-inflammatory and anti-ulcer compounds. For generations, the plant was made into salves and applied to infected wounds and even tumours.

To extract the many active compounds in the leaf, both a dry and wet extraction methods were employed. This allowed us to observe which extraction method would lead to a higher yield of secondary metabolites. Different solvents were also utilized to allow for a variety of different compounds to dissolve. Thus a range of polar, bipolar, and non-polar solvents was used: water (H_2O), very polar molecule to dissolve polar molecules; methanol (CH_3OH) another polar solvent; ethanol (C_2H_5OH) which has both hydrophobic and hydrophilic ends, allowing it to dissolve a wide range of solutes; chloroform ($CHCl_3$), another bipolar solvent; and, acetone (C_3H_6O), a non-polar molecule which readily dissolves non-polar molecules.

RESULTS

The aim of this study was to first quantify the amount of secondary metabolites by performing qualitative and quantitative analysis of the plant leaves' extracts and secondly to assess the cytotoxicity of the relevant plant solvent extracts by MTT (3-(4,5-dimethylthiazol-2-yl)-2,5-diphenyl tetrazolium bromide) assay. The MTT assay is a test which measures NADPH-dependent cellular activity, showing the number of

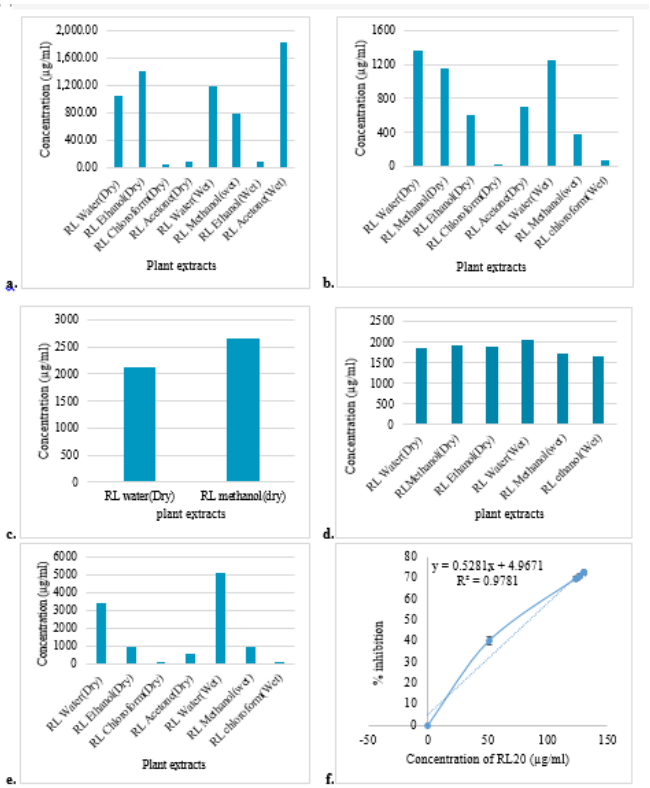

Figure 1: Graphs depicting the amount of phytochemicals present in different extracts of dry and wet RL leaves (a-e) and DPPH activity of RL'20 (f) (N=3, mean±SD). a. total saponins, b. total polyphenols, c. total flavonoids, d. total alkaloids, e. total tannins.

viable cells present (9).

Qualitative and quantitative analysis of phytochemicals in various extracts of RL

From the phytochemical analysis of the *Annona Reticulata* plant, we found that the plant contains a large variety of secondary metabolites and consists of over a thousand µg/ml of various secondary metabolites (**Table 1**). Qualitative data of dry extract of RL showed the presence of flavonoids, polyphenols and alkaloids in methanol and water extracts. Although a slight presence of polyphenols was observed in acetone extract, the flavonoids and alkaloids were completely absent. Saponins and tannins were scarcely seen in the acetone and chloroform extract of dry RL, whereas ethanol extract was lacking flavonoids (**Table 1**). Polyphenols and alkaloids were present in water, and methanol extract of wet RL along with the strong presence of tannins and saponins, as depicted in **Table 1**. Acetone and ethanol extracts of wet RL showed a strong indication of the presence of saponins and alkaloids, respectively. Moreover, the presence of phytochemicals was not evident in its chloroform extract. Methanol dry extract contained high concentrations of polyphenols, flavonoids and alkaloids, containing 1158.27 µg/ml, 2664.00 µg/ml and 1922.79 µg/ml respectively (**Figure 1b, c and d**). Meanwhile, the acetone wet extract contained a very high concentration of saponins, containing 1821.12 µg/ml of saponins (**Figure 1a**). The groups containing a high concentration of tannins were not considered for the preparation of the formulation as they were already a subset of the polyphenol group (**Figure 1e**). Thus, to include a high range of all the tested secondary metabolites, a combination of a wet and dry extract was chosen to create the extract that would be used for the MTT assay.

Thus, it was clear that this plant not only contains a large variety of these phytochemicals but also in large quantities. This abundance of available secondary metabolites indicated that it may potentially have significant anti-cancer properties. The DPPH assay is a test for the antioxidant properties of a substance, by the process of free radicle scavenging, the methanol extract was tested using the aforementioned assay

The methanol dry extract and acetone wet extract were weighed after drying for 72 h. Each dried extract was dissolved in DMSO at 0.001 g/mL concentration. These extracts were subjected to MTT assay. Based on the IC50 values, the extracts were then used to form RL'20 and demonstrate a high DPPH activity of 255.81 µg/ml. This indicates RL'20 is a potent antioxidant (**Figure 1f**).

Cytotoxicity effect of RL'20 on HeLa (cervical cancer) cells

The MTT Assay was carried out using these extracts separately and in combination to determine the cytotoxicity effects after 24 and 48 hours. These results are particularly exciting as we see an herbal extract having potent anti-proliferative impacts on the HeLa cells. The high antioxidant properties are also very exciting as this extract could potentially even reduce the chances of cancer in nearby cells by neutralising free radicles which could lead to catastrophic DNA damage, possibly reducing the risk of cancer.

The IC50 values of methanol dry extract were found to be 27.47 and 12.62 µg/ml at 24 and 48 h of treatment, respectively (**Figure 2a**). Acetone wet extract showed a higher IC50 value of 53.59 µg/ml at 24 h and was similar to that of methanol dry extract at 48 h (**Figure 2b**). IC50 of the formulation, RL'20, was found to be the lowest at 13.34 µg/ml and 5.96 µg/ml at 24 and 48 hours, respectively (**Figure 2c**). It was interesting to note that the 48 hour IC50 value for acetone wet extract was over four times less than the same extract at 24 h. In comparison, the 48 hour IC50 values for the methanol dry extract and combination drug were only around 2.25 and 2.6 times lesser than their respective 24 h IC50 values (**Figure 2**).

This study showed the presence of antioxidants and anti-cancer compounds (saponins, flavonoids, polyphenols, alkaloids, and tannins) in the plant extracts, which demonstrated a level of growth suppression and antioxidant properties. As **Figure 2** reveals, a combination of the extracts had the lowest IC50 value of just 5.69 µg/ml after 48 h treatment and was thus the most potent. This was the most exciting outcome considering the RL'20 contained all the secondary metabolites. The qualitative analysis

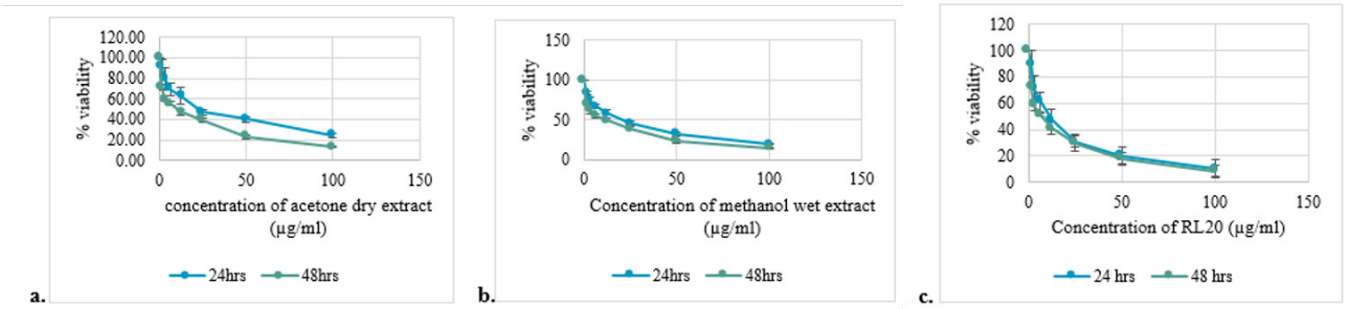

Figure 2: Graphs showing cytotoxicity effect of a. methanol dry extract, b. acetone wet extract and c. RL'20 at 24 and 48h. The data is the representative of three independent experiments performed in triplicates (N=3, mean±SD).

had determined RL'20 shows the most magnificent anti-proliferative properties, leaving only 8.61% of cells viable at its highest concentration after 48 h. The methanol extract also showed relatively high antioxidant properties, and thus probably has cancer prevention properties.

The results for the cytotoxicity assay were auspicious, with each of the three solvents having logarithmic curves for cell toxicity and cell viability (**Figure 2**). It indicated a strong trend, where after 24 h, even the least potent acetone wet extract showed less than 25% cell viability with its highest concentration (**Figure 1**b). At 48 h, the results were ever more prominent, where the methanol dry extract showed the highest cell viability of only around 14%, indicating the potency of the drug increases by time, which could be likely due to the time taken for the secondary metabolites to react on to the cells. Thus, it was clear that the compounds have an anti-proliferative impact on HeLa cells.

Our results demonstrated that saponins, in general, require a more extended period to act upon the cells but are especially potent, as the acetone wet extract and methanol dry extracts 48 h IC50 values were nearly identical even though the acetone extract only has a large amount of saponins and negligible amounts of the other phytochemicals. In contrast, the methanol dry extract has large quantities of polyphenols flavonoids and alkaloids (**Table 1** and **Figure 1**).

As shown in **Figure 2**, the methanol extract has an IC50 value of 87.25 µg/ml and thus has a moderate radical scavenging property. As it has antioxidant activity, which is often known to prevent or fight the onset of cancer (10), it can be hypothesized that this drug can not only fight the growth and spread of cancer, but also help in the prevention of cancer.

DISCUSSION

According to our conclusions, the leaf extracts showed a remarkable effect in both antioxidant and cell viability assays. This experiment therefore can conclude, based on the results of investigations, *Annona Reticulata* is a potent source of bioactive compounds and has a plethora of medicinal properties, such as growth suppressing and anti-proliferative

Solvents	Saponins	Polyphenols	Flavonoids	Alkaloids	Tannins
Water (Dry Extract)	+++	+++	++	+++	+++
Methanol (Dry Extract)	-	+++	+++	+++	-
Acetone (Dry Extract)	+	++	-	-	+
Chloroform (Dry Extract)	+	-	-	-	+
Ethanol (Dry Extract)	+++	++	-	+++	++
Water (Wet Extract)	+	+++	-	+++	+++
Methanol (Wet Extract)	+	++	-	+++	++
Acetone (Wet Extract)	+++	-	-	-	-
Chloroform (Wet Extract)	-	+	-	-	+
Ethanol (Wet Extract)	+	-	-	+++	-

Table 1: Qualitative analysis for the presence of different phytochemicals in various extracts of A. reticulata. '+', '++' and '+++' sign signifies the concentration range of each phytochemical as 1-500, 501-1000 and 1001-2000µg/ml, respectively. '-'signifies absence of the respective phytochemical.

properties. Nevertheless, the anti-cancer properties of the leaf extracts need to further proven. Furthermore, tests are needed to reveal whether the secondary metabolites target just cancerous cells or any dividing cell. The exact mechanism behind these properties are unknown. However, we hypothesized it may be related to anti-inflammatory processes.

The prevalence in Ayurveda has sparked many analyses of the plant; studies of Annona acetogenins isolated from the seeds of A. reticulata showed it caused significant cell death in various cancer lines and suggested potentially promising anti-cancer compounds. These studies on the promising nature of A. reticulata led to our experiment, in which the focus was on the leaves of the plant. According to our results, the plant shows excellent potential as an anti-cancer agent. The usage of this plant could lead to many discoveries in the field of oncology. However, more complex trials and experiments must be conducted on the efficacy of the plant.

MATERIALS AND METHODS

Extraction process: Dry extraction

Leaves were plucked and were shade dried for 48 hours. They were then crushed using a mortar and pestle to get a fine powder. A 1 g:10 ml w/v [1 g of ground dried leaf and 10 ml of solvent] ratio was utilized for extracting the phytochemicals from the all five aforementioned solvents. The leaves were kept in different solvents for 24 hours and the supernatant was centrifuged. The supernatant was collected and stored at 4˚C until use.

Extraction Process: Wet extraction

Leaves were plucked and mashed to a paste using a mortar and pestle. The pulp was left for shade dry for 48 hours. A 1 g:10 ml [1 g of the wet extract of the leaves and 10 ml of solvent] ratio was utilized to dissolve the paste. The leaves were mixed with each solvent and were centrifuged after 24 hours, the supernatant was stored at 4˚C until use.

Qualitative analysis to determine the presence of phytochemicals in each extract

Lambda maxing is a process that identifies the wavelengths at which absorbance is maximum. If there are many dissolved solutes, the lambda max graph may indicate many peaks. and the lambda max wavelength can also behave like a single qualitative parameter to compare the absorption range of different molecules (11). The lambda max curves showed promise as all extracts had shown over ten peaks, indicating the presence of a variety of different dissolved substances in each solvent. Thus, a qualitative analysis of the five secondary metabolites had to be performed on all of the solvents.

The olive oil test was performed to detect the presence of saponins, which utilized vigorous shaking of 0.5 ml of each extract and a few drops of olive oil [~2-3 drops]. A formation of the soluble emulsion after 5 minutes confirms the presence of saponins (12).

For polyphenols, the Folin and Caiocalteu's (FC) reagent test was utilized; ~4 drops of FC reagent and Na_2CO_3 was added to 0.5 ml of the sample and incubated at room temperature in the dark for 20 minutes. The appearance of the blue color shows the presence of polyphenols (13).

The test for flavonoids was performed using the Alkaline reagent test, where 5 drops of 5% NaOH was added to 0.5 ml of extract, which result in yellow color, then few drops of 2 M HCl were added to the solution. The solution turns colorless if flavonoids are present (14).

The test for alkaloids was performed using Dragendorff's analysis, in which 0.5 ml of the extract was added to 0.2 ml of diluted HCl and 1 ml of dragendorff reagent. The presence of alkaloids would be confirmed by the presence of an orange-brown precipitate (15).

To test the presence of tannins, the Ferric Chloride test was performed as 0.5 ml of the extract was mixed with a few drops of 5% $FeCl_3$ and the formation of blue-green color shows the presence of tannins (16).

Quantitative analysis to determine the amount of phytochemicals present in various extracts of RL

Each solvent's absorbance was plotted against a standard absorbance curve to obtain the concentrations of different metabolites in each solvent.

Total Saponins

The Vanillin-Sulphuric acid method (17) was used to determine the total saponin content. 0.25 ml of the sample was added to 0.25 ml of 8% vanillin in ethanol and 2.5 ml of 72% Sulphuric acid. The solutions were incubated for 15 minutes at 60°C and the absorbance was recorded at 765 nm. A standard curve was prepared using Diosgenin.

Total Phenolic content

The total phenolics of the extract were determined using the FC reagent (18). The standard concentrations of gallic acid and samples were mixed with 0.2 ml of FC reagent. After 5 minutes, 1 ml 8% w/v of Na_2CO_3 was added to the solution and volume made up to 3ml with water. The absorbance of the bright blue color was measured after 30 minutes of incubation. The standard plot was prepared using gallic acid and was read at 765 nm.

Total Flavonoid content

Varying concentrations of green tea extracts were mixed with water to make up to 2.4 ml and 0.3 ml of 10% $AlCl_3$ was added. After 5 minutes, 2 ml of 1 M sodium hydroxide was added, the final volume was made up to 10 ml with distilled water and mixed well. The orange color was absorbed in 630 nm. The total flavonoid content was calculated as a green tea extract equivalent on the basis of a standard curve (19).

Total Alkaloid content

2 ml of Dragendorff's solution was added to samples

maintained at 2-2.5 pH with diluted HCl and was centrifuged for 10 min at 1500 rpm. 2 ml disodium sulfide solution was added to form a brown-black precipitate to which 2 ml of concentrated nitric acid was added and the volume was made to 10 ml with water. 1 ml solution was discarded and 5 ml of thiourea was added and the absorbance was recorded. The standard curve was obtained with bismuth nitrate pent-hydrate stock solution (20).

Total Tannin content

0.2 ml sample was added to 0.5 ml of FC reagent and 1 ml of 35% sodium carbonate and the final volume was made up to 10 ml using distilled water. The mixture was shaken and kept at room temperature for 30 minutes. A set of reference standard solutions of tannic acid was prepared using the same method and the absorbance was carried out at 700 nm (21).

Antioxidant assay by DPPH test

DPPH (2, 2-diphenyl-1-picryl-hydrazyl-hydrate) assay is a method by which the antioxidant properties of a particular solution or molecule can be tested. This assay is based on the electron transfer between free radicals (22), a violet color form when oxidized and becomes colorless when reduced. 0.5 ml of the extract was added to 1M DPPH solution in methanol. The absorbance was measured at 517 nm after 30 minutes of incubation at room temperature.

Cytotoxicity assay using MTT (3-(4, 5-dimethylthiazol-2-yl)-2, 5-diphenyltetrazolium bromide) dye

This assay is a colorimetric assay that analyses the cellular metabolic activity (23); thus, the higher metabolic activity, the greater the cell viability. Therefore, the MTT Assay can be used to test the effectiveness of the plant extracts for their anti-proliferative and anti-cancer properties. Two different extracts and a combination of the two were chosen based on the qualitative and quantitative analysis and were tested using the MTT assay (Sigma). The formation of purple formazan crystals inside the mitochondrion indicates the presence of metabolic activity (24), thus higher the intensity of purple color, the higher the number of viable cells in that solution.

HeLa (cervical cancer) cells were obtained from NCCS, Pune. Cells were cultured in Dulbecco's modified Eagle's medium (DMEM) with 10% fetal bovine serum (FBS) (Invitrogen) at 37˚C with 5% CO_2. 0.3 million cells were seeded in a 96 well plate and the extracts were added after 24 h of culture for 24- and 48 h. MTT was added to and dimethyl oxide was used to dissolve the formazan crystals. OD at 545 nm was taken (25) and the cell viability graphs were plotted.

Thus, the IC50 values of the extracts for cell viability could be tested for different times, this allows for even the slower acting metabolites to affect all the cells. IC50 values show the concentration at which there is precisely half the viability of the cells. It is commonly used as a measure of drug potency in pharmacological research. According to the FDA, IC50 represents the concentration of a drug that is required for 50% inhibition in vitro (26). It also allows one to understand how potent the drug is and helps in understanding the results.

Received: July 2, 2020
Accepted: September 14, 2020
Published: February 2, 2021

REFERENCES

1. "Experts Warn against Using Soursop Fruit to Fight Cancer." Cancer *Treatment Centers of America*, 4 Feb. 2020, www.cancercenter.com/community/blog/ 2017/07/ experts-warn-against-soursop-fruit-to-fight-cancer.
2. Gavamukulya, Yahaya, *et al*. "Phytochemical Screening, Antioxidant Activity and in Vitro Anticancer Potential of Ethanolic and Water Leaves Extracts of AnnonaMuricata (Graviola)." *Asian Pacific Journal of Tropical Medicine*, vol. 7, 2014, doi:10.1016/s1995-7645(14)60258-3.
3. "Secondary Metabolite." Secondary Metabolites - *Knowledge Encyclopedia*, www.biologyreference.com/ knowledge/Secondary_metabolites.html.
4. Yildirim, Isil, and TurkanKutlu. "Anticancer Agents: Saponin and Tannin." *International Journal of Biological Chemistry*, vol. 9, no. 6, Jan. 2015, pp. 332– 340., doi:10.3923/ijbc.2015.332.340.
5. Yang, G. "Inhibition of Growth and Induction of Apoptosis in Human Cancer Cell Lines by Tea Polyphenols." *Carcinogenesis*, vol. 19, no. 4, Jan. 1998, pp. 611–616., doi:10.1093/carcin/19.4.611.
6. Chang, Hui, *et al*. "Structurally Related Cytotoxic Effects of Flavonoids on Human Cancer Cells in Vitro." *Archives of Pharmacal Research*, vol. 31, no. 9, 2008, pp. 1137–1144., doi:10.1007/s12272-001-1280-8.
7. Mondal, Arijit, *et al*. "Alkaloids for Cancer Prevention and Therapy: Current Progress and Future Perspectives." *European Journal of Pharmacology*, vol. 858, 2019, p. 172472., doi:10.1016/j.ejphar.2019.172472.
8. Morse, Mark A., and Gary D. Stoner. "Cancer Chemoprevention: Principles and Prospects." *Carcinogenesis*, vol. 14, no. 9, 1993, pp. 1737–1746., doi:10.1093/carcin/14.9.1737.h
9. Stockert, Juan C., *et al*. "Tetrazolium Salts and Formazan Products in Cell Biology: Viability Assessment, Fluorescence Imaging, and Labeling Perspectives." *Acta Histochemica*, no. 3, Elsevier BV, Apr. 2018, pp. 159–67. Crossref, doi:10.1016/j.acthis.2018.02.005.
10. "Antioxidants and Cancer Prevention." Federal Occuptional Health, U.S Department of Health and Human Services, foh.psc.gov/NYCU/antioxidents.asp.
11. Singh, Ak. "Therapeutic Effects of Plant-Extract Synthesized Gold Nanoparticles against Alcohol-Induced Inflammatory Activity - A Proof of Concept." *Archives of Addiction and Rehabilitation*, vol. 1, no. 2, 2017, doi:10.36959/843/425.
12. Al-Othman, Abdulaziz M. "Phytochemical Analysis

and Biological Activities of Selected Medicinal Plants." *Journal of Medicinal Plants Research*, vol. 6, no. 23, 2012, doi:10.5897/jmpr12.
13. Baddi, G. Ait, *et al*. "Qualitative and Quantitative Evolution of Polyphenolic Compounds during Composting of an Olive-Mill Waste–Wheat Straw Mixture." *Journal of Hazardous Materials*, vol. 165, no. 1-3, 2009, pp. 1119–1123., doi:10.1016/j.jhazmat.2008.10.102.
14. Sankhalkar, Sangeeta, and VrundaVernekar. "Quantitative and Qualitative Analysis of Phenolic and Flavonoid Content in MoringaOleifera Lam and OcimumTenuiflorum L." *Pharmacognosy Research*, vol. 8, no. 1, 2016, p. 16., doi:10.4103/0974-8490.171095.
15. "Test Method for Qualitative Analysis for Active Sulfur Species in Fuels and Solvents (Doctor Test)." doi:10.1520/d4952-09.
16. Waniska, Ralph D., *et al*. "Practical Methods to Determine the Presence of Tannins in Sorghum." *Journal of Applied Poultry Research*, vol. 1, no. 1, 1992, pp. 122–128., doi:10.1093/japr/1.1.122.
17. Agarwal, Aastha. "Saponins Standard." *Sapogenin Standard Curve of Total Saponin Content*, ResearchGate, Nov. 2015, www.researchgate.net/figure/ Sapogenin-standard-curve-of-total-saponin-content-Y00161x-0033R-2-0950_fig3_292176981.
18. Javanmardi, J. "Antioxidant Activity and Total Phenolic Content of Iranian Ocimum Accessions." *Food Chemistry,* vol. 83, no. 4, 2003, pp. 547–550., doi:10.1016/s0308-8146(03)00151-1.
19. CHANG, CHIA-CHI. "Estimation of Total Flavonoid Content in Propolis by Two Complementary Colorimetric Methods." *Journal of Food and Drug Analysis*, vol. 10, no. 3, 25 Jan. 2002,https://www/researchgate.net/profile/Rayn_Aarland/post/What_is_the_simplest_method_to_estimate_flavonoids/atttachment/59d62a9479197b8077988fb2/AS:339806593798145@1458027613155/download/Chang_flavonoids.PDF.
20. Saitoh, Fumiyo, *et al*. "The Alkaloid Contents of Sixty Nicotiana Species." *Phytochemistry*, vol. 24, no. 3, 1985, pp. 477–480., doi:10.1016/ s0031-9422(00)80751-7.
21. "Total Phenolic, Total Flavonoid, Tannin Content, and Antioxidant Capacity of HalimiumHalimifolium (Cistaceae)." *Journal of Applied Pharmaceutical Science*, 2015, doi:10.7324/japs.2015.50110.
22. Garcia, Eugenio José, *et al*. "Antioxidant Activity by DPPH Assay of Potential Solutions to Be Applied on Bleached Teeth." *Brazilian Dental Journal*, vol. 23, no. 1, 2012, pp. 22–27., doi:10.1590/s0103-64402012000100004.
23. Stockert, Juan C., *et al*. "Tetrazolium Salts and Formazan Products in Cell Biology: Viability Assessment, Fluorescence Imaging, and Labeling Perspectives." *ActaHistochemica*, vol. 120, no. 3, 2018, pp. 159–167., doi:10.1016/j.acthis.2018.02.005.
24. Stewart, Mj, and Id Watson. "Standard Units for Expressing Drug Concentrations in Biological Fluids." *British Journal of Clinical Pharmacology*, vol. 16, no. 1, 1983, pp. 3–7., doi:10.1111/j.1365-2125.1983.tb02136.x.
25. Mahmood, Hafiz Khalid, *et al*. "Phytochemical And Antioxidant Screening Of Anacylus Pyrethrum, ApiumGraveolens, BoerhaaviaDiffusa, Cinnamomum Cassia Blume, CuscumisMelo Linn, CuscumisSativus Linn, DaucusSativus, FoeniculumVulgare, TrachyspermumAmmii And Theit Effect On Various Human Ailments." *Matrix Science Pharma*, vol. 2, no. 2, Jan. 2018, pp. 06–14., doi:10.26480/msp.02.2018.06.14.
26. Beck B, Chen YF, Dere W, Devanarayan V, Eastwood BJ, Farmen MW, *et al*. "Assay Operations for SAR Support". *Assay Guidance Manual*. Eli Lilly & Company and the National Center for Advancing Translational Sciences, Nov 2017.

JOURNAL OF
EMERGING INVESTIGATORS

Article

Low environmental pH inhibits phagosome formation and motility of *Tetrahymena pyriformis*

Thea Chung*[1], Oliver Weissleder*[1], Elizabeth Lillis[1]
[1] Milton Academy, Milton, Massachusetts
* Authors contributed equally

SUMMARY

***Tetrahymena pyriformis*, single-celled protozoans, populate ponds, lakes, and streams. As 2.57 million tons of carbon dioxide enter the atmosphere every second, Earth's bodies of water acidify rapidly, creating harmful habitats for organisms such as ciliates at the bottom of the food chain, like *T. pyriformis*. Investigating the ability of *T. pyriformis* to feed in acidic pHs presents a deeper understanding of the short-term ramifications of carbon dioxide emissions on freshwater ecological communities. In this experiment, we varied pH from 4.5 to 7.0 by diluting carbonated water. To observe *T. pyriformis* food vesicle formation, we counted the number of phagosomes located in iodine-fixed *T. pyriformis* after a 10-minute feeding period. We hypothesized that increased suspension acidity would reduce *T. pyriformis*' consumption of food vesicles due to inhibited motility functions and phagosome formation during phagocytosis. Our data suggests *T. pyriformis* best generate phagosomes within a pH range of 6.0 to 7.0. Data displayed a low average vesicle count of 0.60 ± 0.16 at a pH of 4.5 and a high average vesicle count of 3.73 ± 0.18 at a pH of 7.0. At a pH of 6.0, average vesicle count plateaued as its rate of increase slowed. We posit that as pH levels decrease, *T. pyriformis* lose feeding competence due to three probable mechanisms: increased membrane density, weakened myosin necessary for vesicle transport, and inhibition of ciliary movement –– all components necessary to initiate and complete phagocytosis.**

INTRODUCTION

Since the late 19th century, our industries, modes of transportation, agricultural operations, and residential needs have required the burning of fossil fuels, a process which releases harmful greenhouse gases into the atmosphere (1, 2). As global emissions have steadily increased due to population growth and its consequent demand, Earth's bodies of water have absorbed unexpected amounts of carbon dioxide, resulting in their acidification through the formation and subsequent dissociation of carbonic acid (3, 4). Even subtle changes in environmental conditions, such as water acidity, can disturb the balance of ecosystems (4). Investigating the potential consequences of acidification on aquatic organisms gives insight on the ecological changes human fossil fuel emissions can cause. Our study of *T. pyriformis* initiates this investigation, starting at the bottom of the food chain.

T. pyriformis are ciliated eukaryotes that inhabit fresh bodies of water, feeding on bacteria through the process of phagocytosis (5, 6). These unicellular paramecia function as model organisms due to their distinct, universal cellular functions such as their food vesicle maturation process (5). Using their cilia (**Figure 1A**), *T. pyriformis* pull bacterial particles into the base of their complex oral groove where they organize their food into fatty membrane vesicles, or phagosomes, using four ciliated membranelles (7). The phagosomes then enter the complex network of membrane trafficking pathways before exiting the organism through egestion (6). Membrane trafficking depends heavily on phospholipids residing in the cytoplasmic leaflet, called phosphoinositides, for vesicle recognition and transport (8, 9). In addition, vesicle transport from the oral apparatus requires the use of myosin motor proteins, composed of fibrous yet

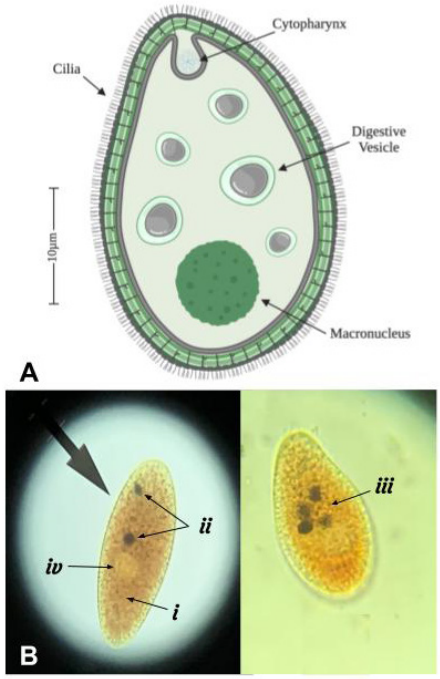

Figure 1: Cellular components of *Tetrahymena pyriformis*. A) Simplistic diagram of a *T. pyriformis* based on a camera lucida image of the organism (17, Abdullah, Shamall). Cellular contents of the organism are labeled. B) A microscopic view at 400X magnification of *T. pyriformis*, fixed with a 20% iodine solution (i, referring to the orange-brown coloration). The left image shows a *T. pyriformis* containing two India Ink food vesicles (ii) after feeding for 10 minutes in a 5.0 pH suspension, while the right image shows a *T. pyriformis* containing four India Ink food vesicles (iii) after feeding for 10 minutes in a 6.5 pH suspension. (iv) points towards the macronucleus of the organism. These photos were taken using an iPhone camera.

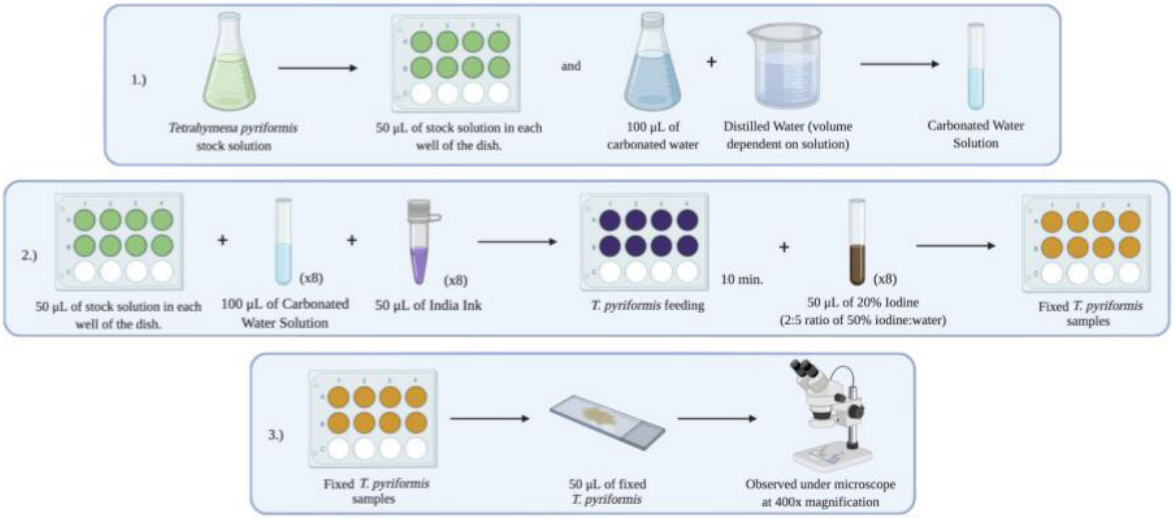

Figure 2: Overview of the stepwise experimental procedure for preparing the samples and the observing the fixed *T. pyriformis*. Step 1.) shows the configuration of the *T. pyriformis* solution, which includes the setup of the multi-well dish, as well as the preparation of the various carbonated water solutions used to alter the environmental acidity. Step 2.) incorporates and describes both the feeding and the fixing processes of the organism. Each of the 8 100 mL carbonated water solutions were separate treatments that varied in pH measurement. Lastly, Step 3.) depicts the sampling and data collection procedures.

dynamic actin molecules crucial for motility (9). All of the molecules work in concert to complete maturation; therefore, if any step is interrupted along the way because of extreme habitat conditions, phagocytosis may not be possible.

The goal of this experiment was to investigate the effect of varying environmental pH on *T. pyriformis'* ability to produce phagosomes containing 2% India Ink, an experimental proxy for food. Through simulating the acidification of freshwater environments due to excess CO_2 in the atmosphere, we aimed to discover optimal feeding pH for *T. pyriformis*. We hypothesized that as acidity increased, *T. pyriformis* would consume less, producing fewer food vesicles, which would implicate their inability to successfully complete phagocytosis. We propose that as environmental pH drops below the neutral freshwater surface conditions of a pH ranging from 7.5–8.5 (10), increased amounts of hydrogen ions (lower pH/acidic conditions) might negatively alter the molecular composition of cilia and membranes, inhibiting *T. pyriformis'* motor functions and vesicle formation processes. Our data uncovers that *T. pyriformis* consume the most food vesicles within an optimal pH range of 6.0–7.0. At any point below a pH of 6.0, *T. pyriformis* lose feeding competence, consuming fewer food vesicles. These results display the danger freshwater acidification poses to even small ciliated organisms, providing reasonable evidence to further research acidification's impact on other aquatic organisms and to uncover the urgency of limiting our fossil fuel emissions.

RESULTS

To determine whether our hypothesis that increased acidity would inhibit phagocytosis and prevent *T. pyriformis* from generating a baseline amount of food vesicles, we prepared seven different treatment groups of the varying acidities: 4.5, 5.0, 5.5, 6.0, 6.2, 6.5, and 7.0, which acted as a negative control, replicating a standard freshwater habitat pH. We created separate treatments by diluting carbonated water, which had a pH of 4.5, with differing amounts of distilled water. Carbonated water mimicked the conditions of a freshwater habitat after absorbing carbon dioxide, and each treatment simulated a more severely acidified environment. After quantifying each treatment's pH using paper pH strips, we mixed *T. pyriformis* and India Ink, a dark dye and proxy for food, into a treatment solution (**Figure 2**). After a 10 minute feeding period, we fixed the *T. pyriformis* with iodine and then, under 400x magnification, counted the number of India Ink food vesicles within 5 different *T. pyriformis* within a specific treatment (**Figure 2**); an increase or decrease in *T. pyriformis'* consumption of food signaled a loss in feeding competency resulting from changes in suspension conditions. The data collected from each *T. pyriformis* at this step represented a pseudo-trial, a replicate collected from within a single trial; yet, pseudoreplicates are not completely independent from one another and therefore cannot solely be used to assess statistical significance. As a result, we repeated these steps three times for each of the 7 treatments, obtaining a total of 15 replicates for every condition. A final treatment (pH = 7.0) without carbonation and without India Ink acted as a second negative control.

As pH increased, *T. pyriformis* formed more India Ink vesicles, consuming the largest mean number of food vesicles of 3.73 ± 0.18 (± standard error) at a pH of 7.0 (negative control), and the smallest mean number of food vesicles of 0.60 ± 0.16 at a pH of 4.5 (**Figure 3**). At a pH of 7.0 with no food available and no carbonation added (second negative control), no *T. pyriformis* held any food vesicles within their bodies. We observed no qualitative changes in morphology *T. pyriformis* across different pH suspensions (**Figure 1B**).

A one-way analysis of variance (ANOVA) performed on our dataset yielded significant variation among our tested conditions ($F(7, 112) = 58.41$, $p = 1.74 \times 10\text{-}34$). A post hoc Tukey's test revealed that mean food vesicle count increased with significance ($p < 0.001$) from 0.60 ± 0.16 to 2.07 ± 0.21 while suspension pH increased from 4.5 to 5.0; then, from a treatment pH of 5.0 to 5.5, mean vesicle count significantly increased ($p < 0.05$) again from 2.07 ± 0.21 to 2.87 ± 0.26 (**Table 1**). No statistical significance was identified between

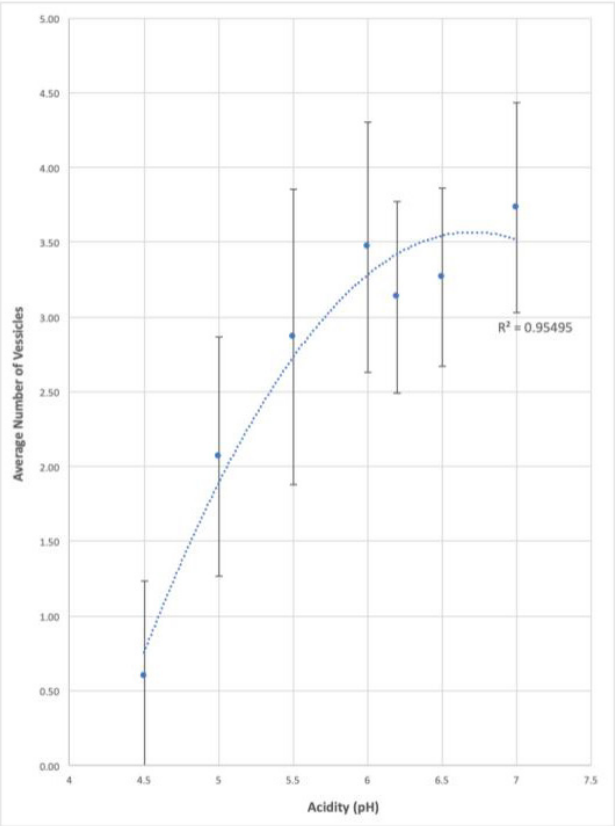

Figure 3: The mean value of India Ink vesicles counted within iodine-fixed *T. pyriformis* in variable pH environments. Means of food vesicles result from 15 replicates (n = 15) collected over 3 trials. Vesicles were counted (at 400X magnification) after *T. pyriformis* were fed India Ink for 10 minutes in various acidic concentrations of carbonated water (4.5 ≤ pH ≤ 7.0). Mean vesicle counts in treatments with a pH of 5.5 and below were statistically significant ($p \leq 0.05$), while data collected in a pH of 6.0 and higher was statistically similar ($p \geq 0.05$). When no carbonation and no India Ink were added to the environment, there were no vesicles observed in any *T. pyriformis* (not shown above). Error bars denote the calculated standard deviation (SD) of each run.

all sequential treatment pairings with pHs of 5.5 and higher (**Table 1**). However, a comparison between pH treatments of 5.5 and 7.0 with mean vesicle counts of 2.87 ± 0.26 and 3.73 ± 0.18, respectively, also yielded statistical difference ($p < 0.025$, **Table 1**). The data set fits the trend of a quadratic polynomial curve with an r2 value of 0.955. Additionally, p-values calculated using two-tailed T-tests between different sets of pseudo-trials within each run were all greater than 0.05, showing statistical similarity, with the exception of two different trials from testing in a pH of 6.0 ($p < 0.0004$).

DISCUSSION

Our data supports the hypothesis that a lower environmental pH decreases the amount of visible food vesicles within *T. pyriformis* after a 10-minute feeding period. However, the data collected also revealed a new element to this trend: as pH increased from acidic to neutral, food vesicle count increased at a decreasing rate. Mean food vesicle count plateaued at pHs higher than 5.5 (**Figure 3**), when data points no longer were statistically different from one another ($p > 0.05$, **Table 1**). But

Treatment Pairs	Tukey HSD p-value
pH 4.5 v. pH 5.0	0.00100
pH 5.0 v. pH 5.5	0.04727
pH 5.5 v. pH 6.0	0.28596
pH 6.0 v. pH 6.2	0.89999
pH 6.2 v. pH 6.5	0.89999
pH 6.5 v. pH 7.0 (no carb)	0.59689
pH 5.5 v. pH 7.0 (no carb)	0.02235

Table 1: Results of a post-hoc Tukey's Test indicating statistical significance between treatments groups. Calculated Tukey HSD p-values are listed for treatment group comparisons labeled in the leftmost column. Green coloration denotes statistical significance ($p \leq 0.05$) while red coloration signals statistical similarity ($p \geq 0.05$).

mean vesicle counts between pH treatments of 5.5 and 7.0 remained statistically different ($p < 0.025$), demonstrating that the optimal feeding environment of *T. pyriformis* lies within a pH range of 6.0 to 7.0. The most probable explanation for this phenomenon is acidity's direct effect on *T. pyriformis'* process of phagocytosis. As the hydrogen ion concentration of their suspension increases, *T. pyriformis'* cell membrane thickness and structure can change rapidly and drastically. Studies investigating other membranes such as phosphatidylcholine bilayers, which occur naturally in eggs, reveal that acidic environments cause decreased head repulsions in phospholipids around a pH of 5.5, increasing interfacial tension and density of the bilayer within nanoseconds (11, 12). Bilayers containing phospholipids with amphiphilic heads occurring in eukaryotic cells, such as *T. pyriformis*, may react similarly to protonation caused by high hydrogen ion concentrations. Increased membrane density could directly inhibit the function of phosphoinositides, which would prevent phagosome transport and organization. Phosphoinositides are essential elements in endosome dynamics, as well as various cell signaling pathways, necessary for regulating the movement of food vesicles throughout phagocytosis (9). Without functional phosphoinositides, food vesicles may not successfully enter membrane trafficking pathways or even reach their respective destinations after phagocytosis, potentially explaining why fewer vesicles were observed in lower pH environments. Though we saw no visible alterations in food vesicle morphology, even subtle changes in membrane density may have hindered phosphoinositide function. Finally, phagosomes rely on actin-based myosin motors to move from the oral apparatus into the cell's interior; yet, acidic environments with a pH of lower than 6.5 can weaken myosin's average force by 20% (13). Even if weakened myosin can still transport phagosomes, they must do so at a slower rate, a discovery which may explain the drastic drop in vesicle count seen in pHs lower than 6.5 (**Figure 3**).

Distilled H_2O (µL)	Carbonated H_2O (µL)	Resulting pH
0	100	≈ 4.5
20	100	≈ 5.0
40	100	≈ 5.5
60	100	≈ 6.0
80	100	≈ 6.2
100	100	≈ 6.5
100	0	≈ 7.0

Table 2: Ratios of distilled water to carbonated water to obtain 6 distinct carbonated water solution pHs. Micropipettes were used to control amounts of each component added into the mixture. Acidity values were measured using paper pH strips.

However, low pH might not hinder only the process of phagocytosis; in environments with pHs lower than 5.0, *T. pyriformis'* cilia can become completely inactivated (14). High hydrogen ion concentrations slow the mechanical activity of cilia in all paramecia, causing an exponential drop in cilia's mechanical speed starting at a pH of around 5.5 (15). Not only does this inhibition of ciliary mechanics prevent *T. pyriformis* from reaching food, but it also prevents them from sweeping food into their oral groove at a normal rate. The critical role of ciliary mechanics in *T. pyriformis'* movement and food consumption offers two explanations for the decreased phagosome production observed below a pH of 5.5.

Ciliary mechanics change in basic solutions as well, solidifying our prediction of a trendline projection that peaks around a pH of 6.5, after which the mean vesicle count would decrease again. At pH solutions above a pH of 7.0, the speed of paramecium's ciliary movement slows, eventually becoming completely deactivated at a pH of 9.5 (15). Other researchers have observed a significant decrease in food uptake of paramecium in basic solutions (14). Based on this information, we predict a decrease in food vesicle count within *T. pyriformis* in more basic solutions, an outcome supporting the idea that *T. pyriformis* feed best in an optimal pH range of 6.5 to 7.0.

A few confounding variables existed in the context of this experiment. Primarily, the size and membrane composition of each food vesicle was inconsistent, meaning *T. pyriformis* with a few large vesicles could have consumed the same quantity of food as ones with many smaller vesicles. Calculating food vesicle area in ImageJ could prove a more accurate method of quantifying food intake. Quickly measuring carbonated water with pipettes generated another source of uncertainty. Bubbles of carbonation would often enter the pipette tip, causing ambiguity in our measurements. To produce more precise results, runs could have been staggered farther apart to eliminate any rush while pipetting. A third source of uncertainty was the determination of pH measurements of each solution using pH strips, since the color of the strips was compared to a limited color scale. The chart increases in whole number increments, so when the color of the strip seemed to lie between two hues, it was difficult to determine the decimal of the pH. Instead, using an electronic pH meter may have increased precision because of its ability to detect minute changes in acidity.

In the future, we could initiate feeding periods after *T. pyriformis* have acclimated to their respective pH suspensions for longer periods of time, to investigate whether *T. pyriformis* can adapt to more acidic environments, better simulating the long-term process of fresh-water acidification. Additionally, studying phagocytosis or other bodily processes in different organisms may further solidify our claims and reveal more consequences of freshwater acidification. We could also collect samples from freshwater ponds, lakes, or streams to study the changing pH levels of our local habitats and how the *T. pyriformis* that reside in them are coping with their environment's varying conditions.

METHODS

Variables and Control Groups

By carbonating water, acidic freshwater environments were replicated by lowering water pH through the reactions: $H_20 + CO_2 \rightarrow H_2CO_3 \rightarrow H^+ + HCO_3^-$. Adding different concentrations of carbonated water to the *T. pyriformis* suspension varied environmental acidity and consequently lowered the overall pH to 4.5, 5.0, 5.5, 6.0, 6.2, and 6.5 respectively. For these six conditions, three trials each consisting of five pseudo-trials were conducted to determine the amount of India Ink vesicles within random *T. pyriformis* in solution. In addition to the six pH solutions listed above, two other control groups were included in the experiment. The first negative control was the original *T. pyriformis* solution with food added but no pH change, and the second negative control group was the same *T. pyriformis* solution with no pH change or food. The first control group served as a baseline for the other tests, since the natural pH that *T. pyriformis* exist in is an average freshwater pH of 7.0 (10). The second control group was necessary to confirm that without food, the *T. pyriformis* would hold no food vesicles.

Configuration of *T. pyriformis* Solutions

T. pyriformis solution (50 µL) was added into 8 separate wells of a 12-well dish. The carbonic acid concentrations, or proportionate mixtures of CO_2 and distilled H_2O, were combined in a separate multi-well dish. The carbonic acid was prepared by placing a bottle of distilled water in a SodaStream® and pressing the carbonation button for 10 seconds, as suggested by the instructions. The pH of the purely carbonated water was around 4.5; this was established as the minimum bounds of the IV. To achieve the other less carbonated solutions, the original carbonated water solution was diluted with distilled water to raise solution pH. Preliminary testing demonstrated that adding 20 µL increments of distilled water to 100 µL of carbonated water would increase the pH by roughly 0.5 per addition (**Table 2**).

Feeding the *T. pyriformis*

After the concentrations were made and the pHs were quantified prior to each trial using pH strips (**Table 2**), the acidic dilutions and food proxy were simultaneously added to the *T. pyriformis* solutions. First, 100 µL of the 4.5 pH solution and 50 µL of 2% India Ink were added to 50 µL of *T. pyriformis* in the first dish well, for a 1:1 ratio of 2% India Ink to *T. pyriformis*. These values, along with the amount of carbonated solution added, were controlled every single trial

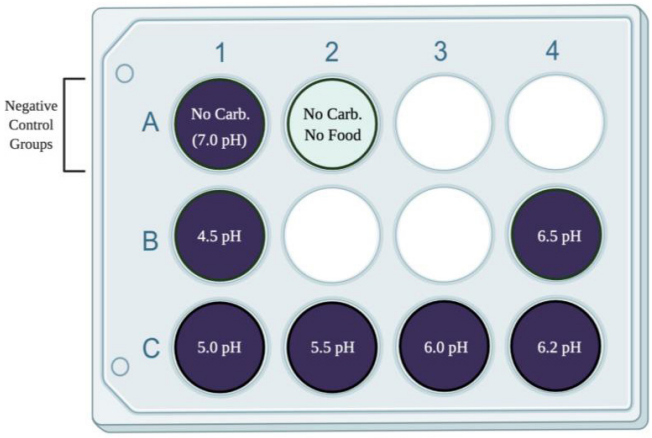

Figure 4: A multi-well dish containing all solutions observed under the microscope during testing. Each solution, with the exception of the two negative control groups, contains 50 µL of *T. pyriformis*, 50 µL of 2% India Ink, and 100 µL of specific carbonated water dilutions, which were all added simultaneously. The first negative control group (well A1) contains 50 µL of *T. pyriformis* and 50 µL of 2% India Ink, whereas the second negative control group (well A2) contains only 50 µL of *T. pyriformis*.

and run to prevent any other variables from influencing our results. Exactly 30 seconds later, a sufficient window of time to refill micropipettes, 100 µL of the 5.0 pH solution and 50 µL of 2% India Ink were added to the 50 µL of *T. pyriformis* in the second well of the dish. This process was continued for the rest of the remaining pH solutions at 30 second intervals (**Figure 3**). In the penultimate well of the dish, 50 µL of 2% India Ink was mixed with 100 µL of distilled water and combined with the 50 µL of *T. pyriformis* solution. In the last well of the dish, the 50 µL of *T. pyriformis* solution was unaltered; it was expected that this *T. pyriformis* solution would confirm that without food, *T. pyriformis* held no food vesicles (**Figure 4**). They were given exactly 10 minutes to feed.

Preparation and Administration of Fixing Solution

During the 10-minute waiting period, the dilute iodine solution used to fix the *T. pyriformis* was prepared. This dilution was generated by mixing 200 µL of 50% iodine with 500 µL of distilled water to create 700 µL of diluted 20% iodine. The 20% solution was used because the 50% iodine made the *T. pyriformis* too dark to inspect under the microscope, an observation confirmed by preliminary testing. After the 10-minute feeding, 50 µL of the 20% iodine solution was added to the first well containing the 4.5 pH solution to fix the *T. pyriformis*, allowing them to be easily observed under a microscope. Next, after 30 seconds, 50 µL of the iodine dilution was added to the second well containing the 5.0 pH solution. This same fixing procedure was repeated for all solutions in the other wells of the dishes again at 30 second intervals, including both control groups (**Figure 4**). After this process was completed, 50 µL of solution from each run was added to a slide and labeled. (**Figure 2**).

Data Collection

These slides were then inspected under a microscope at 400X magnification, and the number of large, dark food vesicles (**Figure 1B**) within five random *T. pyriformis* for each of the eight slides was counted and recorded. Occasionally, microscope focus was adjusted when looking at a single *T. pyriformis* to observe all of its bodily contents, as vesicles can lay on different focus planes within their bodies. After collecting the vesicle data for five random *T. pyriformis*, the first trial was concluded. The second and third trials, each with five pseudo-trials, were commenced in the same manner as the first. Once all data was collected, mean, SD, and standard error calculations were completed. Additionally, an ANOVA and post hoc Tukey's Test were performed in Excel to assess statistical variance among our dataset. In **Figure 2**, SD calculations were used to produce error bars, and Excel was employed to produce a best fit polynomial trend to the data.

ACKNOWLEDGMENTS

The authors would like to thank the Milton Academy Science Department for supplying the materials needed to complete this research and for offering continual guidance throughout the process of publication.

Figures 1A, 2, and 4 were made using BioRender.com.

Received: August 18, 2020
Accepted: November 23, 2020
Published: February 8, 2021

REFERENCES

1. Staff, EIA. "Fossil Fuels Have Made Up at Least 80% of U.S. Fuel Mix since 1900." United States Energy Information Administration, 2 July 2015, www.eia.gov/todayinenergy/detail.php?id=21912.
2. "Global Greenhouse Gas Emissions Data." United States Environmental Protection Agency, www.epa.gov/ghgemissions/global-greenhouse-gas-emissions-data.
3. "Carbon Dioxide Emissions Rise to 2.4 Million Pounds per Second." *CBS News*, 2 Dec. 2012, www.cbsnews.com/news/carbon-dioxide-emissions-rise-to-24-million-pounds-per-second/.
4. Gies, Erica. "Like Oceans, Freshwater Is Also Acidifying." Scientific American, 11 Jan. 2018, www.scientificamerican.com/article/like-oceans-freshwater-is-also-acidifying/.
5. Ruehle, Marisa D., *et al.* "Tetrahymena as a Unicellular Model Eukaryote: Genetic and Genomic Tools." *Genetics*, vol. 203, no. 2, June 2016, pp. 649-65, doi.org/10.1534/genetics.114.169748.
6. Ross, Gary, *et al.* "A Simple Microscopy Assay to Teach the Processes of Phagocytosis and Exocytosis." *Life Sciences Education*, vol. 11, no. 2, 1 June 2012, doi.org/10.1187/cbe.11-07-0060.
7. Cole, Eric S. "The Tetrahymena Conjugation Junction." *Madame Curie Bioscience Database*, 2000-2013, www.ncbi.nlm.nih.gov/books/NBK6002/.
8. Dickson, Eamonn J. "Understanding Phosphoinositides: Rare, Dynamic, and Essential Membrane Phospholipids." *Biochemical Journal*, vol. 476, no. 1, Jan. 2019, pp. 1-23. *Portland Press*, doi.org/10.1042/BCJ20180022.
9. Nusblat, Alejandro D., *et al.* "Conservation and Innovation in Tetrahymena Membrane Traffic: Proteins, Lipids, and Compartments." *Tetrahymena Thermophila*, edited by Kathleen Collins, 2012, pp. 141-75, 159 vols.

Science Direct, doi.org/10.1016/B978-0-12-385967-9.00006-2.
10. *"*pH of Water.*"* *Fondriest Environmental, Inc.*, 19 Nov. 2013, www.fondriest.com/environmental-measurements/parameters/water-quality/ph/.
11. Lähdesmäki, Katariina, *et al. "*Membrane Simulations Mimicking Acidic PH Reveal Increased Thickness and Negative Curvature in a Bilayer Consisting of Lysophosphatidylcholines and Free Fatty Acids.*"* *Biochimica Et Biophysica Acta (BBA)*, vol. 1798, no. 5, May 2010, pp. 938-46. *Science Direct*, doi.org/10.1016/j.bbamem.2010.01.020.
12. Petelska, Aneta D., and Zbigniew A. Figaszewski. *"*Effect of pH on the Interfacial Tension of Lipid Bilayer Membrane.*"* *Biophysical Journal*, vol. 78, no. 2, Feb. 2000, pp. 812-17. *Science Direct*, doi.org/10.1016/S0006-3495(00)76638-0.
13. Woodward, Mike, and Edward P. Debold. *"*Acidosis and Phosphate Directly Reduce Myosin›s Force-Generating Capacity through Distinct Molecular Mechanisms.*"* *Frontiers*, 10 July 2018, www.frontiersin.org/articles/10.3389/fphys.2018.00862/full.
14. Lee, J. Warren. "The Effect of PH on Food-Vacuole Formation in Paramecium." *Physiological Zoology*, vol. 15, no. 4, 1942, pp. 459–465. *JSTOR*.
15. Gray, James. Ciliary Movement, p. 80. Cambridge, Cambridge UP, 2015.
16. Northwestern University. *"*Acidity Can Change Cell Membrane Properties.*"* *Science Daily*, 1 Oct. 2013, www.sciencedaily.com/releases/2013/10/131001124012.htm.
17. Abdullah, Shamall. Tetrahymena pyriformis. A-Photomicrograph (1000X). B-Camera lucida drawing. Apr. 2010.

JOURNAL OF
EMERGING INVESTIGATORS

Article

Observing how the distance from the mouth of a Bahamian mangrove affects biodiversity

Connor J. Fischetti[1], Emilie D. Wolf[1]
[1] The Browning School, New York, New York

SUMMARY

Mangroves are salt-tolerant shrubs that have elaborate root structures and are found on tropical coastlines. Their complex root structure, along with other characteristics, allow mangroves to filter out salt from saltwater. This filtration results in varying salinity levels throughout mangroves and can affect what type of organisms can live in mangroves. Looking at the biodiversity of different sections of a mangrove can give insight into what certain species are attracted to in their habitat. Our experiment focused on determining how the distance from the mouth of a mangrove affects biodiversity. We determined this biodiversity by selecting three sites located at different distances from the mouth of the mangrove. By using the assumption that salinity decreases as you move farther away from the mouth of the mangrove, we were able to compare each site's relative salinity with its biodiversity. At each location, we recorded all marine species and their abundance for a total of twenty minutes. From the data collected, we used a Simpson's diversity index to calculate the biodiversity of each of the sites. We predicted that the site closest to the mouth would have the highest diversity since more animals are adapted to living in saltwater than freshwater. Once we collected the data, it was clear that the site 260 meters away from the mouth had the lowest diversity, and the sites that were 90 and 135 meters away were similar in biodiversity. We also observed that almost all of the fish found were either juvenile or under five inches, which supported our prediction that the majority of fish would be smaller because they use the compact roots as protection from predators. Overall, our hypothesis that biodiversity would be highest near the mouth was partially supported because although the 135-meter site was the most diverse, it was very similar to the 90-meter site. They were both significantly denser in biodiversity than the 240-meter site.

INTRODUCTION

Salinity levels are a crucial component of water ecosystems because they keep more than 75% of the world's organisms alive and biodiversity high (1). Mangroves are unique in the fact that they have varying salinity at different locations (2). The combination of salinity's vital role in the life of aquatic species and mangrove's ability to alter salinity levels offered the opportunity to explore the true effects of varying salinity in a localized habitat. The objective of this study was to determine whether biodiversity changes as a result of a changing salinity gradient based on the assumption that salinity decreases the further away the site is from the mouth of the mangroves.

Mangroves' prop roots, which are exposed, give extra support and an excellent place for other species to claim as home, including species that live specifically around mangroves. Although the ecosystems of mangroves are diverse, many of the fish and shellfish that place themselves there are temporary due to the need to breed or place eggs. The roots of the mangrove trees consist of hard and durable wood that helps to stop large waves and winds from pushing further inland of a coastal region (3). They can also filter out pollutants and trap sediments from the land (4). Apart from their ecosystems, mangroves include a wide variety of species, including the common, red mangroves, black mangroves, and the nipa palm, which are members of the Arecaceae family (4).

A study done in 2001 investigated the correlation between a variety of juvenile fish and mangroves (5). It found that areas with structures similar to mangroves attracted more fish than areas with little structure. They also tested whether juvenile fish were attracted to places with more or fewer algae. Their data showed that structures left to form algae attracted four times the total number of fish than areas with a clean structure or lack of structure (5). The report concluded that the most important characteristic of a mangrove environment for small juvenile fish was the complex structure of roots that provide an abundance of food and protection from predators. As the fish grow, they tend to shift their habitat to mudflats due to a change in diet and reduced vulnerability to predators (5).
Biodiversity is the variety in life on earth on all levels, from physical traits down to the genes of the organisms. Biodiversity is what allows ecosystems to function properly since each species has a unique function to play. (6). In the Bahamas, there is a vast amount of biodiversity. The surrounding water contains many different types of fish and marine life.

A biodiversity index shows how diverse groups of organisms are. It uses the number of species in an environment, as well as the abundance of each of those species. A biodiversity index will show that as the richness and evenness of species increase, so does the diversity. Evenness is defined as how close in numbers each species in the recorded data set are

A biodiversity index will generate a number between one and zero, with one being extremely diverse and zero, no diversity (8).

$$D = 1 - \left(\frac{\sum n(n-1)}{N(N-1)} \right)$$

The diversity formula above (previous page) is known as Simpson's Diversity index. The D in the equation is the diversity value on a scale of zero to one. The value n is representative of the total number of organisms of a particular species, and N is representative of the total number of all species in the data set. By dividing the sum of each species "n(n-1)" value by the "N(N-1)," one obtains the root value, which is then subtracted from 1 to obtain the diversity (D) value (8).

A group of organisms with only one or two species would be considered less diverse than one with the same abundance but multiple species. Simpson's index uses the richness and relative abundance to give the sample set a rating from zero to one (8). One primary assumption we used during calculation is that we accurately identified the species across their different life stages. This diversity value is also limiting because it is hard to compare data from one experiment to another since they could have two drastically different ways of recording the species and their number. For instance, one study may record only adult organisms or record flora and fauna instead of just fauna (8).

The Bray Curtis Index uses the values of two different sites (in this case, the abundance of each species) and the lowest number of shared values to give a value to how different the sites are from one another. This value is then subtracted from one and multiplied by one hundred to find the similarity. This test is limited because the accuracy depends on how many values there are at each site: the more values, the more accurate the index number. The one major assumption that has to be used in calculations is that both site areas are the same size. The formula does not include a space variable and is only working with species count. In this experiment, all sites were equal in area, so we were able to calculate the index without adjustments to the formula (9).

$$BC_{ij} = 1 - \frac{2C_{ij}}{S_i + S_j}$$

We used the above formula, where BC_{ij} is the Dissimilarity value that was subtracted from one and multiplied by a hundred to obtain the similarity value in a percentage form. In the formula, S_i represents the total number of species recorded at one site, and S_j represents the total number of species recorded at the other site. C_{ij} is the sum of only the lesser counts for each species found in both sites. For example, in **Table 2**, Blue Crabs were spotted at both site one and site two, so during the calculation of similarity for the sites, C_{ij} was calculated using the lesser value of each of the shared species, which was the one blue crab at site 2 (9).

We used these formulas to determine whether salinity affects biodiversity in mangroves. Salinity in the oceans is almost always consistent at around 35 PSU but can vary along coastlines where seawater is mixed with freshwater rivers resulting in brackish water. Brackish water presents a unique challenge for wildlife since it requires them to adapt quickly to changing salinity levels. (10).

Salinity levels are a crucial aspect of the distribution of marine and estuary species. Salinity can shape an entire ecosystem and provide specific adaptations for different species. The effects of changing salinity on the ecology of an ecosystem are based mainly on the tolerance of the underlying organism to that change. Salinity levels can vary on both short term and long term scales. Because of this, many organisms have adapted a tolerance to varying salinity levels. Most of the time, estuarine species are euryhaline, meaning that they can tolerate and live in a wide range of salinity. Unlike estuarine species, many other marine species are stenohaline and extremely limited in the salinity level they can tolerate. Lower salinity levels can provide a subsidy for estuarine species by reducing competition in the environment. Salinity levels outside of an organism's tolerance can change their behavior, limit their chance of reproduction and germination, and can reduce their fitness for survival in the environment. Salinity can work synergistically or antagonistically with other environmental factors in making a constantly changing habitat. Salinity levels are also influenced by Anthropogenic activities or human factors such as the ice caps melting and the rapid heating and evaporation in the tropics (11).

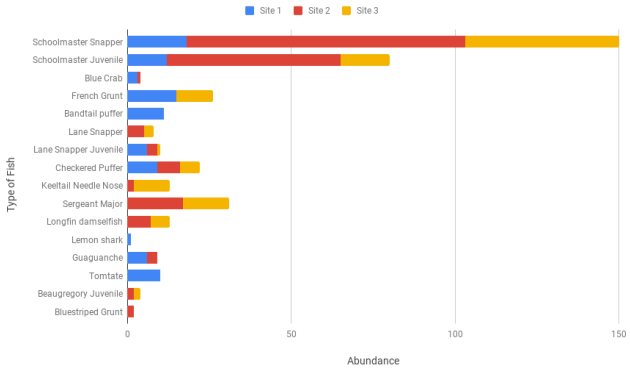

Figure 1: Stacked bar graph of the abundance of each species of fish. Site 2 (in red) had the highest number of different types of fish. For each type of fish recorded throughout the experiment, its total abundance is represented by the multi-colored bar next to its name. Schoolmaster snappers were the most common fish found across our sites. Each bar is separated into different colors representing the abundance for each site. Site 1 is represented in blue, site 2 in red, and site 3 in yellow. The data on the abundance of each fish was acquired by counting the number of its kind that passed through a 225 m^2 perimeter set up at the different sites within two 10 minute windows.

Using the assumption that the salinity gradient decreases further into a mangrove (**Table 1**), it is predicted that the biodiversity will be greater in saltier water or closer to the mouth because fewer organisms have adapted to live in

	Site 1	Site 2	Site 3
Distance from the mouth of Mangrove	260 meters	135 meters	90 meters
Assumed salinity	Lowest	Median	Highest
Depth	40 cm	60 cm	85 cm
Substrate	The sand was much finer than other sites	Coarse sand with many small rocks in the channel	Coarse sand with rocks
Current	Little current	Strong current	Strongest currents
Mangroves density	Less dense than other sites	Densest mangroves	Similar to site 2
Sampling dates and times	April 30, 2019 Trial 1: 10:30am - 10:40am Trial 2: 2:35pm - 2:45pm	April 30 and May 2, 2019 Trial 1: 10:45am - 10:55am Trial 2: 11:10am - 11:20am	April 30 and May 2, 2019 Trial 1: 2:20pm - 2:30pm Trial 2: 2:25pm - 2:35pm
Characteristics	Consistently windier than all other sites	Located at the curve in the creek of mangrove (Fig. 2) Sheltered from the wind	The narrowest part of the mangrove creek Fish hide in the mangroves, few to no fish in open areas

Table 1: Description of Each Site in The Page Creek Mangrove System shown in Figure 2.

Figure 2: Location of Each Site in The Page Creek Mangrove System and Distance from the Mouth of Mangrove in Meters.

fresher water, so there is less competition (11). In addition, it is predicted that the majority of the fish in the mangroves will be either juvenile or small types of fish due to the mangrove's compact and safe environment (6).

RESULTS

A large number of species had been observed at all of the sites (**Table 2**, **Figure 1**). To find the biodiversity of each site, a Simpson's biodiversity index was used to give each site a biodiversity rating from 0 to 1, with one being the most diverse. Site 1, which was located farthest from the mouth of the mangrove (**Figure 2**), was given the lowest rating at 0.12. Site 1 was located 240 meters from the mouth of the mangroves, and it was also much less dense of a mangrove than sites 2 and 3. Site 3 was the second most diverse., with a biodiversity index of 0.21 and the most diverse site was site 2, with an index reading of 0.34. The Simpson index is calculated using both the number of species and richness of the species. We can, therefore, see that it is no surprise that site 2 was the most diverse because it had 12 of the 15 species recorded in the entire mangrove. One can also see in **Figure 1** that site 2

Common Name	Species Name (Author, Year)	Site 1	Site 2	Site 3
Schoolmaster snapper	*Lutjanus apodus* (Walbaum,1792)	18	85	47
Schoolmaster juvenile	*Lutjanus apodus* (Walbaum,1792)	12	53	15
Blue crab	*Cardisoma guanhumi* (Latreille,1828)	3	1	0
French grunt	*Haemulon flavolineatum* (Desmarest,1823)	15	0	11
Bandtail puffer	*Sphoeroides spenglerpia* (Bloch, 1785)	11	0	0
Lane snapper	*Lutjanus synagris* (Linnaeus, 1758)	0	5	3
Lane snapper juvenile	*Lutjanus synagris* (Linnaeus, 1758)	6	3	1
Checkered puffer	*Sphoeroides testudineus* (Linnaeus, 1758)	9	7	6
Keeltail needle nose	*Platybelone argalus* (Lesueur, 1821)	0	2	11
Sergeant major	*Abudefduf saxatilis* (Linnaeus, 1758)	0	17	14
Longfin damselfish	Stegastes diencaeus (Jordan & Rutter, 1897)	0	7	6
Lemon shark	*Negaprion brevirostris* (Poey, 1868)	1	0	0
Guaguanche	*Sphyraena guachancho* (Cuvier, 1829)	6	3	0
Tomtate	*Haemulon aurolineatum* (Cuvier, 1829)	10	0	0
Beaugregory juvenile	*Stegastes leucostictus* (Castelnau, 1855)	0	2	2
Bluestriped grunt	*Haemulon sciurus* (George Shaw, 1803)	0	2	0
Simpson's Diversity Index		**0.1204**	**0.3413**	**0.213**

Table 2: Total Number of Fish and Species Recorded at sites 1,2, and 3 and each Sites Simpson's Index.

	Site 1	Site 2
Site 2	31.7	
Site 3	46.4	63.4

Table 3: Percentage of Similarity Between Each Site Using The Bray Curtis Index.

had the highest abundance of each species found at the site. The adult and juvenile Schoolmaster Snapper were the most abundant at all sites (**Table 2**, **Figure 1**).

In order to compare the similarity between the sites, we used the Bray Curtis Index. The index used the abundance of each species at each site to establish a percentage number to represent their similarity. **Table 3** shows that site 1 was least similar when compared to both site 2 and site 3 with a similarity rating of 31% and 46%, respectively. This low similarity percentage supports and mirrors the diversity test because site 1's index was 0.22 away from site 2's index and 0.09 away from site 3's index. **Table 3** also shows that sites 2 and 3 are 63% similar. The similarity between sites 2 and 3 and the lack of similarity compared to site 1 is due to the site's distance from each other, as shown in **Figure 2**. Site 2 was only 45 meters away from site 3 compared to 125 meters away from site 1 (**Table 1**).

The main outliers observed from the data were the extreme number of both schoolmaster and schoolmaster juveniles observed in site 2 and the extremely low number of lemon sharks observed. The high number of schoolmaster snappers was caused by the second recording of fish at site 2. During that ten minute recording period, the tide was extremely low. In addition to the tide being very low, site 2's mangrove density was also much higher than the other two sites. These two factors caused the high tide number of schoolmasters to hide deeper into the mangroves where we could not see them, while the low tide forced all the fish to come into full view where we were recording. Another small outlier was the lemon shark. During the two days of recording, the only lemon shark that was recorded was at site 1. This outlier was most likely a random and an unusual coincidence.

DISCUSSION

Our hypothesis that the regions closer to the mouth of the mangrove would be more diverse was partly supported by the data. Sites 2 and 3 had higher biodiversity index values than site 1, which was 260 meters away from the mouth of the mangrove and had a lower assumed salinity level. Site 2, however, had the highest biodiversity index instead of the predicted site 3, which was closest to the mouth of the mangrove. Although site 2 had higher biodiversity than site 3, it still supports the idea that the closer to the mouth a site is, the more diversity it will have. It supports this idea because sites 2 and 3 were only 45 meters apart and had the most similar recordings, which means the data was probably just impacted by a small sampling error. Our hypothesis about

Figure 3: Location of Mangrove System in Relation to The Island School on The Island of Eleuthera in The Bahamas.

the majority of fish being small was also supported. Through our observations of the fish, it was clear that the majority of the fish were either small adults or juveniles. In addition, the majority of fish were recorded inside the compact mangroves, which further proved the predicted fact that juvenile and small fish choose mangroves as a habitat because they can use the structure as shelter.

One of the downsides of testing in the field is that several unwanted factors can affect the experiment. One such factor was that site 1 was shallower and contained a much less dense mangrove than the other sites. This difference in mangrove density could have affected our data because it was clear that fish in the mangroves liked to swim in the denser roots while they would tend to stay away from the thinner rooted mangroves. Another factor that could have affected the data was the weather. During the two testing days, there was about half an inch of rain that could have affected the salinity in the mangrove. The current of the mangrove system also could have affected the results. At all testing periods, site 3 had a very strong current compared to the other sites. The increased current most likely resulted in fish taking shelter deeper in the mangrove, where we were not able to record their abundance. A source of error that most likely occurred during the experiment was a miscount of the abundance of fish. There was a significant amount of fish that had to be recorded one by one, and since they were constantly moving around, the same fish may have been recorded more than once. Each team member did their best to record as accurately as possible, but errors always occur when using observation-based data. These errors most likely did not have a huge effect on the data because the miss counts were low enough that it would not have affected the biodiversity index value. One final source of error was the fact that there were multiple people in the mangrove. There were a total of eight individuals in a very small region of the mangrove, many of them not paying attention to where they were walking and how they were disrupting their environment. These disturbances in the testing area most likely caused fish to swim away from our testing site or swim deeper into the mangrove, where we were not able to observe them. Overall, these errors and factors undoubtedly affected the data. However, the effect was not large enough to make a quantifiable difference in the data that would lead to any significance.

Assuming that these results are mainly accurate, there are still limitations that have to be kept in mind when applying the data. One of them is the assumption that as one goes further into the mangrove, the salinity will decrease. We have no evidence of how drastic or slight the change may be. We are just using the assumption that salinity decreases. This limitation only applies when one is looking at the biodiversity at varying salinities. If, however, one is only looking at how biodiversity changes at different distances from the mouth, this assumption does not have to be used, although it can be if wanted. Overall the data collected in this experiment would be most helpful comparing locations with different diversity at different distances from the mouth, not the diversity at different salinities. Using the distance from the mouth value to compare the data, it is clear that the locations closer to the mouth and with more dense mangroves will have more biodiversity.

In future experiments, we recommend that a salinity probe be used to get an accurate reading on the salt levels of each of the sites. It would also be advised that the team be extremely cautious of their footsteps and how they can easily scare the fish away. In the future, it would also be recommended that each site be recorded for longer than twenty minutes in total. The accuracy of the biodiversity index would be significantly more accurate if each site was recorded for more than twenty minutes. Lastly, in the future, it would be highly suggested that a different system of recording the fish be adopted rather than the error-prone manual method.

MATERIALS & METHOD

The mouth of the mangrove system was determined and marked with a stake. Then, a transect line was run from the mouth to points that were 90, 135, and 260 meters away. Each of the points was marked with a stake. A 15 meter by 15-meter perimeter was created around each stake. Then each of the four-team members was placed in the corners of the perimeter with waterproof cameras. A timer was set for 10 minutes. During the 10 minutes, if a team member saw a fish, he would yell out a short description and the quantity he had seen. He would also record the fish with the camera so it could later be identified if not known. The data recorder

Figure 4: Images of each of the sampling sites looking upstream. Site 1 was furthest from the mouth of the mangrove, and site 3 was nearest.

for the team wrote down the description and the quantity of fish into a waterproof notebook. This process was repeated every time a team member spotted a new fish or another number of a previously recorded fish. The number of fish was recorded with a tally system to ensure an accurate number. To ensure that no fish were counted more than once, each team member would track where the fish were going and announce it to the other members so they would not count them again. Once ten minutes had expired, the team moved to the next location and repeated the method of recording fish and their quantity. Each site was recorded for a total of twenty minutes. Once all the data had been collected, the fish were identified. Using the camera footage, the short description, and each person's memory of the fishes, the species name of each fish was found using *Reef fish identification of Florida, The Caribbean, and The Bahamas* by Paul Humann and Ned Deloach. Then using the richness and abundance of fish at each site, a Simpson's diversity index was calculated using Google Sheets.

ACKNOWLEDGMENTS

Spencer Russell, Khai Shulman, and Liam Messenger for help with proposal submission and data collection. Special thanks to The Browning School for funding the expedition and supporting authentic research and to the Island School for providing data recording material, transportation, room and board, and site selection data.

Received: July 18, 2019
Accepted: August 3, 2020
Published: February 8, 2021

REFERENCES

1. "Did You Know...? Marine Life." *MarineBio Conservation Society*, marinebio.org/creatures/facts/.
2. Chen, Ronghua, and Robert R. Twilley. "A gap dynamic model of mangrove forest development along gradients of soil salinity and nutrient resources." *Journal of Ecology* 86.1 (1998): 37-51. https://scholar.google.com/scholar?hl=en&as_sdt=0%2C33&q=A+gap+dynamic+model+of+mangrove+forest+development+along+gradients+of+soil+salinity+and+nutrient+resources&btnG=
3. Britannica, The Editors of Encyclopaedia. "Mangrove." *Encyclopædia Britannica*, Encyclopædia Britannica, Inc., 28 Feb. 2019, www.britannica.com/plant/mangrove.
4. "What Is Biodiversity?" *American Museum of Natural History*, American Museum of Natural History, www.amnh.org/our-research/center-for-biodiversity-conservation/about-the-cbc/what-is-biodiversity.
5. Laegdsgaard, Pia, and Craig Johnson. "Why Do Juvenile Fish Utilise Mangrove Habitats?" *Journal of Experimental Marine Biology and Ecology*, Elsevier, 5 Mar. 2001, www.sciencedirect.com/science/article/pii/S0022098100003312?via%3Dihub.
6. "Mangroves." *Smithsonian Ocean*, 18 Dec. 2018, ocean.si.edu/ocean-life/plants-algae/mangroves.
7. "Bahamas Flora and Fauna." *Bahamas Flora and Fauna*, My Bahamas Travel, 2018, www.my-bahamas-travel.com/bahamasfaunaflora.html.
8. "Simpson's Diversity Index." *Barcelona Field Studies Centre*, Barcelona Field Studies Centre S.L., 28 Nov. 2018, geographyfieldwork.com/Simpson'sDiversityIndex.htm.
9. Glen, Stephanie. "Bray Curtis Dissimilarity." *Statistics How To*, 17 Mar. 2018, www.statisticshowto.datasciencecentral.com/bray-curtis-dissimilarity/.
10. Gates, David M., and Michael B. Thompson. "Biosphere." *Encyclopædia Britannica*, Encyclopædia Britannica, Inc., 24 Sept. 2018, www.britannica.com/science/biosphere/The-cycling-of-phosphorus-and-other-essential-nutrients#ref70878.
11. Smyth, Katie, and Mike Elliott. "Effects of Changing Salinity on the Ecology of the Marine Environment." *Stressors in the Marine Environment*, 2016, pp. 161–174., doi:10.1093/acprof:oso/9780198718826.003.0009.

JOURNAL OF
EMERGING INVESTIGATORS

Article

Repurposing citrus peel waste and its positive effects on our health and communities

Andrew Kim[1] and Joon Om[2]
[1]Montclair Kimberley Academy, Montclair, NJ
[2]Tandon School of Engineering, New York University, Brooklyn, NY

SUMMARY

Every year, more than 30% of food products go to waste. This is approximately 1.3 billion tons of food, which is equivalent to 1.3 trillion U.S. dollars. While conventional solid waste treatments and fertilization of food waste are common, citrus fruit peels require secondary applications and advanced disposal management due to their low pH values and high antimicrobial characteristics. Since citrus fruits are well-known sources of vitamin C and antioxidants, we hypothesized that their peels also contain high amounts of vitamin C and antioxidants. In our study, five common citrus peels including grapefruit, lemon, lime, orange, and tangerine, were used to determine the amounts of vitamin C and total soluble antioxidants. Experimental results showed that lemon peels contain the highest vitamin C concentration (39.68 mg/g sample), closely followed by tangerine peels (37.23 mg/g sample). Lower vitamin C concentrations were extracted from the grapefruit, lime, and orange peels within a 3-hour reaction period with the average concentrations of 26.36 mg/g, 25.20 mg/g, and 24.53 mg/g sample, respectively. Despite containing a relatively low level of vitamin C, grapefruit peels demonstrated the highest antioxidant capacity (48.142 µmol Trolox/g peel sample), followed by orange, lemon, tangerine, and lime. Based on our results, if we were able to repurpose fruit peels and utilize them as a nutrient source, each U.S. individual would be able to meet the daily amount of the recommended vitamin C with 2-3 teaspoons of citrus peels reducing 4.8 pounds of the carbon dioxide (CO_2) equivalent annually at the same time.

INTRODUCTION

The food shortage and undernourishment of approximately 820 million people in the world has long been a global concern (1). Despite this alarming statistic, more than 30% of the food produced for human consumption, which is equivalent to nearly 1.3 billion tons, worth almost 1.3 trillion US dollars, is wasted each year (2). While most of the food waste happens at the processing stages, in industrialized countries, more than 60% of the food waste is produced at consumer levels (3). A previous report shows that the amount of food waste produced per capita in developed countries is about 15 times more than that in developing countries (4). Minimizing food waste through proper management and consumers' habits has the potential to transform the fate of the food waste toward beneficial applications, and the world hunger map would change significantly. In order for this to happen, consumers in industrialized nations need to be aware that even the small changes in our daily lives will dramatically reduce the unnourished population in the world.

Among the various types of food wastes, fruits and vegetables contribute the greatest amount (40–50% of total food waste). These values are exceptionally higher than those in other food groups, such as meat, fish, and dairy products (1). Most of the fruit and vegetable wastes decompose efficiently, and due to high biodegradable properties, composting them and dumping the wastes in landfill sites have been adopted in many countries (5). The conventional solid waste management, however, does not work efficiently for citrus peel waste due to their antimicrobial characteristics (6). As a result, citrus peel waste requires high-cost disposal management and causes potential environmental pollution. Citrus fruits, which account for about 20% of the overall fruit production in the world, have thick peels resulting in a very high (50–70%, w/w) waste production rate (7). According to Statista data, the total citrus fruit production in 2018 was 152.6 million tons, and about 55% of the productions consumed as fresh fruit generating up to 59 million tons of household waste (7, 8). While citrus peel waste from the industrial process can be utilized for the secondary applications or advanced disposal management, it is not practical to collect household citrus peel waste separately for further treatment. Therefore, the household citrus peel waste, in general, ends up with other home trash in landfill sites and threatens the environment by producing methane gas, which has a 25 times higher capacity as a greenhouse gas than carbon dioxide (9). With the low pH of the citrus fruit peels, discharging the citrus waste in the landfill may acidify the land resulting in the increased risk of toxic metal leachate. Various applications of citrus peel waste have been proposed by numerous groups and utilizing these peels as consumable nutritional resources is a particularly effective method for targeting zero waste discharge, even within individual households. Citrus fruits are a well-known source of vitamin C, which is one of the primary antioxidant sources along with polyphenols (10, 11). Therefore, we hypothesize the citrus peels will contain a significant amount of vitamin C that may be beneficial for intake. In this research, we analyzed the amounts of vitamin C and the total soluble

antioxidants to provide data-based nutritional information of citrus peels, including grapefruit, orange, lemon, lime, and tangerine. Moreover, we examined the relationship between easily soluble vitamin C and the amount of total available antioxidants was studied. Considering the broad interests in human health and well-being, the primary objective of this work is to demonstrate how much an individual can reduce their carbon footprint upon utilizing citrus peel wastes, as well as raising awareness of their nutritional content through vitamin C.

RESULTS

The available amounts of vitamin C and antioxidant capacity from grapefruit, lemon, lime, orange, and tangerine peels were investigated to provide nutritional information. The citrus fruits were obtained from a local market and the peel samples were thoroughly air-dried followed by grinding. Uniform particle size samples were obtained by sieving ground peels to determine soluble amounts of vitamin C and total antioxidants using spectrophotometric assays. The amount of vitamin C present in each sample was determined by measuring the absorbance at 510nm. With various prepared different concentrations of ascorbic acid solutions, the determined reference standard curve regression line is Y = 0.0029 X – 0.0387, where X and Y are absorbance and concentration, respectively (Figure 1).

The experimental data indicate that more vitamin C was extracted within 3 hours from the lemon peel (39.3 ± 0.7 mg/g), followed by tangerine peel (36.6 mg/g ± 0.5 mg/g), which were considerably higher values than those from the grapefruit, lime, and orange peels. There was no significant difference in the amount of extracted vitamin C observed in the grapefruit, lime, and orange peels with the 3-hour extraction average values of 26.3 ± 0.7 mg/g, 23.4 ± 1.4 mg/g, and 24.3 ± 0.2 mg/g, respectively (Figure 2).

Since there is no direct total antioxidant determination method available, in this research, Trolox was adopted as a reference antioxidant. Trolox Equivalent Antioxidant Capacity (TEAC) assay was adopted to determine the amount of total soluble amount of antioxidant from the same citrus fruit peels. The TEAC method uses the percent inhibition concept which quantifies the amount of antioxidant by measuring the degree of absorbance decrease at 735 nm in the presence of ABTS radicals (Table 1). The reference Trolox oxidant capacity slope was determined by plotting percent inhibition as a function of concentration (Figure 3). The TEAC value was calculated by comparing the slope of the sample to that for reference Trolox slope.

Despite the relatively low level of vitamin C, grapefruit peel had the highest amount of the antioxidant, followed by orange, lemon, tangerine, and lime (Figure 4). The data also shows that most of the available antioxidants can be extracted within 20 minutes. Considering the experimental results, it should be noted that the amount of dissolved vitamin C could not be used as an indicator to predict the antioxidant capacity

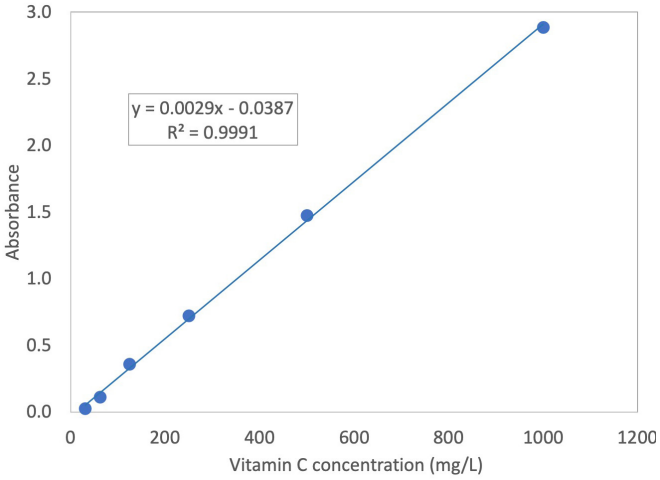

Figure 1: Standard curve used for vitamin C determination. Standard vitamin C solutions at 1,000 mg/L, 500 mg/L, 250 mg/L, 125 mg/L, 62.5 mg/L, and 32.25 mg/L were prepared using a serial dilution method. The experiment was duplicated, and the average value was used.

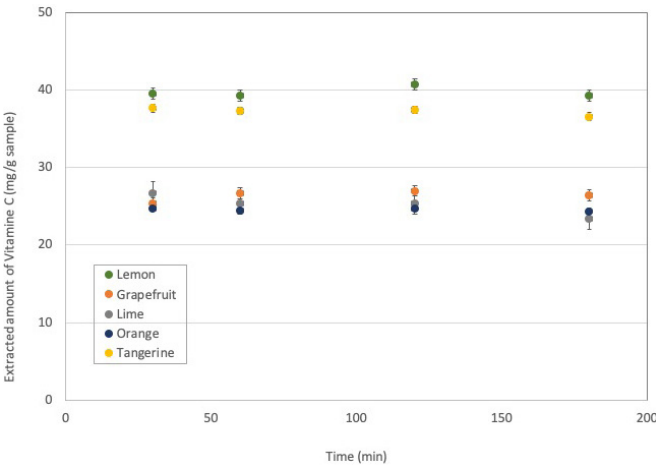

Figure 2: Soluble amount of vitamin C from various citrus fruit peels as a function of reaction period. The experiments were replicated four times and the error bars represent the standard deviations.

from the citrus fruit peels (Figure 5).

This study found that most of the water-extractable antioxidants and vitamin C could be extracted within 30 minutes of the reaction period. The highest amount of antioxidants was extracted from grapefruit peels, and more vitamin C was dissolved from the lemon peels. On the other hand, lime and orange peels showed the least available antioxidant and vitamin C, respectively. Besides, it was failed to observe the proportional relationship between the extracted vitamin C and antioxidant capacity.

DISCUSSION

In order to identify potential secondary applications for the citrus fruit wastes in environmentally-friendly approaches, vitamin C and available soluble antioxidant amounts of five

Trolox (µmol/L)	Absorbance	∆ Absorbance from reference	% Inhibition
250	0.738	0.188	20.3%
125	0.824	0.102	11.0%
62.5	0.877	0.049	5.2%
31.25	0.902	0.024	2.5%
0	0.926	NA	NA

Table 1: An example of % inhibition calculation.

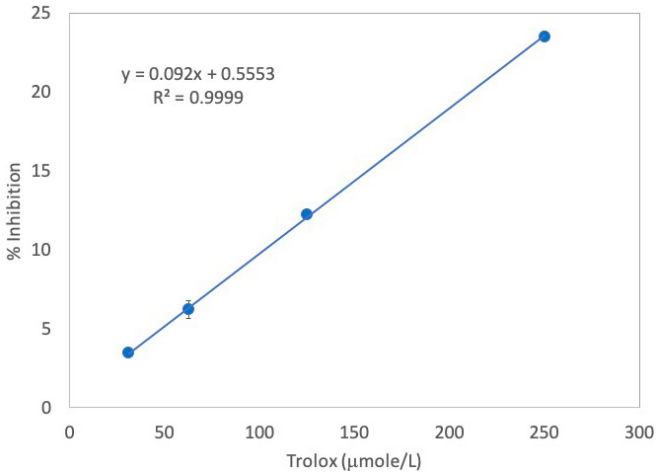

Figure 3. Reference % inhibition graph of standard Trolox solution. The reference Trolox concentrations were 250 µM, 125 µM, 62.5 µM, and 31.3 µM. The experiments were replicated five times and the error bars represent the standard deviations.

common citrus fruit peels — grapefruit, lemon, lime, orange, and tangerine — were analyzed. Reaction periods for this study were limited to up to 3 hours due to experimental and technical difficulties. As the reaction period was extended the solutions became cloudy, resulting in unstable spectroscopic measurements.

The average amounts of vitamin C from the lemon (39.7 ± 0.7 mg/g peel sample) and the tangerine (37.2 ± 0.5 mg/g peel sample) peels were higher than those from the other three peels when measured within a 3-hour reaction period (Figure 2). It should be noted that the extracted vitamin C amounts from grapefruit, lime, and tangerine peels were not significantly different from each other. The highest amount of antioxidants was extracted from the grapefruit peels (48.14 ± 0.05 µmol Trolox / g peel sample) followed by the lemon, orange, lime, and tangerine peels (Figure 4). While additional experiments are required, our studies showed that a higher antioxidant capacity corresponded with increased peel thickness.

Since vitamin C is one of the three major three categories for the natural antioxidants along with minerals and phytochemicals (12), the relationship between total available antioxidants and the extracted amount of vitamin C was observed. However, no proof of the proportional relationship between the amount of vitamin C and the total water-soluble antioxidant capacity was observed in this study (Figure 5).

We observed the five citrus fruit peels adopted in this study showed amounts of both vitamin C and antioxidants. Therefore, those citrus fruit peels could be possible alternative natural resources to provide daily nutritional requirements, thus reducing food wastes and greenhouse gases. The recommended intake of vitamin C for adult females and males, provided by the National Institute of Health (13), are 75 and 100 mg/day, respectively. The required amount can be easily achieved by taking 2–3 teaspoonfuls of dried citrus peels with a reasonable assumption of 2g per one spoonful. When the citrus fruit peels are consumed as nutritional resources, the secondary benefit of carbon footprint decrease, in addition to the household food waste reduction, will be achieved. In 2018, the average citrus fruit consumption per capita in the US was 24 pounds (14). Previous studies reported that the average waste production rate of citrus fruit is 60%, and the amount of carbon footprint produced by citrus fruit waste per capita is the CO_2 equivalent rate of 0.20 kg of CO_2 / kg per orange harvested (7, 15). The information concludes that each person in the US produces 4.8 pounds of carbon dioxide equivalent every year by consuming citrus fruits.

In summary, utilizing citrus fruit peels as an alternative for vitamin C can yield tremendous benefits by lowering total food waste generated; for the standard U.S. household of four, this can be up to 57.6 pounds of citrus-related waste annually. This could help alleviate the costs required to maintain waste transportation and landfill. Other environmental benefits include a reduction in greenhouse gases produced (about 19.2 pounds of carbon dioxide equivalent), which is nearly the same as saving 1 gallon of gasoline (16). Having households adopt these simple and eco-friendly practices is one of the first steps towards paving the way forward into a cleaner and healthier environment.

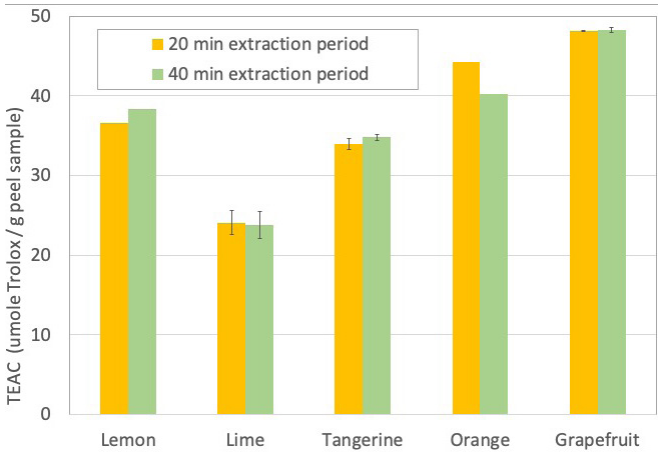

Figure 4. Total water-soluble antioxidant capacity of various citrus fruit peels. Experiments with lime, tangerine, and grapefruit were duplicated and the error bars represent the standard deviation.

Figure 5: The relationship between extracted vitamin C in mg-vitamin C/g-sample and soluble antioxidant amount in μmole-Trolox/g-sample from various citrus fruit peels.

MATERIALS AND METHODS

Typical organic citrus fruit samples including grapefruit, lime, lemon, orange, and tangerine, were purchased from a local market. The peels were collected and air-dried for two weeks to reduce the peel samples' water content. The dried samples were ground using a commercial coffee grinder followed by an additional one-week air dry. For this research, peel particle size was between 0.500 mm and 0.710 mm. To obtain the uniform particle size, the ground sample was sieved using US standard sieve number 25 (0.710 mm), and sieve number 35 (0.500 mm).

0.25 grams of peel sample was mixed with 25mL of water in a 50 mL centrifuge tube for the antioxidant experiment. For the vitamin C experiments, 0.2g of the peel sample was added into a centrifuge tube including 10 mL of water resulting in the mass to water ratios of 20 g/L and 10 g/L for vitamin C and antioxidant experiments, respectively. The tube was fixed to a rotary mixer and run during the experimental period. Approximately 1mL of the solution was taken as a function of time followed by a filtration using a qualitative filter paper (Fisher P5). The filtrate was used for vitamin C and the total antioxidant capacity analysis.

To determine the amount of vitamin C extracted from the samples, a spectrophotometric method proposed by Besada (17) was used. The color developmental 1,10-phenanthroline-ferric ion indicator was prepared in an amber bottle and stored in a refrigerator (4˚C). 0.2 mL of the filtered sample was added to a test tube which included 1mL of the indicator and 0.5 mL of water. The absorbance of the prepared solution was determined at 510 nm after 10 minutes of the reaction period. Fresh 1,000 mg/L L-ascorbic acid stock solution was made and diluted it to prepare various standard solutions to build the standard curve.

The Trolox Equivalent Antioxidant Capacity (TEAC) assay (18) was used in this research to determine the total amount of water-soluble antioxidant capacity. The initial 2,2-azinobis(3-ethylbenzothiazoline-6-sulfonic acid) radical (ABTS•) solution was prepared by mixing same volume of 14 mM ABTS solution and 4.9 mM potassium persulfate solution. The freshly-prepared ABTS• solution was stored in an amber bottle and aged for at least 10 hours before adopting for the experiments. The aged ABTS• solution was diluted to adjust the initial absorbance at 735 nm between 0.8 and 1.2. To determine the change of absorbance (Δ absorbance), 0.1 mL of filtrate was mixed with 2.9 mL of the diluted ABTS• solution and the absorbance was determined after 6 minutes of reaction period. The disappearance of the ABTS• can be expressed as % inhibition, as shown below.

$$\%\ inhibition = \left(\frac{\Delta\ Absorbance}{Absorbance\ of\ reference}\right) \times 100$$
$$= \left(\frac{Absorbance\ of\ reference - Absorbance\ of\ test}{Absorbance\ of\ reference}\right) \times 100$$

With the collected data, % inhibitions at various concentrations were calculated (Table 1) and a plot of % inhibition (Y-axis) vs. sample concentration (X-axis) was built to determine the slope of the trendline (Figure 3). The antioxidant capacity was expressed as TEAC values which were determined by comparing the slopes of the sample and Trolox % inhibition graphs. The unit for the TEAC values for this research can be expressed as:

$$TEAC\ Values\ unit = \frac{unit\ for\ the\ slope\ of\ Sample}{unit\ for\ the\ slope\ of\ Trolox} = \frac{\left[\frac{\%\ inhibition}{g\ of\ Sample\ /\ L}\right]}{\left[\frac{\%\ inhibtion}{\mu mole\ of\ Trolox\ /\ L}\right]}$$
$$= \left[\frac{\mu mole\ of\ Trolox}{g\ of\ sample}\right]$$

REFERENCES

1. "Worldwide Food Waste." ThinkEatSave, http://www.unenvironment.org/thinkeatsave/get-informed/worldwide-food-waste. Accessed 13 March 2020.
2. "Food Loss and Food Waste." Food and Agriculture Organization of the United Nations, http://www.fao.org/food-loss-and-food-waste/en/. Accessed 22 May 2020.
3. "Global Food Waste and Its Environmental Impact | Green Living." RESET.to, https://en.reset.org/knowledge/global-food-waste-and-its-environmental-impact-09122018. Accessed 22 May 2020.
4. https://twosides.info/includes/files/upload/files/UK/Myths_and_Facts_2016_Sources/18-19/Key_facts_on_food_loss_and_waste_you_should_know-FAO_2016.pdf. Accessed 22 May 2020.
5. Arvanitoyannis, Ioannis S., and Theodoros H. Varzakas. "Vegetable Waste Treatment: Comparison and Critical Presentation of Methodologies." Critical Reviews in Food Science and Nutrition, vol. 48, no. 3, Mar. 2008, pp. 205–247.
6. Mehmood, Basharat, et al. "Short Communication: In Vitro Assessment of Antioxidant, Antibacterial and Phytochemical Analysis of Peel of Citrus Sinensis." Pakistan Journal of Pharmaceutical Sciences, vol. 28,

no. 1, Jan. 2015, pp. 231–239.
7. Zema, Demetrio Antonio, et al. "Valorisation of Citrus Processing Waste: A Review." Waste Management, vol. 80, 2018, pp. 252–273., doi:10.1016/j.wasman.2018.09.024.
8. "Fruit: World Production by Type 2018." Statista, 11 Feb. 2020, https://www.statista.com/statistics/264001/worldwide-production-of-fruit-by-variety/. Accessed 22 May 2020.
9. The Zero-Waste Chef. "10 Ideas to Rescue Citrus Peels - Zero-Waste Chef." Zero-Waste Chef, 28 Jan. 2016, https://zerowastechef.com/2016/01/28/10-ideas-to-rescue-citrus-peels/.
10. "Nutritional and Health Benefits of Citrus fruits." Food, Nutrition and Agriculture 24 Nutritional and Health Benefits of Citrus fruits, www.fao.org/3/x2650t03.htm.
11. Du, Guorong, et al. "Antioxidant Capacity and the Relationship with Polyphenol and Vitamin C in Actinidia Fruits." Food Chemistry, vol. 113, no. 2, 2009, pp. 557–562., doi:10.1016/j.foodchem.2008.08.025.
12. Aziz, Manal Azat, et al. "Antioxidant Categories and Mode of Action." IntechOpen,IntechOpen, 6 Nov. https://www.intechopen.com/books/antioxidants/antioxidant-categories-and-mode-of-action.
13. Office of Dietary Supplements - Vitamin C. https://ods.od.nih.gov/factsheets/VitaminC-Consumer/. Accessed 22 May 2020.
14. "U.S. Fresh Citrus Fruit Consumption per Capita, 2018 | Statista." Statista, https://www.statista.com/statistics/257189/per-capita-consumption-of-fresh-citrus-fruit-in-the-us/. Accessed 22 May 2020.
15. Mordini, Manuela, et al. Carbon & Water Footprint of Oranges and Strawberries: a literature review. 2009, Retrieved from https://saiplatform.org/uploads/Library/WG%20Fruit%20-%20ART%20Final%20Report.pdf
16. EPA, U. S., and OAR. Greenhouse Gas Emissions from a Typical Passenger Vehicle. Jan. 2016, https://www.epa.gov/greenvehicles/greenhouse-gas-emissions-typical-passenger-vehicle.
17. Besada, Amir "A Facile and Sensitive Spectrophotometric Determination of Ascorbic Acid." Talanta, vol. 34, no. 8, Aug. 1987, pp. 731–732., doi:10.1016/0039-9140(87)80229-1.
18. Re, Roberta, et al. "Antioxidant Activity Applying an Improved ABTS Radical Cation Decolorization Assay." Free Radical Biology & Medicine, vol. 26, no. 9-10, 1999, pp. 1231–1237., doi:10.1016/s0891-5849(98)00315-3.

Article submitted: May 22, 2020
Article accepted: September 3, 2020
Article published: December 20, 2020

JOURNAL OF
EMERGING INVESTIGATORS

Article

The effects of stress on the bacterial community associated with the sea anemone *Diadumene lineata*

Rebekah Cahill[1], Stacy A. Krueger-Hadfield[2], Will H. Ryan[2]
[1]Jefferson County International Baccalaureate School, Birmingham, Alabama
[2]Department of Biology, University of Alabama at Birmingham, Birmingham, Alabama

SUMMARY

The bacteria found on and inside animals can play important roles in the health and function of the host individual. However, the factors that control which species colonize a host are complex. In this study, we investigated the effect of environmental stress on the composition of the bacterial community associated with the sea anemone *Diadumene lineata*. We grew anemones in both normal and stressful conditions and then cultured bacteria from each individual anemone and its mucus separately on R-2A agar. We found that anemones grown in normal conditions had microbiomes that were distinct from the surrounding seawater, but that the community of bacteria found on stressed anemones was more similar to that found in the seawater. Interestingly, *D. lineata* produces a thick mucous covering when stressed, which may play a role in controlling the microbial community during stressful conditions. We found that the mucus had a distinct community of bacteria with very few taxa present. These results were consistent with findings from corals and other sea anemones that suggested that stressed hosts are less able to control the microbes that colonize their surfaces and that mucus may have antimicrobial properties that influence microbial community assembly. The findings of this study support the use of sea anemones for further investigation of the complex interaction among hosts, microbes, and their environments. Our study also highlights the need to investigate sea anemone mucus further, both as an ecologically important substance and as a potential source for novel pharmaceutical compounds.

INTRODUCTION

As the tools available to study microbes have improved, we have become better able to appreciate the role that microbes play in the health of organisms and ecosystems. It is now understood that bacteria and other microscopic organisms can form close associations with plants and animals and contribute to their health and function (1). In addition, the microbes associated with common plants and animals, generally called the microbiome, can be an important source of new chemicals that may have properties useful to humans (2). Thus, characterizing the microbes associated with plants and animals is an important goal for both basic and applied sciences.

The relationship between a macroscopic host organism and its microbiome is complex. The environment created by the host may control what species of bacteria can thrive nearby. The bacteria can also have a positive or negative effect on the host (e.g., gut microbes aiding in digestion or bacteria causing illness). The bacteria that are capable of colonizing a host depends on the species available in the local environment, and how those species interact with the host organisms (3). Emerging evidence suggests that organisms tend to show a consistent and intimate relationship with a small core set of bacterial types among the hundreds or thousands of species that can be found occasionally on or inside an individual (4). Different parts of the same organism can maintain different microbiomes. For example, the microbiomes of coral tissue and the layer of mucus covering the tissue have been shown to be distinct (4). The composition of both the core and ephemeral bacterial communities that thrive on or near a host can also depend on the environment in which the host is found, as each bacterial species has its own set of requirements for life that must be met before it can grow.

In this study, we measured the influence of the external environment on the community composition of microbial species associated with the sea anemone *Diadumene lineata*. We chose this species because it can live in a wide variety of environments, which may help us understand the role the external environment has in shaping the microbial community. The anemone *D. lineata* is thought to be native to the Northwest Pacific Ocean, including the coasts of Japan and China. However, the species has successfully invaded coastal waters across a variety of regions around the world including the Pacific, Atlantic, and Gulf Coasts of the United States (5). Its documented ability to tolerate weeks of exposure to temperatures between 3° and 29°C and salinities ranging from near freshwater to a high salinity of at least 34 parts per thousand have likely contributed to its success as a widespread non-native species (6,7). *D. lineata*'s status as an invasive species and its broad environmental tolerance make it an interesting subject for studying how the interaction of the environment, the locally available pool of species, and the anemone's physiology shapes the diversity of its microbiome.

Cnidarians, like corals and sea anemones, also have interesting microbiomes because of the properties of the mucus they produce to protect their tissues. The chemical properties of cnidarian mucus appear to influence the composition of bacteria that can colonize these species (4).

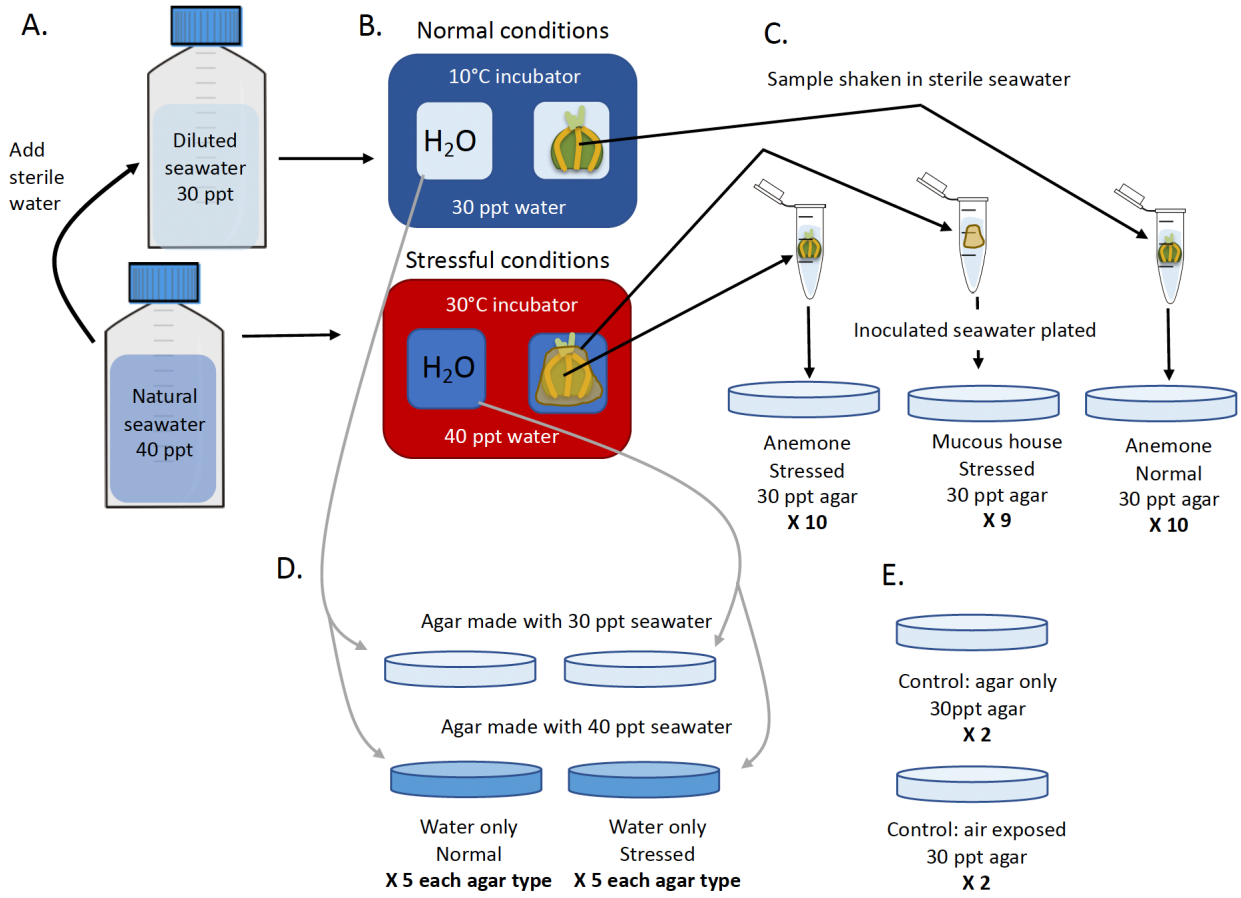

Figure 1. Experimental design. (**A**) Natural, unsterilized seawater was diluted with sterile DI water. (**B**) High and low salinity water were then distributed to plates and placed in to a high and low temperature incubator respectively. The treatment combination of high salinity and high temperature was called "stressful," whereas the low salinity, low temperature treatment was called "normal." (**C**) After two weeks, anemones were removed from each well and placed in a tube of sterilized seawater. Where mucous houses were produced (stressful treatment), the mucous house was placed in a separate tube of sterile seawater. The tube was shaken vigorously to inoculate the seawater with bacteria from the anemone and plated on normal agar. (**D**) An equal amount of water was taken from each of the water-only wells in each treatment and plated individually on agar plates of either normal or high salinity. (**E**) Two sets of control plates were established to ensure that all bacteria observed came from the seawater or anemones. Two normal salinity agar plates were kept sealed to check for contamination in the agar. Two normal salinity agar plates were exposed to the air for a short period to check for contamination from the air.

For example, mucus from the anemone *Actinia equina* has been shown to have hemolytic, cytotoxic, and antibacterial activity in laboratory studies (8). Of interest to our study, *D. lineata*, is known to respond to environmental extremes by secreting a thick mucus coating and remaining sealed inside the structure (hereafter called a "mucous house") until conditions improve (9). It is unknown what role the production of this mucous house has in protecting the sea anemone from harm, but we predicted that the production of such a structure may help protect the sea anemone from harmful changes in the anemone's microbiome, as the host tissue becomes more susceptible to infection under stress.

To better understand the nature of the relationship among the host anemone, mucus, and microbiome, we tested three hypotheses about the factors influencing the microbial diversity associated with this sea anemone. First, the microbiome of the anemone will differ from the seawater surrounding it, second, the community of bacteria associated with the sea anemone will differ under stressful versus normal culture conditions, and third, the bacteria associated with the mucous house will differ from both the seawater and the live anemone tissue.

RESULTS

To understand the role of the external environment on the community of bacteria that are associated with the sea anemone *D. lineata*, we exposed replicate sea anemones and seawater samples to either normal or stressful culture conditions in the laboratory (**Figure 1**). After seven days in culture, we characterized differences in the microbial community between treatment by growing bacteria associated with the seawater, anemones, and mucus produced by the anemone on agar.

Because our methods did not allow us to diagnose the specific bacterial species in the study, we referred to the visually unique colony types as Operational Taxonomic Units (OTUs). Each OTU was assigned an arbitrary letter (A through O), as we were unable to identify bacterial species in

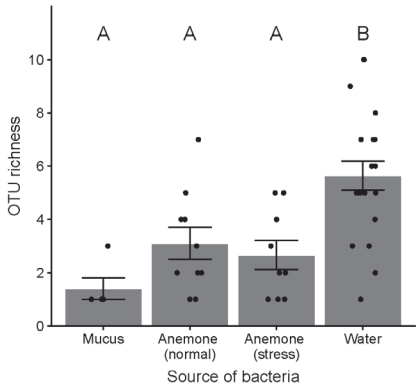

Figure 2. Mean ± standard error OTU richness by source of bacteria. A one-way ANOVA showed that there was a significant difference between groups ($F_{3,40}$ = 8.68, p = 0.001). Tukey HSD post-hoc analysis showed that the water samples had significantly more OTUs on average than the mucus or either type of anemone samples. Different letters above bars denote groups that have significantly different mean OTU richness (pairwise p value between groups unalike letters is less than 0.05). Points are jittered slightly to reduce overplotting.

this study. On average, 3.9 ± 0.39 SE OTUs were found per plate.

To distinguish changes due to the interaction of the anemone and the environment from changes in the bacterial community available in the water due to the experimental conditions, we also characterized the bacterial community in replicate samples of seawater exposed to each treatment condition described above in the absence of sea anemones. We found no effect of either culture environment or agar type on the OTU richness in the water-only samples (Condition: $F_{1,16}$ = 0.01, p = 0.927; Agar: $F_{1,16}$ = 1.96, p = 0.181; Condition by Agar interaction: $F_{1,16}$ = 1.96, p = 0.181), thus samples were pooled to measure the difference in richness by bacterial source.

There was a significant difference in richness among bacterial source (p < 0.001). Post-hoc analysis with Tukey's Honestly Significant Differences test (HSD) showed that water-only samples had significantly more species per sample (5.65 ± 0.55 SE) than the stressed anemones (2.67 ± 0.55 SE), normal anemones (3.10 ± 0.60 SE), or mucous samples (1.4 ± 0.40 SE), which were all similar to each other (**Figure 2**). No bacterial colonies were found growing on either set of controls during the experiment (n = 2 for each control type).

To characterize differences in bacterial community composition among treatments, we used non-metric multidimensional scaling (NMDS), a multivariate ordination technique, to plot the matrix of OTUs absent or present (coded as a 0 or 1) in each petri dish in two-dimensional space. This technique allowed us to quantify and visualize the relative similarity of the bacterial community among dishes, taking into consideration both the frequency and identity of the OTUs present (**Figure 3**). We used the resulting NMDS values assigned to each replicate to test the influence of culture conditions and agar salinity on the bacterial community from the water-only samples with a two-way ANOVA. There

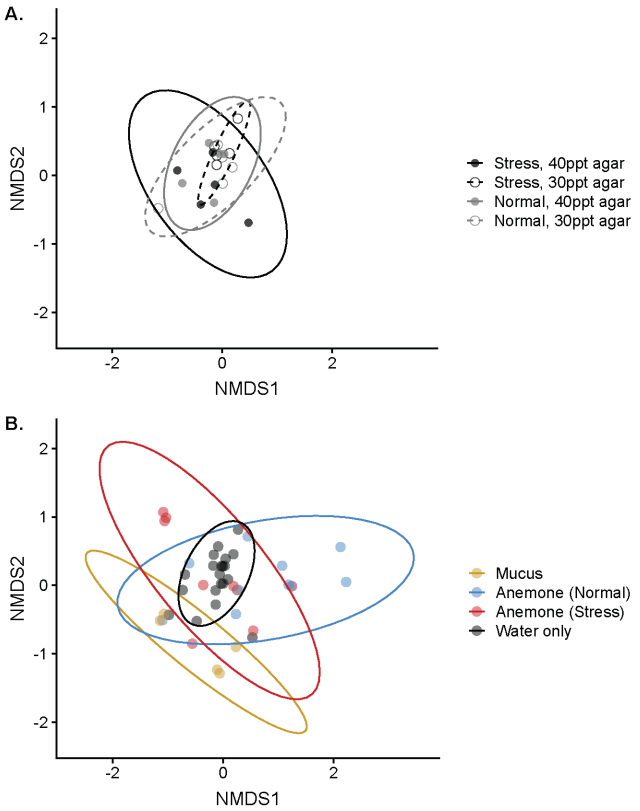

Figure 3. Non-metric multidimensional scaling plots of the bacterial community cultured on agar plates inoculated with fluid from experimental groups. Each point reflects the composition of the community on a single agar plate. Distance between points is correlated with dissimilarity among communities. (**A**) Variation among seawater samples that differed in culture conditions (point color) and the salinity of the agar (open vs. closed points) on which bacteria were plated. There was no significant difference in the average value of NMDS1 or NMDS2 due to either culture condition ($F_{1,16}$ = 0.30, 0.02; p = 0.595, 0.883), agar salinity ($F_{1,16}$ = 0.53, 1.91; p = 0.476, 0.186), or their interaction ($F_{1,16}$ = 0.60, 2.46; p = 0.449, 0.136). (**B**) Variation among communities by source (colors), including anemone-associated bacterial communities when anemones were grown under stressful or normal culture conditions, the mucus collected from stressed anemones, and water (samples combined across treatments). Groups differed significantly below the Bonferroni adjusted alpha (i.e., p < 0.025) along both NMDS1 ($F_{3,40}$ = 4.24, p = 0.011) and NMDS2 ($F_{3,40}$ = 1.31, p = 0.002). Tukey's HSD posthoc analysis showed that normal condition anemones differed significantly from all other groups along NMDS1, and mucus differed significantly from all other groups along NMDS2. The bacterial community associated with stressed anemones did not differ significantly from water only samples (p >> 0.025). Ellipses show 95% confidence intervals for each group.

were no significant differences among water samples along either NMDS graph axis (**Figure 3A**). Thus, we pooled all of the water samples for the next analysis comparing each set of NMDS values among bacterial source (mucus, normal anemones, stress anemones, and water) with a one-way ANOVA for each axis. Differences among groups were significant along both axes below the Bonferroni adjusted alpha of 0.025 (**Figure 3B**). Tukey's HSD post-hoc tests indicated that the microbiome of anemones grown in normal conditions differed significantly from the water-only samples,

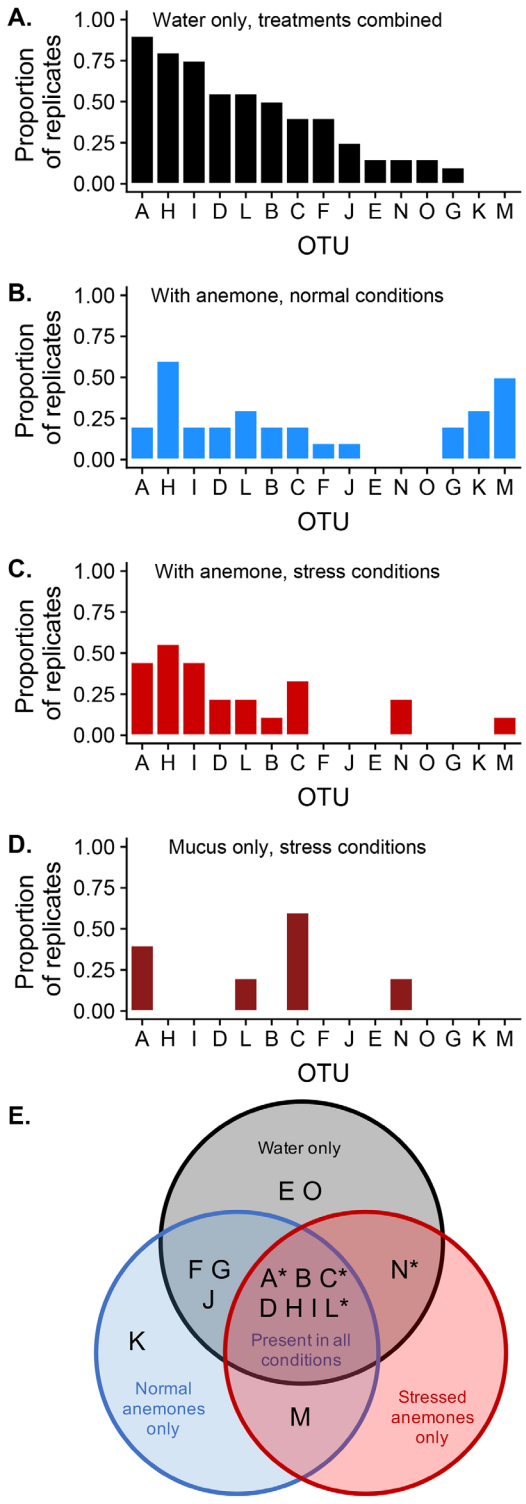

Figure 4. Frequency of occurrence of each OTU on culture plates inoculated with fluid from replicates of each condition. Bar order reflects rank order of commonness to rareness in water-only samples. Bar height indicates the proportion of replicates in which each OTU was found for each condition (panels **A-D**). Panels show the bacterial community composition in (**A**) all water only samples, combined across treatment, (**B**) anemone-associated samples grown in normal conditions, (**C**) anemone-associated samples grown in stressful conditions, and (**D**) excess mucus shed by anemones grown in stressful conditions. (**E**) Venn diagram of occurrence of putative OTUs in cultures grown from each treatment. Letters in overlapping regions indicate OTUs that were found at least once in petri dishes inoculated with fluid from conditions indicated in each circle. Letters in non-overlapping regions indicate OTUs that were unique to a single condition. Asterisks indicate OTUs that were present in mucous samples.

stressed anemones, and mucus (**Figure 3B**). Mucous samples differed significantly from all other treatments along NMDS2. The bacterial community from stressed anemones, however, was statistically similar to that found in the water samples (**Figure 3B**).

The patterns observed in the NMDS were also reflected in the distribution of common versus rare OTUs among treatments (**Figure 4**). The most common OTUs found across water-only plates (A, H, and I; **Figure 4A**) were also the most commonly found among replicates of the stressed anemones (**Figure 4C**). Many of the common OTUs found in water were sparsely found in normal anemone samples, except for H, which was commonly found with anemones also (**Figure 4B**). Likewise, two of the most common OTUs found with normal anemones, K and M, were only identified from anemone samples. OTU richness was low among the mucous samples but seemed to share the most similarities with the stressed anemones (**Figure 4D**). This includes higher representation of taxa A and C relative to normal anemones, as well as N, which was not found in normal anemones at all. The occurrence patterns within each treatment are summarized in a Venn diagram (**Figure 4E**) to demonstrate taxa which may contribute to distinct communities. Of particular interest are the two OTUs which only occurred with anemones (K and M), as well as the two OTUs which only occurred in water (E and O).

DISCUSSION

Emerging patterns from studies of sea anemones and corals suggest that the external environment plays a key role in shaping the richness and composition of associated microbial communities (4). The environment can influence the microbial community directly, by filtering the local species pool, and indirectly, by changing the physiology of the host species. Although the rudimentary techniques by which we have quantified bacterial diversity render our findings preliminary, our results are largely consistent with patterns observed by others.

We found that the composition of the bacterial community was different between unstressed anemones and the surrounding seawater, indicating that the host species can influence the bacterial community that assembles on its surface. Our detection of two OTUs associated with anemones that were not detected in the seawater samples suggested that the host can also cultivate taxa that are either rare or absent in the surrounding environment. Interestingly, when the anemones are stressed – as evidenced by the production of a mucous house – their microbiome becomes more similar to that of the surrounding seawater. This is consistent with

emerging evidence from corals that suggests that stressed hosts have a reduced ability to regulate their microbiomes (10). We did not find an increase in OTU richness or variance among replicate communities in stressed versus normal anemones, as has been reported for the sea anemone *Exaptasia pallida* (11). However, future studies using more sophisticated methods of species identification may uncover cryptic diversity within morphologically similar taxa. Finally, we found that the mucus produced by stressed anemones had a pattern of microbes different from either the seawater or the host anemones. Only four of the fifteen OTUs detected were found within the mucus. The low richness and unique composition of these communities supports the idea that the mucus may have some antimicrobial or otherwise selective properties, consistent with recent findings in corals (4) and other sea anemones (8). Future studies to examine the biochemical properties of anemone mucus and associated bacteria will likely provide fascinating results with insights for both pharmaceutical development and ecological understanding. The patterns we observe suggest that *D. lineata* shares many of the interesting features that have made corals and other sea anemones excellent models for studying the interaction of hosts and microbial communities with the external environment.

There are some important limitations to our findings. Primarily, our use of morphological features to determine bacterial OTUs meant that we likely underestimated the diversity present. In some cases, we may have also overestimated taxonomic diversity by misclassifying colonies of the same type as distinct due to plastic variation in colony morphology. Additionally, our techniques only revealed to us the subset of the bacterial community that is able to be cultured on agar plates. Future studies combining plating techniques with molecular analyses will allow us to estimate what fraction of the available bacteria were culturable and can help us better characterize the diversity present in these communities. However, the absence of bacteria in our negative controls suggests that our aseptic technique was successful. This means that the preserved samples from this and future studies have the potential to provide great insight when analyzed with genetic sequencing.

Understanding the mechanisms of microbial community assembly and succession on and within host species remains an area of active scientific inquiry. One area relevant to the biology of our sea anemone, *D. lineata*, is the role of microbes during species invasion. Our results show that *D. lineata* can both take on microbes from the surrounding seawater and modify the community present on tissues relative to the environment. Both of these qualities may be essential for a species that has been transferred to a new coastline. Continuing studies on the microbial communities of this species across its native and invaded range will allow us to learn much more about the interaction among hosts, microbes, and the external environment.

METHODS

Optimization of stressful versus normal culture conditions

Prior to the current study, a preliminary experiment was carried out to find an appropriate set of conditions to label as "stressful" to the anemones. Anemones were exposed to one of a factorial combination of cool and warm temperatures (10° versus 30°C) and water salinity levels (20, 30, 40 ppt) for two weeks. All anemones survived in all combinations, but the high salinity (40 ppt) and high temperature treatment (30°C) stimulated the most reliable production of mucous houses, thus we deemed these conditions stressful. Anemones grown at 10°C and an ordinary seawater salinity (30 ppt) behaved normally and showed no signs of stress during the experiment; thus, these conditions were deemed normal.

Sample collection

In June 2018, many *D. lineata* individuals were collected from a floating dock at King's Creek Marina in Cape Charles, Virginia. Anemones were transferred on ice in vials of natural seawater from the same site to the University of Alabama at Birmingham. Anemones were moved into vials of sterilized natural seawater collected from the same site and kept at 10°C until the start of the experiment. Under these conditions anemones can survive for long periods without food, which allowed us to avoid the potentially confounding effects of adding microbes associated with food.

Environmental influence on anemone microbiome

We designed an experiment to characterize the bacterial community associated with sea anemones grown in stressful and normal conditions (**Figure 1**). Natural, unsterilized seawater collected from the VIMS Eastern Shore Laboratory in Wachapreague, Virginia was used as a culture medium. Due to natural evaporation, the initial salinity was 40 ppt, which was used for the stress treatment. An aliquot of 40 ppt seawater was diluted with sterile deionized water to 30 ppt for the normal treatment (**Figure 1A**). Salinity was confirmed with a refractometer using aseptic technique at each step to avoid introducing new bacteria to either solution. For each condition, 3 mL of seawater was aliquoted into each of 10 wells of a 12-well tissue culture plate (Thermo Fisher Scientific, Waltham, Massachusetts). Twenty similarly sized *D. lineata* individuals were chosen from among the field-collected samples. The underlying genetic relatedness of the individuals was not known. One anemone was randomly assigned to each water-filled well. Plates were then placed in growth chambers (Percival Scientific, Perry, Iowa) with a 12:12 hour light cycle at either 30°C (stressed) or 10°C (normal) (**Figure 1B**). After seven days, each anemone was carefully transferred into 1.5 mL of sterilized seawater in a microcentrifuge tube using sterilized forceps. Nine out of ten stressed anemones produced mucous houses, while normal condition anemones did not. Each mucous house was carefully separated from its anemone and transferred to a separate tube of sterile seawater. All tubes were vortexed

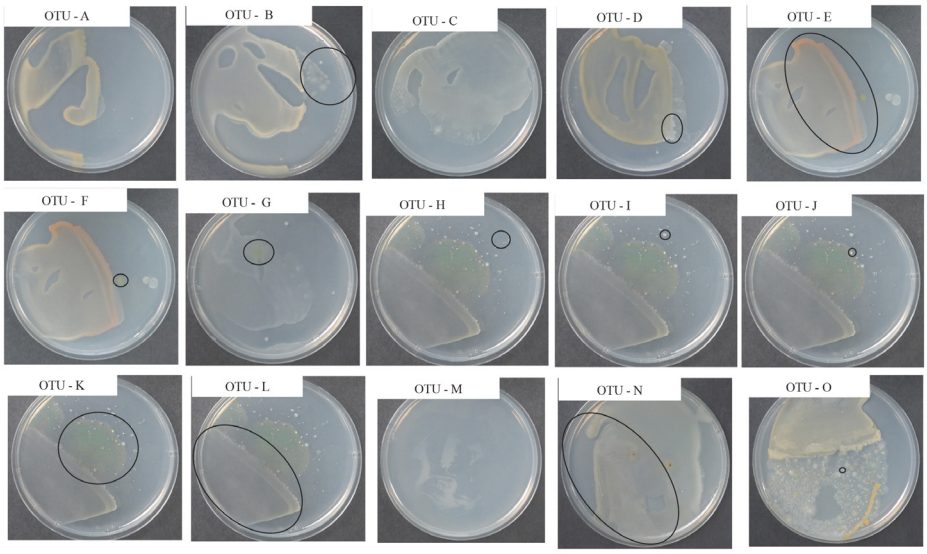

Figure 5. OTU identification guide. These images, along with a written description, were used as a reference to standardize the identification of OTUs across experimental images.

vigorously for 30 seconds to transfer bacteria to the sterile seawater. 1 mL of water from each tube was then spread onto an independent agar-filled petri dish (R-2A media prepared with 30 ppt seawater; Sigma-Aldrich, St. Louis, Missouri) (n = 10, 10, 9 for stressed anemones, normal anemones, and mucous houses, respectively; **Figure 1C**).

Environmental influence on seawater microbiome

Five wells of natural seawater for each culture condition were prepared as above and incubated in the same growth chambers simultaneously with the anemone inhabited plates (**Figure 1B**). After seven days, the water samples were plated. To ensure that the salinity of the agar plate did not inadvertently act as a filter on the bacteria that we observed, we plated one milliliter of water from each condition on R-2A media prepared with both 30ppt seawater and 40 ppt seawater (n = 5 for each combination of treatment by agar type; **Figure 1D**). We compared the influence of culture condition and agar on the OTU richness in water-only samples with a two-way ANOVA.

Controlling for contamination

To ensure that our results were not skewed by bacteria from any source except the samples, we prepared two replicates each of two controls. The first tested for contamination in the agar and consisted of two agar plates which remained closed after pouring and for the duration of the experiment. The second tested for contamination from the air during plate handling and consisted of two agar plates which were left uncovered on the lab bench for 30 seconds, which was much longer than any experimental plate was open during inoculation.

Growing and identifying bacterial colonies

All inoculated agar plates and controls were incubated at 25°C for seven days before photographing the bacterial growth. The images were used, without knowledge of which plate belonged to which treatment, to develop an identification guide of morphologically unique colony types, which were treated as OTUs. Fifteen such OTUs were identified, each assigned a letter A through O (**Figure 5**).

Using the OTU identification guide (**Figure 5**), the photograph of each plate was scored for the presence or absence of each putative taxa. In some cases, colonies had grown together on the plate which prevented us from quantifying the number of colony-forming units as a measure of abundance in each sample. Thus, only the presence and absence patterns were analyzed for this study.

Data analysis

Similarities among the bacterial communities cultured from each treatment were compared in four different ways. First, we compared the OTU richness based on bacterial source (i.e., water, stressed anemone, normal anemone, or mucus) with a one-way ANOVA.

Next, we used NMDS implemented in the VEGAN package of the statistical software R (v 3.5.1) to compare the similarity of the bacterial community among treatment conditions (12, 13). NMDS is a commonly used multivariate ordination technique that allowed us to reduce the complexity of the data for subsequent analysis. This technique was implemented with the metaMDS function in R. Briefly, the major axes of variation are found by first summing the number of differences in the presence or absence of OTUs between each possible pair of samples. Then, the rank order of differences between pairs of samples was used to position each sample on a set of X and Y axes such that more similar samples are plotted nearer to each other. This technique reduces the OTU data for each dish into a single point described by an X and Y value called NMDS1 and NMDS2. These values do not have a biological meaning, per se, but reflect the relative similarity or difference of the species composition between samples.

We used the NMDS values as the response variables in ANOVAs to test two null hypotheses. First, there was no

difference in bacterial community composition among water treatments due to culture condition or agar type, and second, there was no difference in bacterial community composition among the experimental conditions, i.e., found in mucus, with normal anemones, with stressed anemones, and in water samples (pooled across treatments). Because we used some of the same data for both null hypothesis tests, we used a Bonferroni correction to set a more conservative threshold for rejecting the null hypotheses (alpha = 0.025 instead of the conventional 0.05) to reduce the risk of type I error. Where a significant difference was found among groups using ANOVA, we used a Tukey's HSD post-hoc test to determine the pairwise pattern of significant differences among groups.

We then examined the distribution of OTUs within and among treatments by calculating and plotting the proportion of replicates in each condition where each OTU was present. This allowed us to visually compare patterns of commonness and rareness of OTUs among treatments.

Finally, we examined patterns of unique and non-unique OTU occurrences among treatments with a Venn diagram.

ACKNOWLEDGEMENTS

We thank Edward Smith from the Virginia Institute of Marine Science Eastern Shore Lab for field help and logistics, the staff at King's Creek Marina for access to their docks, and Dr. Jeff Morris at UAB for help with bacterial culturing. This project was funded in part by start-up funds from the University of Alabama at Birmingham to Dr. Stacy Krueger-Hadfield and the Office of Postdoctoral Education Career Enhancement award to Dr. Will Ryan. We would also like to thank the four anonymous reviewers whose comments improved this manuscript.

Received: May 19, 2020
Accepted: December 29, 2020
Published: February 15, 2021

REFERENCES

1. Dale, Colin, and Nancy A. Moran. "Molecular interactions between bacterial symbionts and their hosts." *Cell*, vol. 126, no. 3, 2006, pp. 453-465., doi:10.1016/j.cell.2006.07.014.
2. Debbab, Abdessamad, *et al*. "Bioactive compounds from marine bacteria and fungi." *Microbial Biotechnology*, vol. 3, no. 5, 2010, pp. 544-563., doi: 10.1111/j.1751-7915.2010.00179.x.
3. Cuellar-Gempeler, Catalina and Matthew A. Leibold. "Multiple colonist pools shape fiddler crab-associated bacterial communities." *ISME*, vol. 12, 2018, pp. 825-837., doi: 10.1038/s41396-017-0014-8.
4. Hernandez-Agreda, Alejandra, *et al*. "Defining the Core Microbiome in Corals' Microbial Soup." *Trends in Microbiology*, vol. 25, no. 2, Elsevier Ltd, 1 2017, pp. 125-140., doi: 10.1016/j.tim.2016.11.003
5. Ryan, Will H., *et al*. "Environmental Regulation of Individual Body Size Contributes to Geographic Variation in Clonal Life Cycle Expression." *Marine Biology*, 2019, Article 157., doi: 10.1007/s00227-019-3608-z.
6. Ryan, Will H. "Temperature-Dependent Growth and Fission Rate Plasticity Drive Seasonal and Geographic Changes in Body Size in a Clonal Sea Anemone." *The American Naturalist*, vol. 191, no. 2, 2018, pp. 210-219., doi: 10.1086/695496.
7. Podbielski, Imke, *et al*. "Using the Critical Salinity (S Crit) Concept to Predict Invasion Potential of the Anemone *Diadumene lineata* in the Baltic Sea." *Mar Biol*, vol. 3, 2016, p. 227., doi: 10.1007/s00227-016-2989-5.
8. Stabili, Loredana., *et al*. "The Mucus of Actinia equina (Anthozoa, Cnidaria): An Unexplored Resource for Potential Applicative Purposes." *Marine Drugs*, vol. 13 no. 8, 2015, pp. 5276-5296, doi: 10.3390/md13085276.
9. Miyawaki, Mitsuharu. "Notes on the Effect of Low Salinity on an Actinian *Diadumene luciae*." *Journal of The Faculty of Science*, Hokkaido University, Section: 6, Zoology, vol. 10, 1951, pp. 123-126.
10. McDevitt-Irwin, Jamie M., *et al*. "Responses of Coral-Associated Bacterial Communities to Local and Global Stressors." *Frontiers in Marine Science*, vol. 4, 2017, Article 262., doi: 10.3389/fmars.2017.00262.
11. Ahmed, Hanin Ibrahim, *et al*. "Long-Term Temperature Stress in the Coral Model Aiptasia Supports the 'Anna Karenina Principle' for Bacterial Microbiomes." *Frontiers in Microbiology*, vol. 10, 2019, Article 975., doi: 10.3389/fmicb.2019.00975.
12. Oksanen, Jari, *et al*. "vegan: Community Ecology Package". R package version 2.5-4. 2019, www.CRAN.R-project.org/package=vegan.
13. R Core Team. "R: A language and environment for statistical computing". R Foundation for Statistical Computing, 2018, Vienna, Austria. www.R-project.org.

JOURNAL OF
EMERGING INVESTIGATORS

Article

How has California's Shelter-in-Place Order due to COVID-19 and the Resulting Reduction in Human Activity Affected Air and Water Quality?

Olivia Everitt[1], Ashley M. Pierce[2]
[1]Urban School of San Francisco, San Francisco, CA
[2]Unaffiliated Scientist

SUMMARY

As the world continues to battle the novel coronavirus or COVID-19, many states in the USA have restricted outdoor human activity, intending to reduce the number of viral infections. In turn, the number of cars on the streets and factories in operation has decreased. This unique time for the world has created an opportunity to study the impacts of reduced human activity. We collected water and air quality data through field data collection and remote data sites to test how the change in human activity affected the concentration of pollutants in water and air. Throughout California, we studied three test sites in June and July from 2015 to 2020 to compare the collected field or monitored water and air quality data over the past five years. We hypothesized that with the reduction of human activity, and therefore car emissions, the air and water pollutants in all three test locations would decrease for June/July 2020 compared to the last five years. In our study, the air quality improved from 2015 to 2020 in terms of the oxides of nitrogen (NO_x) and ozone (O_3), especially at Lake Tahoe's Placer County. However, the water quality remained relatively constant for the test sites over the course of the study, while it significantly improved Sonoma County's Russian River. Overall, the air pollution in California for June and July somewhat decreased from 2015 to 2020, while the water quality remained fairly constant in June and July during California's shelter-in-place order.

INTRODUCTION

The outbreak of severe acute respiratory syndrome COVID-19, casused by coronavirus 2 (SARS-CoV-2), was deemed a pandemic on March 11, 2020, by the World Health Organization. In California, USA, Governor Newsom issued a shelter-in-place order on March 19, 2020. The shelter-in-place order required citizens to only leave their homes for essential trips, and many nonessential businesses, like restaurants, were closed. As of July 2020, over 19 million cases of COVID-19 were confirmed worldwide, with 541,000 cases in California alone (1). The COVID-19 pandemic offers a unique time to study the effects of a worldwide shutdown. Water and air quality directly affect human health. If pollutant concentrations of either are above the standard, it can lead to human health problems including respiratory infections, lung cancer, and heart disease (2). The pandemic allows us to observe the effects of reduced human activity on the environment.

The worldwide shutdown limited the number of many people in the streets, cars used for transport to work, and the operation of businesses and factories (3, 4). Apple's COVID-19 Mobility Tracking found that driving rates in April 2020, the height of the shelter-in-place order, in California dropped 65% below the baseline and were 18% above the baseline at the end of July 2020 (3). The baseline is an average value of collected movement in a specific location. Apple determined the baseline from the median of a five-week period between January 3rd and February 6th of 2020. The baseline is used to illustrate changes due to COVID-19 and does not account for seasonality or daily changes. Apple calculated this baseline from a time when some people may have already started to reduce activity (5). Similarly, Google's Mobility Tracking showed that California public transit use was down 42% below the same baseline as of July 27, 2020. The Bureau of Transportation Statistics reported that 28.3% of Californians stayed indoors as of July 30, 2020 (6, 7). Reduced human activity corresponded with decreased human-induced emissions from vehicles and industrial operations (8). Particulate matter (PM) and nitrogen oxides (NO_x) decreased, and likely other pollutants (9, 10). The U.S. Environmental Protection Agency (EPA) monitors pollutants in the air and water to protect human health (11). PM, NO_x, and ozone (O_3) are criteria air pollutants and have natural and anthropogenic sources. The EPA also monitors water quality indicators, such as total dissolved solids (TDS) and pH, for human health.

PM is microscopic particles or liquid suspended in the air. $PM_{2.5}$ refers to PM that is 2.5 μm or less in diameter. Due to its fine size, $PM_{2.5}$ can be harmful to humans since it can enter the bloodstream or lungs (12). PM_{10} has a diameter of 10 μm or smaller and cannot move as far as $PM_{2.5}$ because larger-sized particles tend to deposit to surfaces closer to sources (13). Automobile engines produce NO_x and release partially combusted hydrocarbons as a result of burning fossil fuels. Factories also emit pollutants, such as PM and NO_x. NO_x emitted from these sources can lead to the formation of O_3. O_3 is necessary in the stratosphere to protect life on earth from intense ultraviolet (UV) radiation from the sun, but it is not beneficial in the troposphere (14). O_3 at ground level contributes to smog, which can cause health problems and

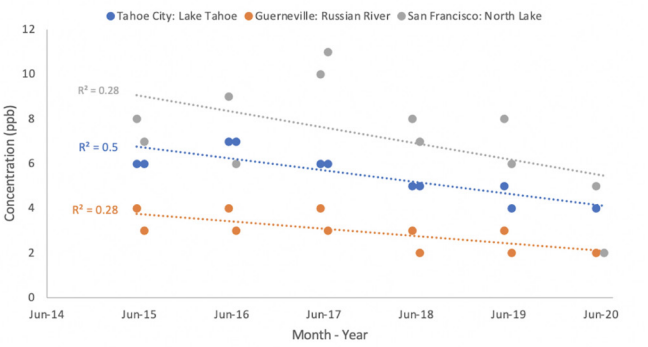

Figure 1. NOx Air Quality Concentrations Reduced from 2015 to 2020. The NO_x concentration (ppb) at three locations in California — Lake Tahoe (blue), Russian River (orange), and North Lake (grey) — was measured in June and July from 2015 to 2020. r^2 values represent a linear regression analysis.

Table 1: Water Quality

Location:	Tahoe City: Lake Tahoe		San Francisco: North Lake		Guerneville: Russian River	
County:	Placer County		San Francisco County		Sonoma County	
Measurement:	pH	TDS (ppm)	pH	TDS (ppm)	pH	TDS (ppm)
mean: 2020/15–19	7.65/NA	39.58/NA	8.82/NA	190.73/NA	8.02/8.10	124.67/132.43
+/- SD: 2020/15–19	NA	NA	NA	NA	0.46/0.17	0.29/5.87
p-value: 2020 to 2015–2019	NA	NA	NA	NA	0.53	0.004

Table 1. Water quality data for Russian River, Lake Tahoe, and San Francisco's North Lake. pH and TDS concentration in each water source was measured. The change in TDS in the Russian River at Guerneville over the 5 years was statistically significant. The nitrogen content in each body of water could not be thoroughly analyzed due to the precision of the tools used.

also harm crops and building materials (15). The $NO_2 \rightarrow NO + \bullet O$ reaction requires sunlight to occur. During the summer months, more UV radiation is present due to an increase in sunlight, resulting in an increase in O_3 creation.

Water quality is also affected by human activity, and since traffic decreased due to COVID-19, there was decreased pollution from toxic particles from car exhaust entering the San Francisco Bay (15). Many factors contribute to water quality, including TDS and pH. TDS are the inorganic and organic substances in a body of water that encompasses any minerals present (16). TDS can be a product of urban and natural runoff from storms, minerals in the water, and industrial wastewater. The EPA states that a TDS concentration below 300 ppm constitutes drinkable water, and above 1200 ppm is considered unhealthy and undrinkable. High TDS can lead to health issues from high concentrations of specific ions, such as nitrate, arsenic, aluminum, copper, or lead (16).

The pH of water is a measure of the number of hydrogen ions present in water. Human activity can affect the acidity or alkalinity of water through industrial and agricultural runoff or wastewater discharge, but natural influences such as rocks, soil, and plant life also alter pH (17). Algae and plants in the lake or body of water consume the dissolved CO2 in the water and create O2 and glucose. Surface water tends to have a pH between 6.5 and 8.5, but throughout the summer, lake surface water typically has a pH between 7.5 and 8.5 (18). While sunlight is present, the water surface will be more basic than a pH of 7 (18). Human input and air pollutants can alter the pH.

Many different factors impact water and air quality, such as the surroundings. The water quality of a city pond compared to a high alpine lake will vary due to differences in human activity and elevation, temperature, and other factors. The air quality can be affected by human-induced pollution and natural sources, such as wildfires and pollen. Based on these concepts, we hypothesized that the decrease in human activity due to California's COVID-19 shelter-in-place would result in a decrease of air and water pollutants at all three test locations: Russian River, Lake Tahoe, and North Lake in Golden Gate Park. We collected water data manually for June and July 2020. We used available air and water data from monitoring networks for the previous five years and compared it with our collected data for June and July 2020. Analysis of collected samples and monitoring data indicates that decreased human activity due to COVID-19 has likely improved California's air quality in San Francisco, Placer, and Sonoma counties. In contrast, water quality has remained fairly constant in these locations in June and July 2020.

RESULTS

To test the water quality of the Russian River, Lake Tahoe, and North Lake in Golden Gate Park, pH, NO_x, and TDS we measured these concentrations with a testing kit and various meters, and compared it to data pulled from monitoring networks including, the U.S. Geological Survey (USGS), the National Water Information System (NWIS), and the San Francisco Estuary Institute (SFEI). Data for each county's air quality were collected from the Bay Area Air Quality Management District (BAAQMD) and California's Air Resources Board (CARB). The overall results show minimal change in air and water quality during the June and July sample periods with reduced human activity due to COVID-19 compared to data from the previous five years. Though, there were some differences likely due in part to reduced human activity.

The average nitrogen concentration of Lake Tahoe in 2018 was 20.9 ppb with a maximum allowable of 210 ppb. The standard pH for the lake was between 7.0 and 8.4, which is the accepted range for pH values in Lake Tahoe. Keep Tahoe Blue states that the average TDS for the lake is 47.5 ppm (19).

NO_x concentrations significantly decreased from June/July 2015 to 2020 in San Francisco (p-value = 0.01) and Tahoe City of Placer County (p-value = 0.01). However, the change in concentration for Guerneville of Sonoma County (p-value = 0.07) was not statistically significant (**Table 2**). In San Francisco, the mean concentration of NO_x in June/July of 2020 (3.5 ppb, n = 2) was lower than the mean concentration for 2015 to 2019 (8.0 ± 1.6 ppb, n = 10). The r^2 value (r^2 = 0.28) suggests a weak negative correlation for NO_x concentrations

Table 2: Air Quality										
Location:	Tahoe City: Lake Tahoe				Guerneville: Russian River			San Francisco: North Lake		
County:	Placer County				Sonoma County			San Francisco County		
	NO_x (ppb)	O_3 (ppb)	$PM_{2.5}$ ($\mu g/m^3$)	PM_{10} ($\mu g/m^3$)	NO_x (ppb)	O_3 (ppb)	$PM_{2.5}$ ($\mu g/m^3$)	NO_x (ppb)	O_3 (ppb)	$PM_{2.5}$ ($\mu g/m^3$)
mean: 2020/15–19	3.50/5.78	43.00/47.90	5.75/11.58	16.30/17.10	2.00/3.10	23.50/25.74	5.40/5.21	3.50/8.00	26.00/32.20	7.85/6.38
+/- SD: 2015–2019	0.95	4.04	3.34	3.22	0.74	2.39	1.28	1.63	3.94	1.96
p-value: comparing 2020 mean to 2015–2019 mean concentration for June/July	0.01	0.14	0.04	0.74	0.07	0.25	0.84	0.01	0.06	0.33

Table 2. June and July monthly averages for NO_x for Tahoe City's Placer County, Guerneville's Sonoma County, and San Francisco County. O_3 concentrations in ppb, and $PM_{2.5}$ and PM_{10} in µg/m³

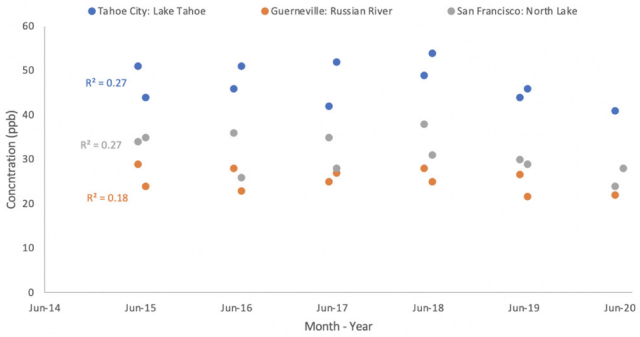

Figure 2. O_3 Air Quality Concentrations Remained Fairly Constant from 2015 to 2020. The O_3 concentration (ppb) at three locations in California — Lake Tahoe (blue), Russian River (orange), and North Lake (grey) — was measured in June and July from 2015 to 2020. r^2 values represent a linear regression analysis with only San Francisco County being significant (r^2 = 0.27).

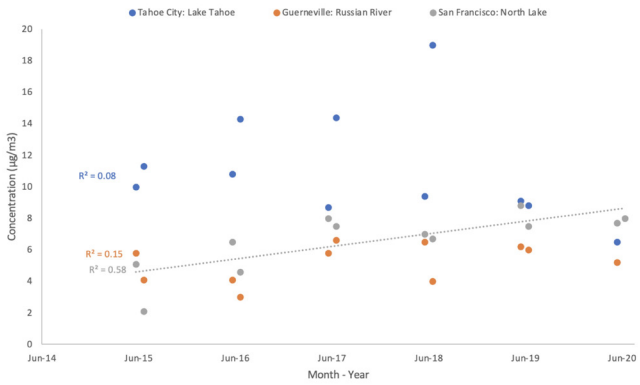

Figure 3. $PM_{2.5}$ Air Quality Concentrations Increased in San Francisco County from 2015 to 2020. The $PM_{2.5}$ concentration ($\mu g/m^3$) at three locations in California — Lake Tahoe (blue), Russian River (orange), and North Lake (grey) — was measured in June and July from 2015 to 2020. r^2 values represent a linear regression analysis. The change in $PM_{2.5}$ in Tahoe City and Guerneville did not present a significant correlation over time (r^2 = 0.077, r2 = 0.147) while the increase in $PM_{2.5}$ in San Francisco over the 5-year period was significant (r^2 = 0.58).

over time. The mean NO_x concentration in Sonoma County for June/July of 2020 (2 ppb, *n* = 2) was lower than the mean concentration for 2015 to 2019 (3.10 ± 0.74 ppb, *n* = 10), with a weak correlation (r^2 = 0.28) over time (**Figure 1**). Tahoe City of Placer County NO_x concentrations in June/July of 2020 (3.50 ppb, *n* = 2) were lower than the mean concentration from 2015 to 2019 (5.78 ± 0.97 ppb, *n* = 10) and had a negative correlation (r^2 = 0.5) over time.

O_3 concentrations at all three locations were not significantly different (**Table 2**). The mean O_3 concentration in San Francisco County for June/July of 2020 (26 ppb, *n* = 2) was lower than the O3 concentration between 2015 and 2019 (32 ± 3.9 ppb, *n* = 10) with a p-value of 0.06 and the weak negative correlation (r^2 = 0.27) over time. Additionally, the O_3 from 2015 to 2020 in Sonoma County with a mean O_3 concentration in June/July of 2020 (23.5 ppb, *n* = 2) was not significantly different (*p*-value = 0.25) in comparison to the mean concentration from 2015 to 2019 (25.7 ± 2.4 ppb, *n* = 10). The r^2 value (0.27) suggests a weak negative correlation between the O3 concentrations of June/July between 2015 and 2020 (**Figure 2**). For Placer County, the O_3 concentration in June/July of 2020 (43.00 ± 2.83 ppb, *n* = 2) was lower than the O_3 concentration between 2015 and 2019 (47.90 ± 4.04 ppb, *n* = 10) but was not statistically significant (*p*-value = 0.14). The r^2 value (0.18) for Placer County suggests no linear correlation between the June/July O_3 concentrations from 2015 to 2020.

The PM2.5 data shows a significant decrease (**Figure 3**) in concentration for Tahoe City with a concentration in June/July of 2020 (5.75 ± 1.06 µg/m³, *n* = 2) that was lower than the $PM_{2.5}$ concentration between 2015 and 2019 (11.58 ± 3.34 µg/m³, *n* = 10, *p*-value = 0.04). The r^2 value (0.08) for Tahoe City around Lake Tahoe suggests no correlation between the concentration of $PM_{2.5}$ over the past five years. In both San Francisco and Guerneville, the variation in $PM_{2.5}$ was not statistically significant (**Table 2**). In San Francisco, the mean PM2.5 concentration in June/July of 2020 (7.85 µg/m³, *n* = 2) was not statistically different from 2015 and 2019 (6.38 ± 1.96 µg/m³, *n* = 10, *p*-value = 0.33). The r^2 value (0.58) demonstrates a mild positive correlation between the $PM_{2.5}$ concentrations over the five years. The mean $PM_{2.5}$ concentration in June/July of 2020 (5.40 µg/m³, *n* = 2) was not statistically different than the PM2.5 concentration between 2015 and 2019 (5.21 ± 1.28 µg/m3, *n* = 10, *p*-value = 0.84) for Guerneville in Sonoma County. The r^2 value (0.15) suggests no correlation between the change in the concentration of

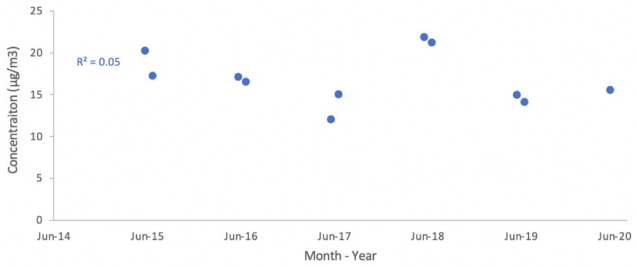

Figure 4. PM_{10} Air Quality Concentrations Remained Constant in Lake Tahoe's Placer County from 2015 to 2020. The PM_{10} concentration (µg/m^3) at Lake Tahoe in Placer County (blue) was measured in June and July from 2015 to 2020. The r^2 value (r^2 = 0.05) represents a linear regression analysis.

PM2.5 and the past five years.

The PM10 concentration in Tahoe City for June/July of 2020 (16.30 µg/m^3, n = 2) was not statistically different (Table 2) than the PM_{10} concentration between 2015 and 2019 (17.100 ± 3.215 µg/m^3, *n* = 10, *p*-value = 0.74). The r^2 value (0.05) suggests no correlation of the mean PM_{10} concentration over the past five years (**Figure 4**).

DISCUSSION

As the COVID-19 pandemic continued to affect human activity, we tested how this daily change carried over to the environment through the air and water quality of three locations in California from 2015 to 2020. The TDS and pH levels of Lake Tahoe and North Lake in San Francisco did not see a significant change, but the TDS concentrations in the Russian River decreased significantly. While most of the collected data showed a slight decrease in air pollution in 2020 during June and July, likely due to altered human activity resulting from the COVID-19 shelter-in-place order, most of the difference was not statistically significant. Water quality was not affected by the decrease in human activity, except for the Russian River, which showed a significant decrease in TDS. San Francisco is a heavily populated city of 883,305 people within 47 mi2 as of 2018 (20). The shelter-in-place order decreased driving activity by 75% below the baseline in April 2020 and remained 26% below the baseline as of late July 2020 (3). The reduction in car emissions in the city likely affected the air quality in San Francisco. The closing of ski resorts in March and a decrease in tourism contributed to the decrease in human activity on the roads and the water of Lake Tahoe (21, 22).

The mean NO_x concentration from 2015 to 2019 was significantly more than that in 2020 for Lake Tahoe at Tahoe City (**Table 2**) could be a result of decreased human activity. However, automobile activity in Placer County had increased 50% over the baseline as of July 26, 2020, after dropping 60% below the baseline in mid-April amidst the height of the lockdown order (3). While the change in road traffic affected the NO_x air quality concentrations in Placer County, the O_3 air quality remained fairly constant over the five year period. The return of automobile activity in July likely accounts for concentrations of O_3 in Placer County during June and July of 2020 (**Table 2**) that were not significantly different from the previous five years.

The $PM_{2.5}$ concentration in the air at Lake Tahoe slightly decreased (**Table 2**) significantly from 2015 to 2020, but the PM10 concentration did not significantly change. The reduction in $PM_{2.5}$ between 2015–2019 and 2020 could have resulted from a decrease in industrial activity. The notably higher $PM_{2.5}$ in July 2018 and PM_{10} concentrations in June and July of 2018 are likely a result of the Ferguson wildfire near Yosemite in Mariposa County, which began in early July, and the Carr fire near Redding, CA, which occurred in late July (23, 24). The air quality in terms of $PM_{2.5}$ and NO_x around Tahoe City at Lake Tahoe slightly improved due to the change in human activity because of COVID-19.

The significant drop in NOx concentrations in San Francisco from 2015 to 2020 (**Table 2**) may be partially attributed to the difference in human activity due to the shelter-in-place order. The decrease in average O_3 concentrations 2015–2019 compared to 2020 (**Table 2**) is not significant (*p*-value = 0.06) to signify an impact by the reduced human activity due to the shelter-in-place order. Though the data is not statistically significant, it could have been significant with a higher sample size. The $PM_{2.5}$ concentrations in San Francisco did not show a significant difference. However, eLichen's determined that the shelter-in-place order caused a 19.7% decrease in $PM_{2.5}$ in San Francisco from late March to early April (25). Our data was collected from June and July of 2020, when human activity had begun to increase again, which may account for statistically insignificant concentrations compared to previous years.

The Guerneville $PM_{2.5}$ concentration was not statistically significant (Table 2). NO_x and O_3 air concentrations were also not statistically different from the previous five years. There can be no determined correlation between the shelter-in-place order due to COVID-19 and the reduced human activity and air quality in Sonoma County in June and July 2020.

Between 1980 and 2012, Lake Tahoe's total nitrogen concentration had been between 0.013 and 0.019 ppm, while the average nitrogen content in 2018 was 0.21 ppm (26, 19). The 2020 data revealed 0 ppm for both nitrite and nitrate in Lake Tahoe, Russian River, and North Lake. The detection limit of the API Freshwater Test Kit was between 0 and 5 ppm. Based on the previous concentrations of nitrogen in Lake Tahoe, it is likely that the concentrations in 2020 were in the same range within the 0–5 ppm measurement. Similarly, the nitrogen concentrations at the Russian River in Guerneville were undetectable by the API Freshwater Kit. The daily averages from June 2, 2011, were 0.193 ppm nitrate, 0.0032 ppm nitrite, and 0.331 ppm total nitrogen. The NO_x data cannot be properly analyzed to determine an effect from the shelter-in-place on the river's nitrogen concentrations because those levels of nitrogen are undetectable by the API test kit. With the same issue, North Lake in San Francisco's Golden Gate Park had daily averages from June 16, 2014, with a nitrate concentration at 1.575 ppm, nitrite at 0.0365 ppm, and total

nitrogen at 2.765 ppm, while the API kit measured 0–5 ppm for all nitrogen concentrations.

The pH of Lake Tahoe has standard measurements between 7 and 8.4 pH. The average pH of Lake Tahoe between June 27th and 29th of 2020 was 7.65, which falls in the standard range, implying that the shelter-in-place order, lessening human activity on and off the water, did not affect the pH of Lake Tahoe. The average TDS measurement was within the acceptable range for Lake Tahoe, indicating the human activity change also did not affect TDS in the water during June and July 2020.

The average pH of North Lake in 2020, taken from daily averages between June 30, 2020, and July 2, 2020, was 8.82 (**Table 1**). There was no accessible pH data from the past five years for North Lake, making a comparison of the pH unavailable. The average TDS in North Lake from June and July 2020 was 190.73 ppm. To compare, the average TDS from 1988 was 264.5 ppm. Despite this 32-year difference, it is apparent that the minerals and ions present in the water have greatly decreased, but interpreting this difference as attributable to limited human activity is not reasonable.

Since June and July of 2015, the pH in the Russian River near Guerneville has remained constant around a pH of 8. The difference in mean pH from June and July 2015–2019 was not statistically significant in comparison to the mean pH from 2020 and was not noticeably impacted by human activity changes as a result of COVID-19. The mean TDS in June and July 2015–2019 was significantly higher (**Table 1**) compared to the mean from 2020 and might have been impacted by the reduction in human activity due to the shelter-in-place order around California. With a lack of human activity, sources of ions entering the water may have been reduced, decreasing the TDS concentration of the Russian River. The snowpack in 2020 measured 53% of the average snow for April, meaning it was a dry snow season in California (27). Less snowpack leads to less snowmelt entering California's water system, which could also reduce the sediment and suspended ions in the Russian River.

The null hypothesis that the shelter-in-place order did not affect either the water or air quality in any of these three locations could not be fully rejected. It is possible that the decrease in human activity might have contributed to improvements in NO_x and $PM_{2.5}$ concentrations in the air around Placer County and Lake Tahoe, as well as decreased TDS in the Russian River at Guerneville. The hypothesis that the pollutants in water and air would decrease in all locations was not fully supported by the data.

In every scientific experiment, we must account for sources of error and limitations when collecting and analyzing data. This data set encompasses the June and July daily and monthly averages from 2015 to 2020 for Sonoma County, Russian River; San Francisco County, North Lake; and Placer County, Lake Tahoe. Air and water quality were analyzed to determine if California's shelter-in-place order due to the COVID-19 pandemic affected air and water pollution. Lake Tahoe, Russian River, North Lake, and their counties do not fully represent California's air and water quality due to their small sample size in comparison to the state. The sample size of two for 2020 also makes it difficult to offer a complete comparison from the five years before. Perhaps if there was a larger amount of data for 2020, the difference in pollution concentration would have been higher. Additionally, varying times of day and weather can affect the turnover of the water, which impacts the TDS readings. Though all the water quality data were collected during the day while the sun was present, pH could have also been affected by the difference in the time of the sample collection. The difference in the time of day for manually collected field data varies from that of the remotely monitored data from 2015–2019 and could impact the comparison of data, leaving room for error in the data analysis. The data for water quality from Lake Tahoe and North Lake monitoring networks are averages and standards, which cannot be directly compared to daily averages to demonstrate an overall understanding of differences in water quality. Lastly, the method and instruments used for manually collecting the water data were much less precise than the historical monitored data methodology. The comparison of field and monitoring data cannot be fully accurate due to differences in how the data was collected.

Each data site represented a different location type in California. The urban environment of San Francisco compared to the rural town of Guerneville and the high elevation mountain area of Lake Tahoe yields results about varying situations and different effects from the shelter-in-place order. In San Francisco, driving was below the baseline average by 18%, walking decreased by 42%, and public transit lines have decreased to 66% below the baseline for July of 2020 (3). However, with a denser population in the city than Guerneville and Tahoe City, the difference in air pollution, except for NO_x, from 2020 and 2015–2019 did not vary notably from the other counties. The air pollutant concentrations in San Francisco have been significantly higher because more automobiles move through the city daily. However, the O_3 concentration in Tahoe City was higher than that of San Francisco. Since San Francisco is located on the Pacific Ocean, the sea breeze brings the cold air to the land, thus causing the warmer air in the city to rise, creating a circular flow. The O_3 concentration in San Francisco is then impacted by this cycle, which also depends on the air temperatures and sunlight. It transports the O_3 to a location where it can get trapped like a mountain range or valley (28). Lake Tahoe is surrounded by the Sierra Nevada mountains, which may hold in and contain the O_3, increasing the O_3 concentration despite a smaller population of people and automobiles. Air pollution from the Sacramento Valley travels up the mountains to the Lake Tahoe basin, potentially increasing the O_3 concentration (29, 30). The mixing caused by the cumulonimbus clouds that form in Lake Tahoe can increase the concentration of O_3 in the troposphere because they act as wet chemical reactors and increase NO_x production through lightning and potentially increase O_3 by

downmixing air from the stratosphere, therefore increasing ozone concentration (31).

Overall, our data demonstrated a slight decrease in air pollution and a decrease in water pollution in the Russian River, while water quality remained stable in the other locations. The difference in location sites affects the air and water quality of each county since pollution concentrations vary based on environmental factors and activity levels. Our data did not fully support the hypothesis that air and water pollution would decrease in all three locations for June and July 2020. With the statewide shelter-in-place order, pollution concentrations had the potential to decrease and create a healthier living environment. While not all aspects of air or water quality demonstrated significant results, the reduced human activity highlights the ability to mitigate human-produced pollutants and potentially the effects of climate change.

METHODS

With the ongoing COVID-19 pandemic, we wanted to test how the reduction in outdoor human activity affected the air and water qualities throughout California. To do so, we tested three bodies of water and their surrounding counties air quality to determine any changes in pollution levels. San Francisco County's North Lake in Golden Gate Park (37.7699° N, 122.5024° W) with an elevation of 80 meters, is located approximately 122 meters from a well-used road: Fulton Street. Sonoma County's Guerneville, California lies along the Russian River, which runs along a road for most of its length, with a population of 4,808 within 10 mi2 as of 2018 (32). The Russian River location (38.50803° N, 122.9874° W) at an elevation of 18 meters is not near the road but is a well used river. In Placer County's Tahoe City (39.1687° N, 120.1424° W), Lake Tahoe is not near a road but is at a much higher elevation of 1,905 meters and is fed from fresh snowmelt. Out of these three data sites, San Francisco saw a more substantial decrease in human activity by the shelter-in-place due to its higher population and human activity (3).

Water quality was measured by a TDS and pH meter as well as an API Freshwater Test Kit (Mars Inc., McLean, VA). The Ketotek KT-3 Portable pH Meter (Ketotek Corporations, Xiamen, Fujian) can detect pH from 0.00 to 16.00 with ± 0.01 pH accuracy. The Ketotek KT-2 Portable TDS Meter (Ketotek Corporations, Xiamen, Fujian) can detect total dissolved solids from 0 to 9990 ppm with a ± 2% accuracy. In Tahoe City, Lake Tahoe, measurements were taken off of a pier with a water depth of approximately 2 meters. Each of the meters has a five-centimeter section that can be submerged in water, so the data represents the surface water at each site. The data from the Russian River near Guerneville was taken at the end of a dock that was 3 meters long, but the depth of the water was about 3.5 meters. Lastly, at the North Lake in Golden Gate Park, data was taken from the shore off of a ramp in the water. The water was only 30 centimeters deep at this location.

To test the nitrate and nitrite concentrations in the water, the API Freshwater Test Kit was used where 5 mL of each water sample was tested by following the instructions to use the liquid test bottles. For the nitrite testing, five drops of the solution were put into the water sample, and the color would appear after shaking the test tube and letting it sit for five minutes. The process for nitrate was very similar, except the color of the water sample would change based on the amount of each analyte present, and the best fit choice was determined regarding the new color of the water. This process was repeated three times for each analyte per water site per day and each site was tested for three consecutive days. Water was collected between 11 am and 3 pm for each test location. The API test kit was able to measure nitrite concentration in 0.25 ppm intervals, whereas nitrate was measured in 5.0 ppm intervals, and both were based on the color of the sample compared to a reference color supplied with the kit.

Table 3: Precision of Instruments (Used in Field Data Collection)			
Instrument	**Use**	**Precision**	**Detection Limit**
API Freshwater Test Kit	Nitrate concentration	0.25 ppm	5.0 ppm
API Freshwater Test Kit	Nitrite concentration	5.0 ppm	160 ppm
Ketotek TDS meter	TDS concentration	0.01 ppm	9990 ppm
Ketotek pH meter	pH concentration	0.01 pH	16 pH

Table 3. Precision and method detection limits for the instruments used in collecting water samples through field data collection.

USGS remote water data from the NWIS was used for Russian River water quality from June 2015 to July 2020 (33). To collect that data, isokinetic sampling methods were used for flowing water. Isokinetic sampling captures particles that flow through a certain area to determine the concentration of the compound or particle. Since the dam for the Russian River opens mid-June each year and closes on the 1st of October, isokinetic sampling was performed due to the water flowing through the river. Since the remote water quality data from USGS and NWIS provided conductivity data, but TDS data was collected for this experiment, conductivity was converted into TDS: $TDS ppm_{500}$ = 500 * (C(µS/cm))/1000 mS/cm.

The San Francisco Estuary Institute (SFEI) collected water samples and data for North Lake using the Seabird CTD, YSI 556, WTW 340i meter (34). This instrument is able to measure many water quality functions and provides nitrate, nitrite, and total nitrogen data for North Lake in San Francisco's Golden Gate Park (35). However, there was no pH data available for North Lake.

UC Davis Tahoe Environmental Research Center provided nitrogen data for Lake Tahoe through their State of the Lake Reports. The nitrogen data was collected from a Shimadzu UV-1700 series Spectrophotometer that uses light absorption to determine the matter concentration of a solution (36). The pH and TDS standards for the lake were determined by the handheld Hanna pH meters with a 0.02 unit resolution and a handheld Oakton TDS Tester Conductivity meter that has a

10 µS/cm resolution (26).

The Bay Area Air Quality Management District (BAAQMD) provided air quality data for San Francisco (37). To obtain NO_x data, a chemiluminescent analyzer was used (38). Chemiluminescence is based on the amount of light given off when nitric oxide and O_3 react to determine the concentration of nitric oxide. To determine the concentration of NO_2 in an air sample, the samples are passed through a catalyst to reduce NO and are then measured by chemiluminescence to quantify the NO_x emissions (38). The minimum sensitivity of the analyzer is ± 2% of the full scale. Particulate matter was measured isokinetically through stack glasses and filtered through glass fibers. The weight of the particulate matter was calculated gravimetrically after separating from excess water. The minimum sensitivity of particulate matter measurements is 0.001 gr/SDCF (39). To measure the O_3 concentration in the air, BAAQMD uses a Thermo Electron/Thermo Environmental Instrument Model 49i. This instrument is placed at each monitored site and analyzes the O_3 in the air from 0.05 to 1000 ppb (40). Air filters through between every 10 and 300 seconds to continuously collect data measurements for the O_3 concentrations (41).

The California Air Resources Board (CARB) provided air quality data for the Russian River through Sonoma County and for Lake Tahoe through Placer County (42). PM concentration was determined through Optical Particle counters (OPC), which measure the light scattered by particles to determine the number and size of particles in the air. OPC uses lasers and detectors to capture the light. Spectroscopy was also used to collect data in terms of particulate matter. Light is passed through an air sample, and the amount of light that is absorbed is directly proportional to the compound or particles. Once the air samples are filtered and have gone through isolation processes, spectroscopy was also used for gaseous pollutants: NO_x and O_3. These gaseous pollutants were measured through testing the conductivity of each water sample as well. Conductivity quantifies the varying flow of electricity between two electrodes. The change in electrical conductivity is directly proportional to the concentration of the measured compound. Thermal conductivity works by measuring the varying resistance across a circuit in relation to a reference circuit because of the increased concentration of a gaseous compound.

A *t*-test was performed on the data to determine statistical significance and the reported *p*-values are based on an *alpha* of 0.05. The 2015–2019 data was compared to the 2020 data for both water and air quality to analyze any difference in concentration over the five year period. The data was formatted into figures and tables through Google Sheets and Excel computer programs.

ACKNOWLEDGEMENTS

I would like to thank the Headwaters Science Institute for the opportunity to conduct research and my family for their constant support and patience throughout this project.

Received: September 3, 2020
Accepted: January 25, 2020
Published: February 15, 2021

REFERENCES

1. Johns Hopkins University & Medicine. "Coronavirus Resource Center." Coronavirus Resource Center. *Johns Hopkins University & Medicine*, https://coronavirus.jhu.edu/map.html. Accessed 28 July 2020.
2. Departmental News. “Health Consequences of Air Pollution on Populations.” World Health Organization, *World Health Organization*, Nov. 2019, www.who.int/news/item/15-11-2019-what-are-health-consequences-of-air-pollution-on-populations#:~:text=Exposure to high levels of people who are already ill. Access 29 July 2020.
3. Apple "COVID-19: Mobility Trends Reports." *Apple*, www.apple.com/covid19/mobility/. Accessed 28 July 2020.
4. Bates, Amanda E, *et al*. “COVID-19 Pandemic and Associated Lockdown as a ‘Global Human Confinement Experiment’ to Investigate Biodiversity Conservation.” Biological Conservation, *Elsevier Ltd.*, 10 June 2020, www.ncbi.nlm.nih.gov/pmc/articles/PMC7284281/.
5. Google. "Community Mobility Reports Help." *Google*, support.google.com/covid19-mobility/answer/9824897?hl=en#:~:text=A%20baseline%20day%20represents%20a,value%E2%80%94it's%207%20individual%20values. Accessed 3 Aug. 2020.
6. Google. "COVID-19 Community Mobility Report." *Google*, 27 July 2020, www.gstatic.com/covid19/mobility/2020-07-27_US_California_Mobility_Report_en.pdf. Accessed 1 Aug. 2020.
7. Bureau of Transportation Statistics. “Daily Travel during the COVID-19 Pandemic.", U.S. *Department of Transportation*, www.bts.gov/browse-statistical-products-and-data/trips-distance/explore-us-mobility-during-covid-19-pandemic. Accessed 8 Aug. 2020.
8. Hamwey, Robert. “Environmental Impacts of Coronavirus Crisis, Challenges Ahead.” UNCTAD, *United Nations Conference on Trade and Development*, 20 Apr. 2020, unctad.org/news/environmental-impacts-coronavirus-crisis-challenges-ahead. Accessed 28 July 2020.
9. Smith, Darrell. “Fires and Climate Change Polluted California's Air. Has Coronavirus Shutdown Helped?” Sacbee, *The Sacramento Bee*, 21 Apr. 2020, www.sacbee.com/news/california/article242181921.html. Accessed 28 July 2020.
10. Lunden, Melissa, and Meghan Thurlow. “The Stunning Impact of COVID-19 Social Distancing on Air Pollution.” Greenbiz, *Greenbiz Group Inc.*, 31 Mar. 2020, www.greenbiz.com/article/stunning-impact-covid-19-social-distancing-air-pollution. Accessed 5 Aug. 2020.
11. Environmental Protection Agency. “Criteria Air Pollutants.” *EPA*, 17 Nov. 2020, www.epa.gov/criteria-air-pollutants#:~:text=Criteria Air PollutantsThese pollutants are,oxides, nitrogen oxides and lead. Accessed 23 Oct. 2020.

12. California Air Resources Board." Inhalable Particulate Matter and Health (PM2.5 and PM10) | California Air Resources Board, *California Environmental Protection Agency*, ww2.arb.ca.gov/resources/inhalable-particulate-matter-and-health. Accessed 31 July 2020.
13. United States Environmental Protection Agency. "Ground-Level Ozone Basics." *EPA*, 10 Sept. 2020, www.epa.gov/ground-level-ozone-pollution/ground-level-ozone-basics#:~:text=Ozone can be "good" or,ultraviolet radiation from the sun. Accessed 6 Aug. 2020.
14. Tedesco, Marco. "Coronavirus Is Improving Water Quality - For Now, At Least." State of the Planet, *Columbia University*, 5 June 2020, blogs.ei.columbia.edu/2020/06/08/coronavirus-improving-water-quality/. Accessed 28 July 2020.
15. Safe Water. "TDS and pH." *Safe Water*, www.safewater.org/fact-sheets-1/2017/1/23/tds-and-ph. Accessed 28 July 2020.
16. Fondriest Environmental, Inc. "pH of Water." Environmental Measurement Systems, *Fondriest Environmental, Inc.*, 23 Jan. 2019, www.fondriest.com/environmental-measurements/parameters/water-quality/ph/#:~:text=Pollution in the air, soil,known as acid rain ²¹. Accessed 28 July 2020.
17. Lake Access. "pH: Measuring the Acidity and Alkalinity of Lakes." *Lake Access*, www.lakeaccess.org/russ/ph.htm. Accessed 28 July 2020.
18. Keep Tahoe Blue. "17th Annual Snapshot Day Report, A Lake Tahoe Basin and Truckee Watershed Citizen Monitoring Event." *Keep Tahoe Blue*, 2017, www.keeptahoeblue.org/download/document/766/2017-Snapshot-Day-Report.pdf. Accessed 5 Aug. 2020.
19. U.S. Department of Commerce. "Census Glossary." *U.S. Department of Commerce.* www.census.gov/glossary/#term_Populationestimate.
20. O'Neil, Rebecca. "Economy impact: Truckee, North Tahoe lean on small business as backbone amid coronavirus crisis." Tahoe Daily Tribune, 4 May 2020. *Tahoe Daily Tribune*, www.tahoedailytribune.com/news/investigating-the-impact-truckee-north-tahoe-lean-on-small-business-as-backbone-of-economy-amid-coronavirus-crisis/. Accessed 28 July 2020.
21. "Tahoe City Demographics." *Point2Homes*, www.point2homes.com/US/Neighborhood/CA/Tahoe-City-Demographics.html#:~:text=Tahoe%20City%20is%20an%20area,City%20and%201%2C021%20female%20residents. Accessed 28 July 2020.
22. "2018 Incident Archive." *CAL FIRE*, www.fire.ca.gov/incidents/2018/. Accessed 6 Aug. 2020.
23. "Situation Intelligence: Ferguson Fire, California Wildfires." *World Aware*, www.worldaware.com/resources/intelligence-alerts/situation-intelligence-ferguson-fire-california-wildfires#:~:text=The%20Ferguson%20fire%20ignited%20on,was%20only%2030%20percent%20contained. Accessed 6 Aug. 2020.
24. ELichens. "IMPACT OF COVID-19 ON AIR QUALITY IN SAN FRANCISCO." *eLichens*, www.elichens.com/impact-of-covid19-on-air-quality-in-san-francisco. Accessed 28 July 2020.
25. UC Davis Tahoe Environmental Research Center. "TAHOE: STATE OF THE LAKE REPORT 2019." *UC Davis*, 2019, terc.sf.ucdavis.edu/sites/g/files/dgvnsk4286/files/inline-files/9_nutrients_5.pdf. Accessed 5 Aug. 2020.
26. Arcuni, Peter. "As April Begins, California's Snowpack is About Half of Normal." *KQED*, Apr. 2020, www.kqed.org/science/1960807/as-april-begins-californias-snowpack-is-about-half-of-normal. Accessed 5 Aug. 2020.
27. Li, Qian, *et al.* "Measurement-Based Investigation of Ozone Deposition to Vegetation under the Effects of Coastal and Photochemical Air Pollution in the Eastern Mediterranean." *Science of The Total Environment*, 25 July 2018, www.sciencedirect.com/science/article/pii/S004896971832518X.
28. Dolislager, Leon J., *et al.* "An Assessment of Ozone Concentrations within and near the Lake Tahoe Air Basin." *Atmospheric Environment*, 2 July 2009, https://doi.org/10.1016/j.atmosenv.2009.07.017.
29. Bose, B.H. "Air quality in Tahoe up and down." Tahoe Daily Tribune, *Swift Communications*, 19 Dec. 2001, www.tahoedailytribune.com/news/ air-quality-in-tahoe-up-and-down/. Accessed 31 July 2020
30. Seinfeld, John H. "The Effects of Meteorology on Tropospheric Ozone." Rethinking the Ozone Problem in Urban and Regional Air Pollution, Washington D.C., *National Academy Press*, 1992, p. 95.
31. World Population Review. "Guerneville, California Population 2020." *World Population Review*, 2020, worldpopulationreview.com/us-cities/guerneville-ca-population. Accessed 28 July 2020.
32. U.S. Geological Survey. "USGS Water Data for the Nation." *National Water Information System*, 2016, nwis.waterdata.usgs.gov/nwis/uv?cb_00010=on&cb_00095=on&cb_00300=on&cb_00400=on&format=html&site_no=11467000&period=&begin_date=2020-07-03&end_date=2020-07-06. Accessed 20 July 2020.
33. San Francisco Estuary Institute. "Contaminant Data Download and Display (CD3)." Contaminant Data Download and Display (CD3) | San Francisco Estuary Institute, *SFEI*, 1 January 1970, www.sfei.org/rmp/data. Accessed 28 July 2020.
34. Trowbridge, Philip, *et al.* "Quality Assurance Program Plan for The Regional Monitoring Program for Water Quality." *SFEI*, www.sfei.org/sites/default/files/biblio_files/2017_RMP_QAPP_Final_Signed_8.2.17.pdf. Accessed 31 July 2020.
35. TERC. "Tools & Technology." *UC Davis*. Accessed 9 Aug. 2020.
36. BAAQMD. "Air Pollution." *Bay Area Air Quality Management District*, 2020, www.baaqmd.gov/about-air-quality/current-air-quality/air-monitoring-data/#/airp?id=316&style=chart&zone=-1&date=2020-06-28&view=monthly. Accessed 28 July 2020.
37. BAAQMD. "OXIDES OF NITROGEN, CONTINUOUS SAMPLING." *Bay Area Air Quality Management District*, 17

July 2017, www.baaqmd.gov/~/media/files/records/mop/vol-4/st13a.pdf?la=en. Accessed 28 July 2020.
38. BAAQMD. "ST-15 Particulate Sampling." *Bay Area Air Quality Management District*, 17 July 2017, www.baaqmd.gov/~/media/files/records/mop/vol-4/st15.pdf?la=en. Accessed 28 July 2020.
39. EPA. "DESIGNATED REFERENCE AND EQUIVALENT METHODS." *U.S. Environmental Protection Agency*, 15 June 2020, www.epa.gov/sites/production/files/2019-08/documents/designated_reference_and-equivalent_methods.pdf. Accessed 28 July 2020.
40. "Model 49i - User Manual". *Thermo Fisher Scientific*, tools.thermofisher.com/content/sfs/manuals/epm-manual-model%2049i.pdf. Accessed 28 July 2020.
41. CARB. "Air Monitoring Technology." *California Environmental Protection Agency*. California Air Resources Board, ww2.arb.ca.gov/capp-resource-center/community-air-monitoring/outline-of-measurement-technologies#cond. Accessed 5 Aug. 2020.

JOURNAL OF
EMERGING INVESTIGATORS

Article

The Protective Antioxidant Effects of Sulforaphane on Germinating Radish Seeds Treated with Hydrogen Peroxide

Venkata Siva Dasuri[1] and Mr. John Churchill[1]
[1] Norwood High School, Norwood, Massachussetts, USA

SUMMARY

Free radical chain reactions result when atoms containing unpaired electrons bind with biomolecules and alter their biological functions, contributing to the progression of diseases such as atherosclerosis, cancer, and diabetes. Antioxidants, such as vitamin E and sulforaphane, are effective neutralizers of free radicals and prevent cellular damage. This present study is conducted to determine the relative effectiveness of sulforaphane against free radicals generated by hydrogen peroxide (H_2O_2) compared with the known antioxidant vitamin E. In this experiment, H_2O_2 is a source of free radicals and germinating radish seeds are models to test the protective effects of antioxidants against free radicals. Generally, H_2O_2 diffuses into the cell and dissociates to form hydroxyl radicals through Fenton reactions. Based on current literature, the hypothesis is that sulforaphane is more effective than vitamin E in inhibiting free radicals from 1% H_2O_2 on germinating radish seeds due to its activation of different antioxidant pathways compared to vitamin E's direct neutralization of free radicals. The 1% H_2O_2-treated radish seeds show lower germination rates than seeds treated with sulforaphane and vitamin E with 1% H_2O_2. Furthermore, the germination rate is higher in sulforaphane with 1% H_2O_2-treated seeds compared to vitamin E and 1% H_2O_2 treated seeds. In summary, these experiments show sulforaphane is more effective than vitamin E in neutralizing the free radical effects of H_2O_2 on radish seed germination. These results point to sulforaphane's potential use as a dietary supplement to counteract free radical effects on cellular levels, helping to prevent the progression of certain diseases.

INTRODUCTION

Free radicals are atoms or molecules that are hazardous to cell health and are the root cause of several degenerative diseases (1, 2). Free radicals have an unpaired electron in their outer shell configuration that makes them highly reactive (3, 4). To achieve a stable electron configuration, the free radicals attracting electrons from biomolecules such as proteins, lipids, or nucleic acids in the cell (5). Because of the removal of an electron, the biomolecules thus become unstable. As a result, this instability results in a cascade of chain reactions that alter their biological function, eventually leading to either cell degeneration or death (6). Some sources of free radicals in our system come from burned or smoked food, alcohol, pre-manufactured goods, ionizing radiation, radioactive substances, and various types of machine exhaust (7). Free radical reactions are implicated in many degenerative diseases, including atherosclerosis, cancer, inflammatory joint disease, asthma, diabetes, senile dementia, and degenerative eye disease, by damaging genetic material within cells (8, 9).

Thus, many living organisms have evolved with certain molecules or enzyme systems that largely counteract the damage arising from free radicals. Nevertheless, naturally occurring compounds in our diet called antioxidants also play a role in neutralizing the free radicals (10). Antioxidant molecules either directly neutralize free radicals at the source by donating an electron through an ionic bond or by indirectly activating antioxidant enzymes that can neutralize free radical reactions (11), thereby protecting the biological molecules.

Antioxidant molecules vary in their neutralizing properties to counteract free radicals. vitamin E is well-known as an effective antioxidant against free radicals and one of the most abundant and significant lipophilic radical-scavenging antioxidant *in vivo* that forms a-tocopheroxyl radicals as the intermediate in its free radical scavenging reaction (12, 13). Recent studies demonstrate phytochemical ingredient molecules like Sulforaphane, richly found in cruciferous vegetables such as broccoli, brussels sprouts, and cabbage, can be cytoprotective and act as an antioxidant molecule, acting through the activation of various antioxidant enzymes in response to free radical stress (14). However, the relative effectiveness of various antioxidant molecules against free radicals is not known.

The model of action through which antioxidants neutralize free radicals differs in cellular systems (3). The antioxidant molecule vitamin E neutralizes free radicals at the source by donating an electron through an ionic bond (15), whereas sulforaphane has been shown to activate a cascade of antioxidant enzymes in response to free radical stress in the cellular system (14). However, both actions help protect biological molecules. These differences in the mode of antioxidant action between sulforaphane and vitamin E could be a reason for the observed differences in their effectiveness in counteracting free radical effects on germinating radish seeds. However, the mechanisms of action of antioxidants need further investigation to explore the reasons for the relative differences in their effectiveness as an antioxidant.

Our study aims to investigate the relative effectiveness of sulforaphane as an antioxidant molecule to counteract the effects of free radicals generated by 1% H_2O_2 in comparison with another known antioxidant, vitamin E (16, 17). We

hypothesize sulforaphane is more effective than vitamin E in inhibiting the effects of free radicals on the germinating radish seeds treated with 1% H_2O_2 based on existing research suggesting that vitamin E upregulates antioxidant defenses as an exogenous antioxidant while sulforaphane activates endogenous defenses instead to neutralize free radicals (18). Specifically, evidence shows sulforaphane controls the expression of genes involved in the neutralization and elimination of reactive oxidants via the activation of nuclear factor erythroid 2-related factor 2 (NRF2) pathway, although the sulforaphane's mechanisms are not completely understood at this time (19). In this experiment, H_2O_2 is used as a source of free radicals and the germinating radish seeds are used as models to test the protective effects of antioxidants in neutralizing free radicals. Previously, H_2O_2 was determined to be detrimental to the seed germination process as a toxic molecule and this observation is consistent with the results of this experiment; however, H_2O_2 in very small amounts can be conducive to seed germination as a signaling molecule (20). In the current study, H_2O_2 is used at concentrations that negatively affect the seed germination process.

RESULTS

After three days of incubating radish seeds in the presence of 1% H_2O_2 with or without antioxidants, seed germination rates are recorded and analyzed. A representative picture of germinating radish seeds with different treatments is shown in **Figure 1**. **Table 1** displays the summary of the radish seed germination results obtained with four different individual experiments. In all, the experiment derived significant results based on a one-way ANOVA test with p<0.05.

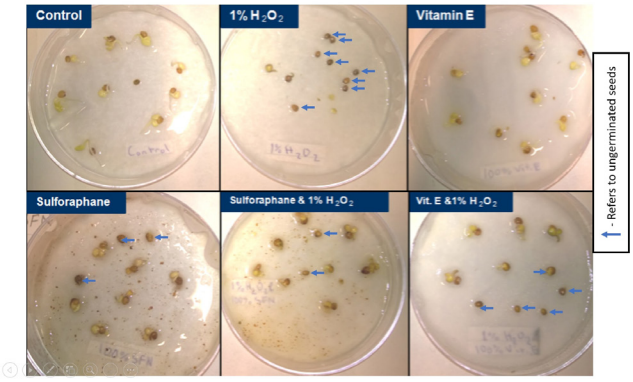

Figure 1. Representative images of radish seed germination exposed to H_2O_2 and antioxidants. As described in the methods section, radish seeds were treated either with 1% H_2O_2 antioxidants alone, or 1% H_2O_2 in combination with either of the antioxidants, Sulforaphane and Vitamin E. The radish seeds were incubated for 72 hours, images of the petri dishes were taken, and the germination rates were analyzed.

H_2O_2 is used as a source of free radical generation in this study. An optimum concentration of H_2O_2 for the seed germination experiments is initially determined by testing the seed germination rate using different concentrations of H_2O_2. 1% H_2O_2 concentration is found to be an optimum concentration for the germination experiments as the rate of radish seed germination was definitely 0% when used at a concentration of 3%. The rate of germination of radish seeds is about 12% when H_2O_2 is used at a concentration of 1%, which is sufficient to vastly inhibit seed germination.

The radish seeds from the control group show an average germination rate of 97.5% (**Figure 1; Table 1**). However, the seeds treated with 1% H_2O_2 had a 12.5% germination rate, which is the lowest of all the treatments and point towards the strong inhibition of H_2O_2 on seed germination. Furthermore, the treatment of radish seeds with either sulforaphane or vitamin E did not have significant effects on seed germination, resulting in a germination rate of 90% and 97.5% respectively when compared to the seeds treated with water alone (**Table 1; Figure 2**).

Experimental Results of Seed Germination

	Control	Vitamin E	Sulforaphane	Vit. E + 1% H2O2	SFN + 1% H2O2	1% H2O2
Experiment 1	10	10	9	4	10	0
Experiment 2	10	9	10	4	8	0
Experiment 3	10	10	7	5	8	3
Experiment 4	9	10	10	8	9	2
Average	9.75	9.75	9	5.25	8.75	1.25
STDEV	0.500	0.500	1.414	1.893	0.957	1.500
SEM	0.250	0.250	0.707	0.946	0.479	0.750
t-test		1.000000	0.355918	0.003705	0.113532	3.83E-05

ANOVA Single Factor Test Results based on above table

Source of Variation	SS	df	MS	F	P-value	F crit
Between Groups	231.2083	5.0000	46.2417	29.9946	3.95E-08	2.7729
Within Groups	27.7500	18.0000	1.5417			
Total	258.9583	23.0000				

Table 1. A single factor ANOVA test for a robust comparison between the test groups was performed to determine the overall significance of the results. Statistical student *t*-test analysis was then performed on four independent sets of 10 healthy radish seed germination experiments, comparing each of the treatments to the control group containing only radish seeds and water. The germination rate of radish seeds treated with H_2O_2/antioxidants alone or in combination of both were recorded, and the results were analyzed using Student's t-test to determine the significant differences in the germination rate between the treatment groups. Significant differences in seed germination rate were observed in treatment groups treated with 1% H_2O_2 and Vitamin E+ 1% H_2O_2 when compared with control treated group but not with any other groups, suggesting Vitamin E is less effective than sulforaphane in neutralizing H_2O_2's free radical toxicity and its inhibition of germination.

The seeds group treated with vitamin E plus 1% H_2O_2 display an average seed germination rate of 52.5%, and the germination rate was significantly lower when compared to the control group with p <0.05. The radish seeds treated with sulforaphane and 1% H_2O_2 yielded a seed germination rate of 87.5%, which is higher compared to the rate of germination of seeds in the presence of vitamin E with 1% H_2O_2 but not significant (p-value>0.05) when compared to the control group (**Table 1; Figure 2**). The vitamin E with 1% H_2O_2 group is thus significantly different from the control

group with a $p<0.05$ and the sulforaphane with 1% H_2O_2 group is not significantly different from the control group treated with a $p=0.1135$, suggesting sulforaphane is relatively more potent in acting against free radical stress caused by H_2O_2 on germinating radish seeds when compared with vitamin E. In all, the statistical tests performed demonstrate the sulforaphane with 1% H_2O_2 group have a similar germination pattern as the control group while the vitamin E with 1% H_2O_2 did not, thus suggesting vitamin E is less effective than sulforaphane in neutralizing H_2O_2's free radical toxicity and its inhibition of germination.

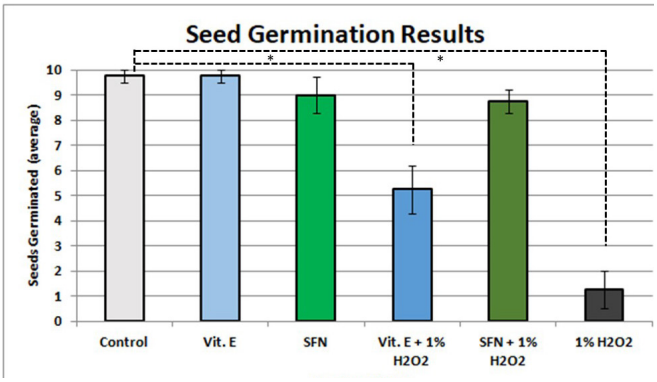

Figure 2. Sulforaphane maintained seed germination rates in the presence of H_2O_2 more effectively than vitamin E. Bar graph below gives a summary of the radish seed germination results from four different experiments. The error bars represent the standard error of the mean (SEM) between individual experiments. The difference between treatment groups is considered significant (*) when the *p*-value is $p<0.05$ based on student *t*-test results. Significant differences in seed germination rate were observed in treatment groups treated with 1% H_2O_2 and Vitamin E and 1% H_2O_2 when compared with control-treated group but not with any other groups indicating the sulforaphane-rich broccoli extracts are effective in neutralizing the effects of 1% H_2O_2.

DISCUSSION

This study was designed to determine the effectiveness of sulforaphane (from broccoli sprout extracts) in preventing the effects of free radicals on germinating radish seeds. Our experimental results support that sulforaphane-rich broccoli extract is more effective in neutralizing the free radical effects of H_2O_2 on germinating radish seeds when compared to the antioxidant, vitamin E.

The control group containing seeds treated with water alone exhibited an average germination rate of 97%, suggesting that the conditions used such as water, seed bed, temperature, water, and light were optimal for the germination of the radish seeds. The seeds treated with H_2O_2 plus sulforaphane alone showed a similar germination rate to the control group, indicating that sulforaphane is effective in preventing the free radical effects on germinating radish seeds under the experimental seeds. In contrast, the seeds treated with vitamin E and H_2O_2 showed an average germination rate of 50%, which indicates that vitamin E is less effective in neutralizing H_2O_2 effects when compared to sulforaphane.

The results from the present study show that sulforaphane rich-broccoli extract can act as an effective antioxidant and suggest that this extract is more potent than vitamin E in counteracting free radical effects. In effect, this study is helpful to further expand on existing research regarding sulforaphane and its potential effects and uses as an endogenous antioxidant. By demonstrating the higher effectiveness of sulforaphane over vitamin E in the context of H_2O_2 free radical toxicity and inhibition of germination, this research highlights the untapped therapeutic potential of sulforaphane as a potent antioxidant. By demonstrating these statistically significant results using radish seeds as an experimental model, this study will encourage other researchers to further investigate the mechanisms of how sulforaphane activates the NRF2 pathway as well as which enzymes are central to its function. We hope to open the path for the thorough investigation of sulforaphane including, but not limited to, its definite model of action in addition to its beneficial effects in mammalian cells and humans overall.

By using this research to demonstrate sulforaphane is effective in combating the free radical effects of H_2O_2, we can say that it would be beneficial for individuals to incorporate cruciferous vegetables, known to be an excellent source of sulforaphane, into their diets. Thus, this study has real-life applications as people could develop healthier eating habits by including sulforaphane rich-broccoli and other foods containing sulforaphane in their diet. As a natural antioxidant, sulforaphane can work as a defense against the free radical effects in our body with implications for preventing or delaying the underlying degenerative disease such as atherosclerosis, cancer, inflammatory joint disease, asthma, diabetes, senile dementia, and eye disease (8, 21, 22).

MATERIALS AND METHODS

Solution Preparations and Treatment Group Setup

The solutions for each of the experimental groups were prepared using a graduated cylinder. For this experiment, there were 6 petri dishes (100mm by 15mm; RGF) with 10 radish seeds in each (Seeds of Change) that had different 10 mL treatments added to each one (see **Figure 1**). First, coffee filter disks were placed in each petri dish at the bottom to produce a foundation for seed germination to occur. Ten mL of distilled water was added to the control group and 10 mL of 1% H_2O_2, diluted from 3% H_2O_2, was added to the comparative control group. Next, the contents of a broccoli extracts rich with sulforaphane pill (400 mcg per 20:1 broccoli sprout extract capsule; Swanson, Green Foods) were added to 10 mL of water, stirred well, filtered, and added to the petri dish labelled as SFN. This step was repeated for the vitamin E pill (400 IU per dose; Spring Valley) and the solution was added to the vitamin E petri dish. The concentration of the sulforaphane-related treatment was 400 mcg per 10 mL of its corresponding solution per experimental group and is comparable to the 400 IU or 20,000 mcg concentration of

vitamin E per 10 mL of its corresponding solution as both are the recommended daily dose of the antioxidant as established by dietary guidelines. Finally, for the experimental groups, the vitamin E pill and Sulforaphane pill were each added into a 10 mL solution of 1% H_2O_2. The solutions were stirred well, filtered, and added into their respective petri dishes labeled as "vitamin E + 1% H_2O_2" and "SFN + 1% H_2O_2". The petri dishes were then kept 3 feet away from a tube light at a temperature of around 73°F for 72 hours. Finally, pictures were taken and the seeds that had germinated from each petri dish were counted (see **Table 1**). This experiment was repeated four independent times.

Data Analysis

The average number of seeds germinated and the SEM (standard error of the mean) per experimental condition were calculated using Microsoft Excel. The significance (*p*-value) of the effectiveness of the treatment, compared to control treatment, on germinating radish seeds was calculated using a one-way ANOVA test to determine significance and a *t*-test to compare the means of each experimental group and the control group (see **Table 1 & Figure 2**).

ACKNOWLEDGEMENTS

We would like to thank the JEI editors for their detailed feedback and helpful suggestions on the manuscript throughout the submission process.

Received: July 20, 2020
Acccepted: November 30, 2020
Published: February 19, 2021

REFERENCES

1. Mathis, T., S. Vignot, C. Leal, J. P. Caujolle, C. Maschi, M. Mauget-Faÿsse, L. Kodjikian, S. Baillif, J. Herault, and J. Thariat. "Mechanisms of phosphenes in irradiated patients." *Oncotarget*, vol. 8, no. 38, 2017, pp. 64579-64590. doi:10.18632/oncotarget.18719

2. Jan, A. T., M. Azam, K. Siddiqui, A. Ali, I. Choi, and Q. M. Haq. "Heavy Metals and Human Health: Mechanistic Insight into Toxicity and Counter Defense System of Antioxidants." *International Journal of Molecular Sciences*, vol. 16, no. 12, 2015, pp. 29592-29630. doi:10.3390/ijms161226183

3. Ahmadinejad, F., S. G. Møller, M. Hashemzadeh-Chaleshtori, G. Bidkhori, and M. S. Jami. "Molecular Mechanisms behind Free Radical Scavengers Function against Oxidative Stress." *Antioxidants*, vol. 6, no. 3, 2017, pp. 51. doi:10.3390/antiox6030051

4. Sun, Yinnan, K. Yang, Q. Cao, et al. "Homogenate-assisted Vacuum-powered Bubble Extraction of Moso Bamboo Flavonoids for On-line Scavenging Free Radical Capacity Analysis." *Molecules*, vol. 22, no. 7, 2017, pp. 1156. doi:10.3390/molecules22071156

5. Black, J. R., M. S. Islam, H. L. Carmichael, B. L. Slaten, B. K. Little, and G. Mills. "Radical Chain Reduction of CCl4 Initiated by Illumination of SPEEK Solutions." *The Journal of Physical Chemistry A*, vol. 121, no. 20, 2017, pp. 3918-3928. doi:10.1021/acs.jpca.7b00240

6. Deng, Yuen, E. L. Lee, K. Chong, and Z. A. Almsherqi "Evaluation of radical scavenging system in amoeba Chaos carolinense during nutrient deprivation." *Interface Focus*, vol. 7, no. 4, 2017, pp. 20160113. doi:10.1098/rsfs.2016.0113

7. Yang, Lili, G. Liu, M. Zheng, et al. "Highly Elevated Levels and Particle-Size Distributions of Environmentally Persistent Free Radicals in Haze-Associated Atmosphere." *Environmental Science and Technology,* vol. 51, no. 14, 2017, pp. 7936-7944. doi:10.1021/acs.est.7b01929

8. Gupta, R. K., A. K. Patel, N. Shah, et al. "Oxidative stress and antioxidants in disease and cancer: a review." *Asian Pacific Journal of Cancer Prevention,* vol. 15, no. 11, 2014, pp. 4405-4409. doi:10.7314/apjcp.2014.15.11.4405

9. Florence, T.M. "The role of free radicals in disease." *Australian and New Zealand Journal of Ophthalmology,* vol. 23, no. 1, 1995, pp. 3-7. doi:10.1111/j.1442-9071.1995.tb01638.x

10. Baschieri, Andrea, L. Pulvirenti, V. Muccilli, R. Amorati, and C. Tringali. "Chain-breaking antioxidant activity of hydroxylated and methoxylated magnolol derivatives: the role of H-bonds." *Organic and Biomolecular Chemistry*, vol. 15, no. 29, 2017, pp. 6177-6184. doi:10.1039/c7ob01195d

11. Lephart, Edwin D. "Skin aging and oxidative stress: Equol's anti-aging effects via biochemical and molecular mechanisms." *Ageing Research Reviews,* vol. 31, 2016, pp. 36-54. doi:10.1016/j.arr.2016.08.001

12. Niki, Etsuo. "Role of vitamin E as a lipid-soluble peroxyl radical scavenger: *in vitro* and *in vivo* evidence." *Free Radical Biology and Medicine,* vol. 66, no. 1, 2014, pp. 3-12. doi:10.1016/j.freeradbiomed.2013.03.022

13. Tantavisut, Saran, A. Tanavalee, S. Honsawek, et al. "Effect of vitamin E on oxidative stress level in blood, synovial fluid, and synovial tissue in severe knee osteoarthritis: a randomized controlled study." *BMC Musculoskeletal Disorders*, vol. 18, no. 1, 2017, pp. 281. doi:10.1186/s12891-017-1637-7

14. Jiao, Zongxian, J. Chang, J. Li, D. Nie, H. Cui, and D. Guo. "Sulforaphane increases Nrf2 expression and protects alveolar epithelial cells against injury caused by cigarette smoke extract." *Molecular Medicine Reports*, vol. 16, no. 2, 2017, pp. 1241-1247. doi:10.3892/mmr.2017.6700

15. Jiang, Qing. "Natural forms of vitamin E: metabolism, antioxidant, and anti-inflammatory activities and their role in disease prevention and therapy." *Free Radical Biology and Medicine,* vol. 72, 2014, pp. 76-90. doi:10.1016/j.freeradbiomed.2014.03.035

16. Tantavisut, Saran, A. Tanavalee, S. Honsawek, et al. "Effect of vitamin E on oxidative stress level in blood, synovial fluid, and synovial tissue in severe knee osteoarthritis: a randomized controlled study." *BMC Musculoskeletal Disorders*, vol. 18, no. 1, 2017, pp. 281. doi:10.1186/s12891-017-1637-7

17. Menon, Shreya, C. Lu, R. Menon, J. Schwartz, and Y. Guan. "Effects of Antioxidants in Human Cancers: Differential Effects on Non-Coding Intronic RNA Expression." *Antioxidants,* vol. 5, no. 1, 2016, pp. 1. doi:10.3390/antiox5010001
18. Patel, Bijal, et al. "Concerted redox modulation by sulforaphane alleviates diabetes and cardiometabolic syndrome." *Free Radical Biology & Medicine,* vol. 122, no. 1, 2018, pp. 150-160. doi:10.1016/j.freeradbiomed.2018.02.004
19. Nguyen, Truyen, et al. "The Nrf2-antioxidant response element signaling pathway and its activation by oxidative stress." *The Journal of Biological Chemistry*, vol. 284, no. 20, 2009, pp. 13291-13295. doi:10.1074/jbc.R900010200
20. Wojtyla, Łukasz, et al. "Different Modes of H_2O_2 Action During Seed Germination." *Frontiers in Plant Science*, vol. 7, no. 1, 2016, pp. 66. doi:10.3389/fpls.2016.00066
21. Sita, Giulia, P. Hrelia, A. Graziosi, and F. Morroni. "Sulforaphane from Cruciferous Vegetables: Recent Advances to Improve Glioblastoma Treatment" *Nutrients,* vol. 10, no. 11, 2018, pp. 1755. doi:10.3390/nu10111755
22. Bahadoran, Z., P. Mirmiran, F. Hosseinpanah, M. Hedayati, S. Hosseinpour-Niazi, and F. Azizi. "Broccoli sprouts reduce oxidative stress in type 2 diabetes: a randomized double-blind clinical trial." *European Journal of Clinical Nutrition*, vol. 65, no. 8, 2011, pp. 972-977. doi:10.1038/ejcn.2011.59

JOURNAL OF
EMERGING INVESTIGATORS

Article

Role of environmental conditions on drying of paint

Deepti Aggarwal, Riya Dutta, Bhaskar Dutta
Troy High School, Troy, Michigan

SUMMARY

Most manufacturing industries paint their products to protect them from environmental degradation and enhance aesthetics. Reducing paint drying time is an important step in improving production efficiency and reducing costs. To find the most effective way to dry paint, we performed a series of 60 experiments by varying different environmental conditions: humidity, lighting, substrate roughness, and paint color. We hypothesized that decreased humidity would lead to faster drying, ultraviolet (UV) light exposure would not affect the paint colors differently, white light exposure would allow for longer wavelength colors to dry at a faster rate than shorter wavelength colors, and substrates with higher roughness would dry slower. We constructed a custom paint booth to control the environmental conditions for a variety of painted samples and regularly weighed the samples to monitor the drying rate. Our experiments showed that trials under high humidity dried slightly faster than trials under low humidity, contrary to the hypothesis. We found that white paint had the slowest drying rate compared to red, yellow, and blue paints under ambient and white light, while under UV light the drying rate of all paints were similar to one another. Colored paints dried the fastest on a metal substrate followed by canvas and then wood, following the increase in roughness of the substrate. Overall, our studies show that the paint drying process is very much dependent on its surrounding environment, and optimizing the drying process requires a thorough understanding of the environmental factors and their interactive effects with the paint constituents.

INTRODUCTION

Manufacturing industries, whether they deal with cars, toys, refrigerators, or anything in between, all have one thing in common: they paint their products. This painting process involves the essential step of paint drying following its application on the products during mass production. The time it takes for paint to dry varies for these products; if the time is reduced, the production to market time would be reduced with important financial implications and an increase in efficiency (1-2). Currently, some companies place painted products in ovens to quickly dry them or use radiation heaters. In the case of automobiles, paint tunnels with low humidity hot air are often used for accelerating the paint drying process (3).

Paints are made of microscopic colloidal particles in a liquid. As paint dries, the liquid evaporates, and the paint particles move at different speeds according to their size and settle into layers. Various environmental factors, such as temperature, air flow, and humidity can affect the evaporation rate of liquids (4). These changes can affect the chemical and physical boundary conditions in the drying paint layer and further affect the forces and accelerations on the colloidal particles. The interaction forces acting between these colloidal particles in suspension play an important role in the process of paint drying (1). There are four stages of paint drying (**Fig. 1**). The first stage is known as settling. In this stage, the particles of the paint fit into place and begin to stop moving; no noticeable differences in weight or paint dryness are evident here. The second stage, known as squashing, is used to measure the rate of paint drying, as this is where paint rapidly declines in weight and the solvent evaporates quickly. The third stage is called inversion. This stage results in a small increase in weight for the paint samples due to air becoming trapped in the now solid paint. This stage may or may not be present in all paint drying processes. The fourth and final stage of paint drying is known as diffusion. From here, the paint gradually declines in weight, and continues evaporating solvent until no more evaporation is possible, at which point the sample is considered “cured” (5-6). Paint

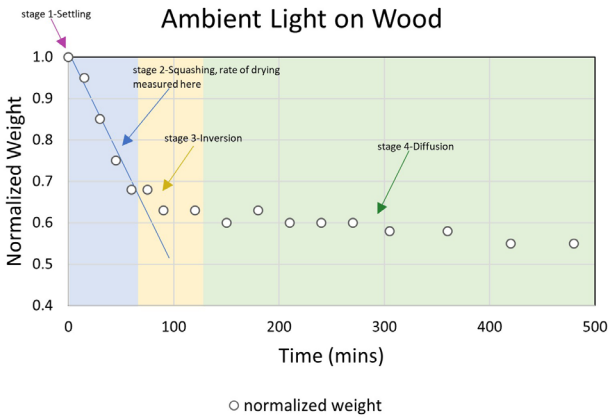

Figure 1. Four independent stages of paint drying as indicated by preliminary testing. The rate of drying was measured from the slope of the blue section of the plot in stage 2 (Squashing). Most of the solvent evaporated in this stage. The yellow section represents stage 3, inversion, and the green section represents stage 4, dispersion.

particles also coalesce in the final stage of drying. Companies may use latex paints or short-wave infrared curing to increase paint drying speed and efficiency (7). The current study aims to investigate the role of the above-mentioned environmental factors on paint drying in order to better understand the drying process and, in turn, aid in improving the efficiency of the process.

For these experiments, the drying rates of household acrylic paints were tested under different environmental conditions to evaluate the effect of individual factors (8). The goal of this study was to find out how the environmental conditions such as humidity, lighting, paint color, and substrate affect the rate of drying of household acrylic paint. For each of the various independent variables to be tested, we formulated a different hypothesis. We hypothesized that a decrease in room humidity will promote faster evaporation of the liquid solvent in the paint and result in a higher paint drying rate. We predicted that painted samples exposed to ultraviolet (UV) light would not exhibit a correlation between the color of the paint and rate of paint drying. Under white light, however, we hypothesized that colors characterized by shorter wavelengths will dry at a slower rate than colors characterized by longer wavelengths because shorter wavelengths have more energy. If shorter wavelengths of light are reflected, then less energy is being absorbed. Finally, we hypothesized that a higher substrate roughness will mean thicker layers of paint at the troughs and would result in a slower drying rate. The goal of this study was to find the environmental conditions that could increase the speed of paint drying and potentially increase efficiency of the relevant manufacturing processes. Trials under high humidity dried slightly faster than trials under low humidity. We also found that white paint had the slowest drying rate compared to red, yellow, and blue paints under ambient and white light. However, under UV light, the drying rate of all paints were similar. Colored paints dried the fastest on a metal substrate followed by canvas and then wood, following the increase in roughness of the substrate.

RESULTS

In this study, we conducted a series of experiments to investigate how environmental conditions such as humidity, lighting, paint color, and substrate affected the rate of drying of household acrylic paint. We performed a total of 60 trials, each spanning a total test time from 500 minutes to up to 1700 minutes. Each experiment involved applying paint of a specific color on either a canvas, wood, or metal substrate, and subsequently measuring the weight of the substrate at periodic time intervals. The rate of the drying process is expressed as the normalized weight loss per unit time (**Equation 1**) during the squashing stage of the paint drying

$$\text{Normalized weight loss at time 't'} = \frac{\text{Initial paint weight} - \text{Paint weight at time 't'}}{\text{Initial paint weight}} \quad \textbf{(1)}$$

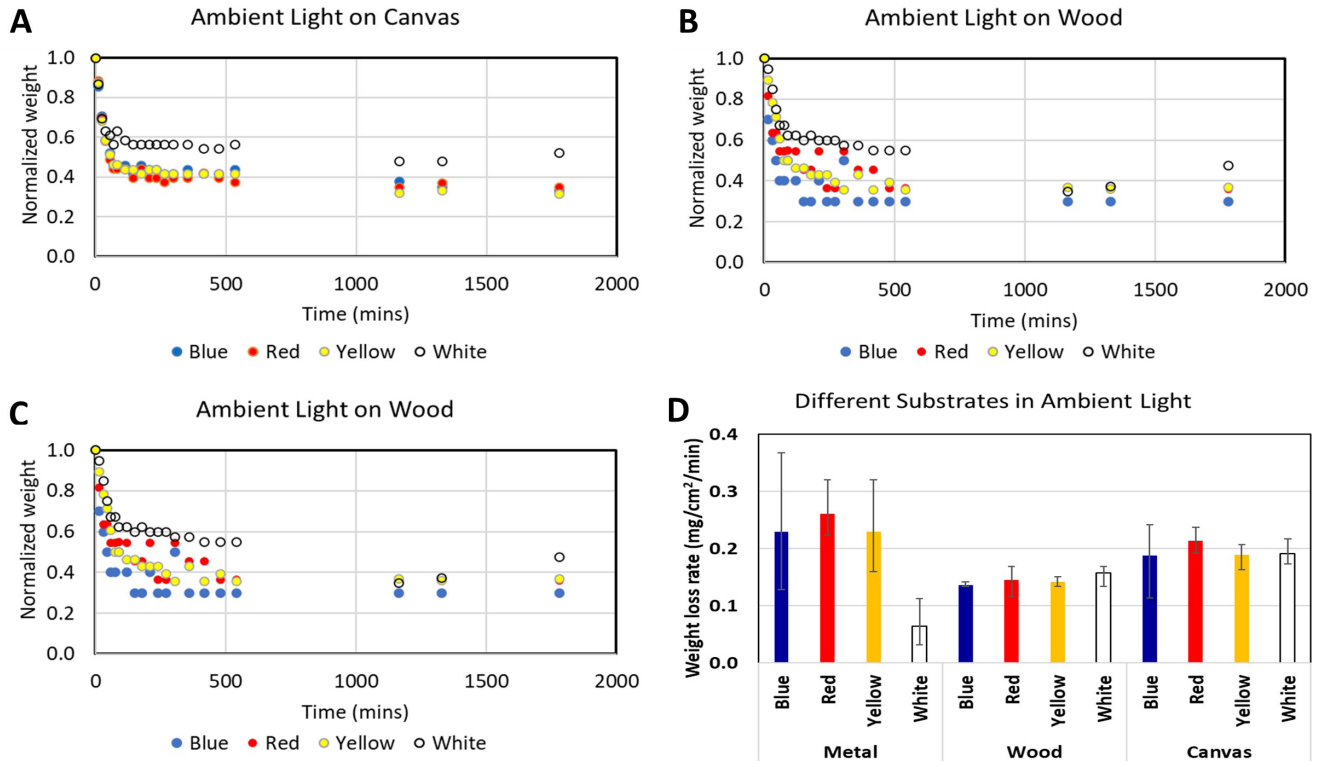

Figure 2. Control and modified roofs. Craft store birdhouse roofs were modified with different mitigation devices. **a)** Control roof with no mitigation device. **b)** Rounded edge mitigation device. **c)** Barrier edge mitigation device. **d)** Upright airfoil mitigation device.

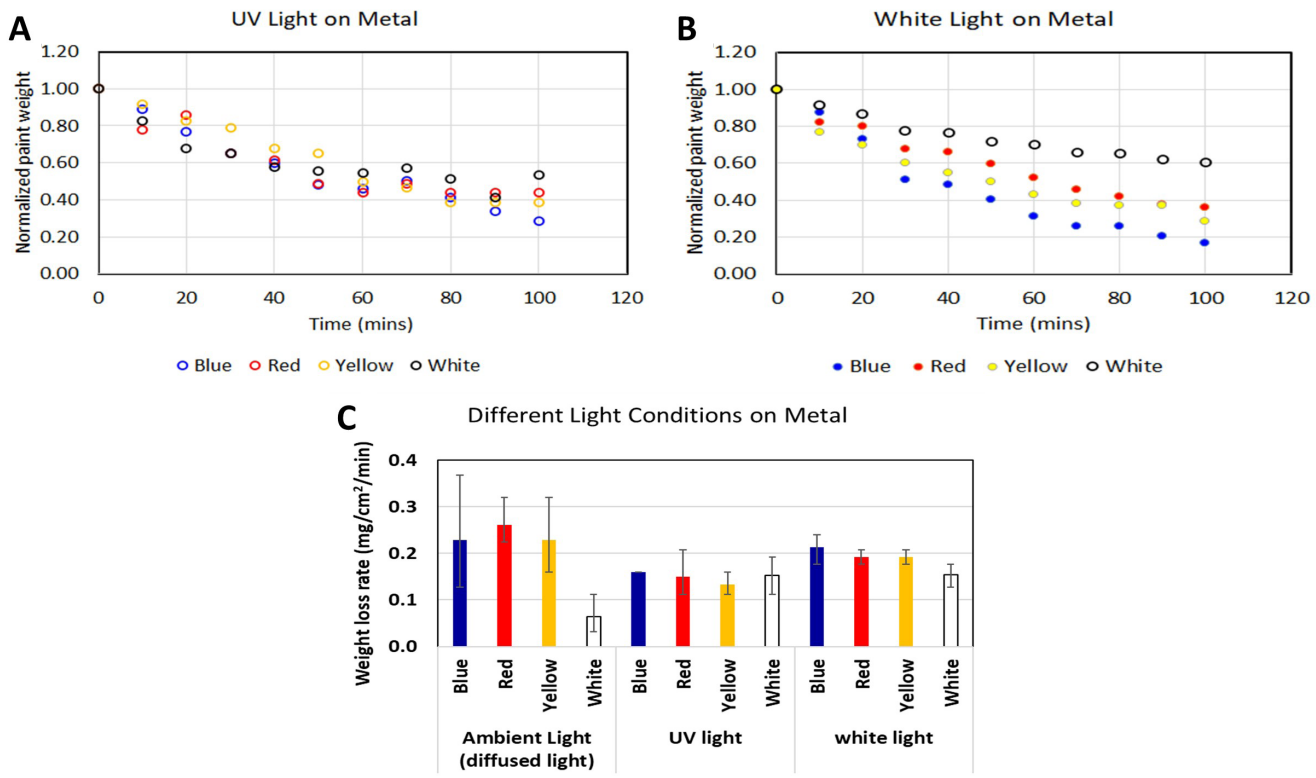

Figure 3. Drying rates (squashing stage) of different paint colors in A) UV light, **B)** white light, and **C)** ambient light on a metal substrate. Under UV light, there was no observable difference between the drying rates of the different colors. Under white light and diffused light, white paint dried at a slower rate compared to the other colors. The error bar shows the max and min of each data set.

process:

The overall trend of the normalized weight loss for all the samples during drying was exponential decay (**Fig. 1**). The normalized weights declined from 1.0 down to between 0.3 and 0.5 until the plateau at about 100 minutes (**Figs. 2 and 3**). Almost 80% of the total weight loss occurred within the first 100 minutes, and the remainder over the next 400 minutes. Since paint samples on different substrates had different surface area, we calculated the drying rate as weight loss per unit area per unit time to allow proper comparison between different substrates.

Next, we analyzed the effect of several variables on the rate of paint drying. Since we hypothesized that the drying rates of different painted substrates under ambient light would be influenced by surface roughness, we used a surface profilometer to determine roughness of canvas, metal, and wood substrate samples. The mean (standard deviation) of the surface roughness in the z direction from peak to valley of the canvas was 26.79 µm (2.73 µm). The roughness of the wood was the greatest at 34.17 µm (2.56 µm), and metal roughness was the least at 0.56 µm (0.06 µm) (**Table 1**). The drying rates of paint in ambient light on these substrates varied depending on which substrate we used (**Fig. 2**). For blue, red, and yellow paint, the metal had the highest drying rate (blue: 0.23 mg/cm²/min, red: 0.26 mg/cm²/min, yellow: 0.23 mg/cm²/min), followed by canvas (blue: 0.19 mg/cm²/min, red: 0.21 mg/cm²/min, yellow: 0.19 mg/cm²/min) and then wood (blue: 0.14 mg/cm²/min, red: 0.15 mg/cm²/min, yellow: 0.14 mg/

Table 1. Substrate sizes, average amount of paint applied on each substrate, average paint area and approx. paint weight per unit area on different substrates.

Type of Substrate	Substrate roughness (µm)	Sample area (mm x mm)	Average paint weight at start (g)	Average paint surface area (mm^2)	Paint weight per unit area (mg/mm^2)
Metal	0.56	25 x 25	0.142	625	0.23
Wood	34.17	45 x 40	0.268	1120	0.24
Canvas	26.79	65 x 65	0.468	2025	0.23

cm²/min). These results support our hypothesis that rougher surfaces (wood in this case) dry more slowly. However, the drying rate of white paint was much lower on metal, while the drying rates of white paint on both wood and canvas were much higher. This indicates that the surface roughness is not the only influencing factor in the process of paint drying.

Next, we investigated the effect of various lighting on the drying rates of the four colors on metal substrates. Metal substrates were chosen because metal is commonly used in a wide range of industrial manufacturing processes. Under ambient light, the blue, red, and yellow paints dried at similar rates (0.23, 0.26, and 0.23 mg/cm²/min, respectively), while the white paint dried much more slowly (0.06 mg/cm²/min). Under direct white light, all three colors had similar drying rates, with blue at 0.21 mg/cm²/min, and red and yellow both at 0.19 mg/cm²/min, but white at a slightly lower rate of 0.15 mg/cm²/min. The drying rate of all paints were similar under UV light (blue: 0.16 mg/cm²/min, red: 0.15mg/cm²/min, yellow: 0.13 mg/cm²/min, white: 0.15 mg/cm²/min) (**Fig. 3**). These results show that slower drying of white paint occurs under white light and ambient light, but not in the presence of UV light.

Finally, we studied the effect of humidity on the drying rate of blue paint on various substrates because the average paint drying time of blue paint was in between the rest of the drying times (**Fig. 4**). In lower humidity (31%), the average drying rates were approximately 0.16, 0.11, and 0.16 mg/cm²/min for metal, wood, and canvas, respectively. In higher humidity (43%), the average drying rates were slightly higher (0.23, 0.14, and 0.19 mg/cm²/min for the metal, wood, and canvas substrates, respectively).

DISCUSSION

In the three experiments conducted, the four stages of paint drying were clearly visible when the normalized weights were plotted over time (**Fig. 1**). In the present experiments, the second drying stage or the squashing period varied from 60 to 100 minutes, while we observed the complete drying between 500 to 1700 minutes for various conditions.

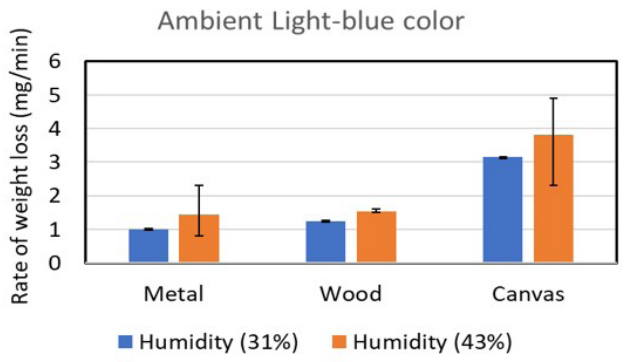

Figure 4. Drying rates (squashing stage) of blue paint on different substrates in ambient light at high (43%) and low (31%) humidity levels. At both humidity levels, drying rate is fastest on metal, followed by canvas and slowest on wood. On all three substrates, blue paint dries faster under higher humidity. The error bar shows the max and min of each data set.

When analyzing and comparing the weight loss data of various paints under different conditions, we normalized the weight of the paint by taking the weight change as a fraction of the original paint weight (**Equation 1**). As seen in **Figs. 1-3**, the starting point was 1.0 and over time the weight decreased until it reached a plateau, indicating the fraction of solids in a particular paint. We tried to apply a similar amount of paint per unit area of substrate in all the experiments (**Table 1**), the actual weight of each sample varied marginally from one to another. Normalizing the paint weight helped to eliminate the effect of this weight variation between different experiments and allowed a direct comparison between various experiments.

After we established the general trend for paint drying, the effects of specific variables were tested. We first considered the substrate type. Using a surface profilometer, we determined that the order of substrate roughness from least to greatest was metal, canvas, then wood (**Table 1**). For the blue, red, and yellow paints, the drying rate was the highest on metal, followed by canvas, and the rate was the slowest on wood substrates (**Fig. 2D**). This observation supports our hypothesis that the increased roughness of the substrate decreases the rate of paint drying. It is possible that a surface with higher roughness reduces the rate of solvent evaporation due to higher surface asperity in these samples. However, it is important to note that the drying behavior of white paint did not support this hypothesis and showed that the metal substrate had the lowest drying rate compared to wood and canvas. This clearly indicates that there are possibly other factors, such as the volume of solids in different types of paints, the paint composition, and the interaction of the paint with the substrate material, that may play a more important role in paint drying than surface roughness alone. This could be a potential future study.

We expected the lighting exposure to affect the paint drying rate because different colored paints would reflect different amounts of visible light energy. In addition, acrylic paints are known to absorb UV light very slowly (7) and consequently result in slow drying under UV light. The light that is absorbed by the paint provides additional energy for evaporation of the paint solvent, mainly water. It is well known that light colors in the visible spectrum are associated with specific wavelengths and energies, starting with blue (475nm wavelength), yellow (550nm wavelength) and red (680nm wavelength) in the order of increasing wavelength and decreasing associated energy (9). Red paints reflect red light wavelengths and absorb the rest and are therefore expected to absorb the highest amount of energy among the three colors. This is followed by yellow paint that reflects only yellow wavelength and therefore absorbs the second highest amount of energy. The third is the blue paint that reflects only blue wavelength, and therefore absorbs the least amount of energy among the three colors. White paints reflect all colors and therefore is expected to

absorb the least amount of energy among all the paints in the current study. We expect that a higher amount of absorbed energy promotes a higher rate of evaporation and faster rate of paint drying.

Our hypothesis was that under white light, paint colors with increasing wavelength (blue, followed by yellow, and then red) would be associated with a decrease of drying rate because colors characterized by shorter wavelengths would reflect wavelengths of light with higher energy and therefore dry slower. We found this to be incorrect, as under white light as well as under ambient light drying rate of all three colors, blue, yellow and red were similar to each other even though blue has the shortest wavelength and red has the longest (**Fig. 3B**) wavelength. This apparent contradiction of the hypothesis and the drying rate of different paint colors indicates that the paint constituents possibly play a bigger role than the light reflection of individual colors in the process of paint drying. However, all the studies under white light and ambient lighting clearly show that white paint dries more slowly than the colored paints as predicted by our current hypothesis (**Fig. 3C**). The relatively slower drying rate of the white paint may be attributed to the reflection of most of the light by white paint. Studies in the literature have reported that white paints containing titanium dioxide (TiO_2) and acrylic can reflect up to 92% of incident light (10). Under UV light on metal, all paints seemed to dry at the same rate, which is possibly due to the fact that UV radiation is not reflected differently by any visible paint colors (**Fig. 3A**).

Finally, we studied the role of humidity on the rate of drying. We hypothesized that in ambient lighting, reduced humidity will increase paint drying rate. This is expected as reduced humidity will promote convection and aid evaporation of solvents from the paint. However, our humidity experiments with blue paint on metal showed that higher humidity yielded marginally higher drying rates (**Fig. 4**). These results do not line up with published literature (1, 6) and our hypothesis. As indicated in literature, air flow is a critical factor in the process of paint drying and possibly the most dominant factor (8). In the current experiments, the low humidity trials were performed in the closed paint booth with minimal air movement to isolate the paint booth from the rest of the room and to prevent the ambient humidity altering the humidity of the paint booth. While this allowed the paint booth to have lower humidity than the rest of the room, it also shut out air circulation and reduced convection and evaporation. Thus, we attributed this as the cause of lower drying rate at lower humidity levels during the current study. In conclusion, air movement and humidity are inter-related in the paint drying process and need to be tested independently.

One important factor in the drying process was the relationship between the paint color and underlying solvent, or the ratio of the paint to solid volume (11). Solid content in a paint mainly refers to the residue that is retained in the paint after drying and this mainly consists of pigments, binders and certain additives. In comparison to the other colors, we found the white paint had a higher volume of solids (50% vs. 30-40% for blue, red, and yellow) in the present study. This variation in the solid volume was unavoidable even though we used the same brand and type of paint across all the trials. The colored paints simply require less volume of solid than the white paint. Higher volume of solid in the white paint means lower solvent content and this further highlights the fact that the drying rate of white paint was slower even with lower solvent content.

In the current study, the experiments were conducted under a controlled environment, with only one variable intentionally being altered in each variable trial. We repeated each experimental condition three times and used an average value for further analysis of data. Nonetheless, there were some instances where experimental error may have affected the data. One example is that each time we opened the paint box to perform weight measurements the paint box environment may have been affected by outside air flow. Another potential source of error is the drying rate calculation from the recorded weight loss data. As mentioned in the introduction and results section, we calculated the drying rate from the slope of the weight loss graph during the squashing stage. Weight loss is typically linear in this stage and end of squashing is marked by a significant change in the slope of the plot (**Fig. 1**). We took care to calculate drying rate from this section of the plot. Large sample size and repeated trials helped to reduce the impact of these errors.

In the future, this study could be expanded in multiple ways. Two lessons learned from the current experiments are the importance of accounting for as many confounding variables as possible and examining the hypotheses in light of unexpected findings. An experimental scheme based on the design of experiments and a detailed statistical analysis using analysis of variance could be employed to examine the effect of different variables that interact with each other. A future study isolating the effect of humidity from the effect of air flow is needed to better understand the effect of humidity on the paint drying process. In addition, various types of paints could be tested, such as back paints vs white paints, and water-based paints vs. oil-based paints that have different pigments and different solvents and/or different concentrations of solvents to understand the effect of the pigments and solvents on drying. Since paint drying has a very important application in the manufacturing industry, studies involving the drying of paint on curved vs. flat surfaces and on larger samples may be of significant interest to the industrial community. The research question is broadly applicable to all manufacturing products from refrigerators to airplanes and across various industries. Shortening the paint drying process through environmental changes will help to improve drying efficiency and be easy to implement.

METHODS

The experiments were performed in a paint booth measuring 0.9m (length) x 0.5m (width) x 0.9m (height), built from a used cardboard box. The paint booth included a

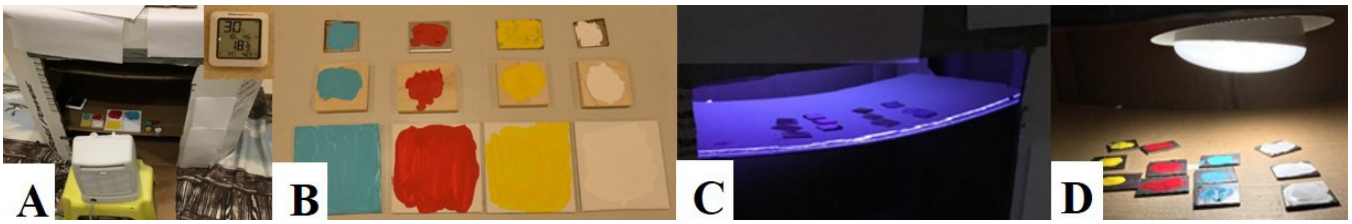

Figure 5. Experimental design. A) Paint booth with thermometer and hygrometer. **B)** Substrates and colors used. Bottom to top: canvas, wood, and metal. Left to top: blue, red, yellow, and white paint. **C)** UV light inserted into the top of the paint booth. **D)** White light inserted into the top of the paint booth.

window for easy access to samples and shelves to hold the samples (**Fig. 5A**). The goal of this paint booth was to control as many environmental factors as possible. Temperature and humidity were measured using a ThermoPro TP50 digital hygrometer (**Fig. 5A**). The average temperature during all the experiments was recorded between 20ºC and 24ºC, approximately room temperature. Acrylic paints from the same brand (Apple Barrel) were used for all experiments (**Fig. 5B**). A Zeiss Surfcom130A profilometer was used to measure substrate surface roughness prior to painting. The weight of the paint samples was measured in an AMIR digital weighing scale with 500g maximum capacity at 0.01g increments. The independent variables tested included the lighting, humidity, substrate type, and paint color. All experiments were performed in ambient light, white light (**Fig. 5D)**, and UV light (**Fig. 5C**). Normal humidity and low humidity conditions were achieved by placing silica gel desiccants in the paint booth for the low humidity and leaving the box unaltered for the normal humidity. Three substrates (wood, canvas, and metal) were used in the experiments. Four paint colors were tested: Caribbean blue, yellow, white, and apple red. Details of the substrate size, initial paint weight, paint area, and paint weight per unit area are given in **Table 1**. We attempted to maintain similar values for 'paint weight per unit area' for all experiments to allow a better comparison of results among the various experiments.

The first step of our experiments was to measure and record the weight of each unpainted sample of wood, canvas, and stainless steel (**Fig. 5**). We used this to normalize the weight in calculations, so the mass of the original sample does not affect the rate (**Equation 1**). Each substrate was then hand painted using nylon/polyester 3-inch brushes with either acrylic Caribbean blue, yellow, white, or apple red paint (**Fig. 5B**). The weight of the painted samples of wood, canvas, and metal (with different colors) was recorded as a function of time (**Fig. 2**). New samples were used for each experiment and experiments for every variable were repeated three times.

The samples were placed in the paint booth and weighed every 15 minutes for the first 90 minutes. Measurements were taken at longer intervals for up to 500 minutes in all cases and continued up to 2000 minutes if the normalized weight continued to decline. However, in later experiments, since the second stage (squashing) was the focus of interest for this study, strict measurements were taken only up until the point of inversion. Prior to each trial, the temperature and humidity in the paint booth were recorded using a thermometer and hygrometer. Experiments (total of 60) were repeated to test varying conditions of lighting, humidity, substrate, and paint color. The data were calculated as the mean of three trials and plotted along with the error bars, showing the max and min of each data set, and analyzed. Paint weight loss was plotted as the normalized weight at time t, defined as the ratio of the difference between the initial weight and weight at time t to the initial weight. By applying regression analysis in the linear "squashing" region, the slope of the plot (mg/min) was calculated, and this was used to determine the rate of paint drying (**Fig. 1**).

Received: September 23, 2020
Accepted: February 14, 2021
Published: February 20, 2021

REFERENCES

1. Saranjam, Nazli. "Transport Phenomena in Drying Paint Films", tspace.library.utoronto.ca/bitstream/1807/76813/1/Saranjam_Nazli_201611_PhD_thesis.pdf, Accessed 12/17/2019.
2. "Paint", www.britannica.com/technology//paint, Accessed 12/17/2019.
3. www.beccainc.com/dry-paint-technologies-available/, accessed 12/29/2020.
4. justpaint.org/technical-notes-on-drying/, Accessed 12/29/2020.
5. Drying of Water-based Paints, www.maths-in-industry.org/miis/312/1/Drying-of-water-based-paints.pdf, Accessed 1/12/2019.
6. Heat and mass transfer in latex paints during drying, Stuart G Croll, J. of Coatings Technology, Vol 59, No 751, Aug 1987. pp. 81-92.
7. The effects of temperature and air humidity on drying of waterborne paint products, Hong Diep Bui, Ph.D. Thesis, Industrial Management, Centria University of Applied Sciences, October 2017
8. "Drying Parameters Application Guidelines." *Teknos*, www.teknos.com/globalassets/teknos.uk/industry/industrial-

JOURNAL OF
EMERGING INVESTIGATORS

Article

Development and implementation of enzymatic and volatile compound-based approaches for instantaneous detection of pathogenic *Staphylococcus aureus*

Divya Nori[1], Evani Patel[2], Amanda Martinez[1]
[1]Milton High School, Milton, Georgia
[2]Kennesaw Mountain High School, Kennesaw, Georgia

SUMMARY

***Staphylococcus aureus* (*S. aureus*) has a mortality rate of up to 30% in developing countries. In contrast, the mortality rate of *S. aureus* in the U.S. is less than 5%. One reason for the six-fold increase in fatality in underdeveloped communities is lack of access to a rapid, accurate, and user-friendly diagnostic method to enable timely detection of these infections. The purpose of this experiment was to determine if enzymatic and volatile compound-based approaches would perform more quickly in comparison to existing *S. aureus* diagnostic methods and to evaluate these novel methods on accuracy. Further, we sought to implement them in a reusable 3D-printed instantaneous detection device. A combination of droplet transmission tests and direct contact tests were developed and evaluated to create a comprehensive method by which individuals can diagnose their condition as pathogenic *S. aureus*, incorrect use of device, or another infection. We hypothesized that the approaches developed in this study would perform more quickly than existing approaches. Ultimately, our device provided results in less than 30 seconds, which is much quicker than existing methods that take anywhere from 10 minutes to 48 hours based on approach. Statistical analysis of accuracy provides preliminary confirmation that our device based on enzymatic and volatile compound-based approaches can be an accurate and time-efficient tool to detect pathogenic *S. aureus*.**

INTRODUCTION

Staphylococcus aureus, hereby referred to as *S. aureus*, is the second-most common healthcare-associated infectious bacteria (1). Pathogenic *S. aureus* can infect many organs, the most common being the respiratory tract. *S. aureus* is a leading cause of death in hospitalized patients, with a mortality rate of up to 30% in underdeveloped communities (2). Pathogenic strains are often the cause of ventilator-associated pneumonia or a bacterial infection following influenza, both of which can be lethal conditions if not detected quickly (3). For *S. aureus*, respiratory droplets are the primary mode of transmission, presenting a potential path by which a solution can be created. The ability to diagnose a respiratory tract staph infection in a cost-effective, self-administrable, and time-efficient manner is critical to reducing the mortality rate in developing countries. Current diagnostic methods include the swabbing and incubation of respiratory tract cultures, but results from these traditional tests take up to 48 hours to determine a definitive diagnosis (4). However, some rapid diagnostic testing methods have been researched in prior literature.

Polymerase chain reaction (PCR) is one method that has been pursued for potential early detection of *S. aureus* in the respiratory tract. The genetic biomarker that provides *S. aureus* with pathogenic properties is amplified and can therefore be more easily detected (5). However, PCR is not easily accessible in the developing world, and is not a viable diagnostic approach in patients' homes or smaller clinics due to the need for lab access (6). A rapid diagnostic method developed for *S. aureus,* known as the "rapid staph test" employs a latex fixation test and a lateral flow test. The latex fixation test or latex agglutination is used in the identification of microorganisms. If *S. aureus* antibodies are present, latex beads covered with antigens will firmly clump together to form a mass. The lateral flow test is more widely used, and if *S. aureus* antibodies are present when a sample is applied to nitrocellulose film, a visible line will form. However, while these tests are more accessible than PCR, they are not widely available in developing countries and are not reusable (7). Creating a diagnostic method that could be used more than once would allow for an entire community in a developing country to use a single test device. To bridge the gap seen in prior literature, four biochemical tests were assessed for time-efficiency and accuracy in this study. The tests were evaluated individually in flasks and later evaluated together within the device to ensure efficacy of the diagnostic tool.

The four biochemical tests evaluated are cost-effective, compound-based, and easily interpretable, making them unique from previous tests. Two of the tests, the calcium hydroxide test and hydrogen sulfide test, are droplet-based, meaning that the result will be displayed when the user exhales into the device. The remaining two tests, the hyaluronidase test and catalase test, are direct contact approaches meaning

that they are intended to analyze a sample that the user takes from the back of their throat using a sterile swab which is provided to the user with the device. Both testing methods ensure that patients in developing nations would not need additional equipment to perform the tests, and the patients could easily administer it themselves. The calcium hydroxide test was chosen to indicate to the user whether they are using the device correctly. To ensure that the gas sample is not contaminated by the outside air and is primarily the user's breath, the calcium hydroxide test detects the presence of carbon dioxide. This is because exhaled air consists of 4% to 5% carbon dioxide by volume which is a 100-fold increase over the amount of carbon dioxide in the air (8). Aqueous calcium hydroxide solution reacts with carbon dioxide gas to produce carbonic acid. Phenolphthalein indicator, a chemical compound that is colorless in acidic solutions and pink in basic solutions, turns clear when in contact with carbonic acid, providing a colorimetric indication of proper device use.

Hyaluronidases are a family of enzymes that breakdown the substrate hyaluronate. Several microorganisms have genes that encode hyaluronidase, including bacteria in the *Bacteroides*, *Treponema, Clostridium,* and *Propionibacterium* genera. Species in these genera can be found in the human gastrointestinal tract, intestines, or skin, but the only bacteria present in the human respiratory tract that produce hyaluronidases are *S. aureus, Streptococcus pyogenes*, and *Streptococcus pneumoniae* (9). Detecting the hyaluronidase enzyme would establish the presence of one of these three bacterial species, providing the rationale for the development of this test. When hyaluronidases come into contact with hyaluronic acid, hyaluronate is degraded into an oligosaccharide (10). If an oligosaccharide is produced in the enzyme reaction product, a chemical indicator for simple sugars such as Benedict's solution can detect the presence of hyaluronidase and establish that one of the three bacteria is present. Benedict's solution changes from blue to green when in the presence of a sugar polymer such as an oligosaccharide. The user is instructed to not eat anything for three hours before swabbing the back of their throat for this test so that traces of extraneous sugar are not present. This would help ensure that the activity of hyaluronidase is being detected and lower the chance of a false positive. While this method has not been used as an enzymatic assay for hyaluronidase in the past, we attempted to provide evidence for the efficacy of this approach due to its easy interpretability for users who are self-administering the test.

The catalase test was chosen as one of the contact-based tests for this device to differentiate between *S. aureus*, *S. pyogenes*, and *S. pneumoniae* (after a positive result for the hyaluronidase test). *S. aureus* is catalase positive, while *S. pyogenes* and *S. pneumoniae* are catalase negative because all streptococci lack the enzyme catalase (11-12). Currently, *S. aureus* is speculated to use hyaluronidase as a virulence factor. However, since this has not been supported with sufficient evidence, a more fool-proof approach to identify the pathogenicity of the bacterial strain is necessary (13). Pathogenicity must be established to attribute the positive result of the hyaluronidase test to a *S. aureus* infection and not a hyaluronidase enzyme encoded by human cells or non-pathogenic *S. aureus* (14-15). Pathogenic staphylococcus strains release hydrogen sulfide-based cytotoxins called volatile sulfur compounds (VSCs). While for some species of bacteria both the non-pathogenic and pathogenic strains produce hydrogen sulfide, it has been established that both dimethyl-disulfide and methanethiol are released by pathogenic *S. aureus* and not by non-pathogenic strains (16-17). The hydrogen sulfide test turns a copper sheet from copper colored to black in the presence of dimethyl-disulfide or methanethiol. The color change is based on the reaction between the VSC and copper that produces copper sulfide and copper oxide (18-19). When the results from the calcium hydroxide test, hyaluronidase test, catalase test, and hydrogen sulfide test are interpreted in conjunction, a patient's condition can be identified as pathogenic *S. aureus*, incorrect use of device, or a different infection (result cannot be determined with this device). The two direct contact tests (catalase and hyaluronidase) and two breath-based tests (calcium hydroxide and hydrogen sulfide) were developed to create a diagnostic process that will perform accurately and efficiently when hosted in a 3D-printed reusable device.

The central aims of this study were to determine the plausibility of using enzyme biomarkers and volatile compounds released by bacteria to enable early detection, engineer a device applying these findings to detect *S. aureus* in a patient's respiratory tract, and compare the results to existing diagnostic approaches. We hypothesized that the approaches developed in this study would perform more quickly than existing approaches. The null hypothesis can be rejected in favor of this alternate hypothesis because after repeated testing, the device was able to perform in under 30 seconds which is less than the time taken to perform the rapid staph test (10 – 20 minutes) and the *S. aureus* culture test (24 – 48 hours). After Fisher's exact test analysis, a significant difference was observed in hyaluronidase test results between *S. aureus* and *Staphylococcus epidermidis*, hereby referred to as *S. epidermidis*. Non-pathogenic *S. aureus* released a gas (verified by air pressure readings) whose chemical composition triggered a negative result for the hydrogen sulfide test. Therefore, this study provides preliminary confirmation that gaseous metabolites and enzymes can be used to identify certain bacterial infections. Our hypothesis was supported because volatile compound and enzymatic approaches performed in less time than existing methods.

RESULTS

Before assessing the effectiveness of the diagnostic tests, throughout the bacterial incubation process, an air pressure sensor to monitor the production of gas by *S. aureus* and verify that gaseous metabolites were being released. The measured air pressure inside the flask increased over time from 101.325

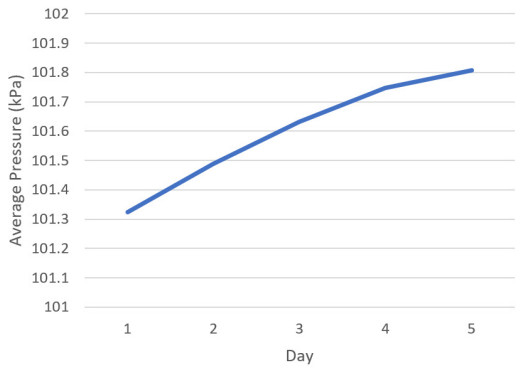

Figure 1. Average air pressure in the Erlenmeyer flasks over time. Each flask contained 50 mL of *S. aureus* broth, and the rate of gas production remained fairly constant as time went on.

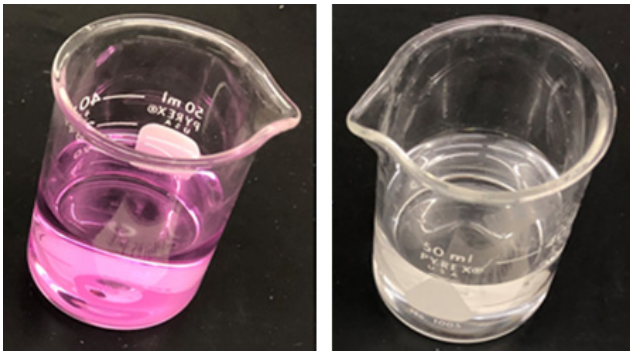

Figure 2. Color change observed due to the reaction of calcium hydroxide and carbon dioxide. Left is before reaction with the addition of phenolphthalein indicator, whereas right is after reaction.

kPA to 101.807 kPA (**Figure 1**). The bacteria produced gas in a way that closely resembled a linear pattern. The linear gas trend was maintained throughout the gas collection process, indicating that the gas production rate remained constant.

The calcium hydroxide test and hyaluronidase test were then evaluated individually in flasks, and the rationale for this portion of the experiment was to determine the optimal conditions for each test. The metric for the calcium hydroxide test was volume of test solution.

We evaluated a range of solution volumes to determine which exhibits the quickest color change (**Table 1**). A direct correlation between solution volume (volume of calcium hydroxide solution onto which the user breaths) and average time in seconds taken to reach a color change was observed. The lowest time taken to reach a color change was 5.1 seconds with a solution volume of 2 mL. Other factors such as room conditions were controlled for, and the samples of healthy breath were taken from the two student researchers, eliminating the need for outside human participants. The researchers blew onto the liquid as they would normally exhale. After identifying the optimal test solution volume of 2 mL, our next experiment was to confirm the observed color change of the calcium hydroxide test when breath is released correctly (**Figure 2**). The beakers initially contained 2 mL of bright pink solution consisting of H_2O, $Ca(OH)_2$, and phenolphthalein. After reacting with carbon dioxide, the solution became transparent (**Figure 2**).

Next, we evaluated metrics for the hyaluronidase test for *S. aureus,* a strain encoding the hyaluronidase enzyme, and *S. epidermidis,* a strain not encoding the hyaluronidase enzyme (**Table 2**). We collected data for several test solution compositions (solvent-solute ratios), and the hyaluronidase test performed the quickest when the solvent-solute ratio was 3:1 with a time of 6.5 seconds (**Table 2**). The solvent was hyaluronic acid, and the solute was Benedict's solution, which was used to detect the presence of an oligosaccharide when hyaluronic acid was degraded by hyaluronidase. This shows that in the device, the volume of hyaluronic acid should be three times the volume of Benedict's solution for the most time-efficient results. This optimal 3:1 acid-indicator ratio was used to confirm the hyaluronidase test's color change with *S. aureus* and *S. epidermidis*. *S. epidermidis* failed to react, so the color remained bright blue/teal (**Figure 3**). *S. aureus* did

Table 1. Time taken to reach a color change from pink to clear for the calcium hydroxide test across different solution volumes.

Test	Sample	Volume of Test Solution (mL)	Average time in seconds (across four trials)
Calcium Hydroxide	Healthy body (breath)	25	64.2
Calcium Hydroxide	Healthy body (breath)	10	28.6
Calcium Hydroxide	Healthy body (breath)	5	8.3
Calcium Hydroxide	Healthy body (breath)	2	5.1

Table 2. Time taken to reach a color change from blue to green for the hyaluronidase test across different ratios of hyaluronic acid and Benedict's solution in the test solution.

Test	Sample	Solvent-Solute Ratio Solution (mL)	Average time in seconds (across four trials)
Hyaluronidase	*S. aureus* (culture)	5 to 1	9.4
Hyaluronidase	*S. aureus* (culture)	3 to 1	6.5
Hyaluronidase	*S. aureus* (culture)	1 to 1	7.9
Hyaluronidase	*S. epidermidis* (culture)	5 to 1	No Reaction
Hyaluronidase	*S. epidermidis* (culture)	3 to 1	No Reaction
Hyaluronidase	*S. epidermidis* (culture)	1 to 1	No Reaction

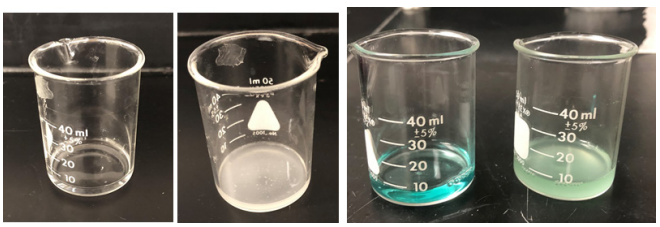

Figure 3. The first panel (starting from the left) shows the result of the catalase test after failing to react with *E. faecalis*, and the second panel shows the result of the catalase test after reaction with *S. aureus*. The third panel shows the result of the hyaluronidase test after failing to react with *S. epidermidis*, and the fourth panel shows the result of the hyaluronidase test after reaction with *S. aureus*.

react, and the color of the solution changed from bright blue to pale green (**Figure 3**).

We next evaluated the catalase and hydrogen sulfide tests individually (**Table 3**). For the catalase test, the average time taken for a color change with the *S. aureus* culture was 4.5 seconds (**Table 3**). The original hydrogen peroxide solution was transparent, and when the *S. aureus* culture reacted, a milky white color resulted (**Figure 3**). However, the *E. faecalis* did not react with the hydrogen peroxide solution, so the beaker remained transparent. The hydrogen sulfide test did not result in a reaction because tested bacterial strains were non-pathogenic (**Table 3**).

We then used CAD software to develop device design prototypes. Our final design involves an opening through which the patient can easily breathe into the compartments, and this opening is designed to streamline the air into the desired locations (**Figure 4**). The bottom portion of the device contains four compartments, one for each test, and the top and bottom portions of the device are sealed together in an airtight fashion. Using this device, we performed a series of 30 final trials (**Figure 5**). These 30 trials consist of 10 *S. aureus* trials, 10 *E. faecalis* trials, and 10 *S. epidermidis* trials, and all of the tests were conducted using non-pathogenic bacteria because pathogenic bacteria were not available to us.

Using data from these final trials, we calculated the Fisher's exact statistic value. We began with the hyaluronidase test, and the null hypothesis was that there is no significant difference in hyaluronidase test results between *S. aureus* and *S. epidermidis* within the device. The alternate hypothesis was that there is a significant difference in hyaluronidase test results between *S. aureus* and *S. epidermidis.* If the computed Fisher's exact test value was less than a p-value of 0.01, the null can be rejected in favor of the alternate hypothesis. The device color sensor detected a pale green color for nine of the non-pathogenic *S. aureus* trials when hosted in the device and detected a blue color for one of the non-pathogenic *S. aureus* trials (**Table 4**). A blue test solution was detected for all 10 of the *S. epidermidis* trials by the device color sensor. The Fisher's exact test statistic value was 0.0001 which shows that the result was significant at $p < 0.01$. The null hypothesis was rejected, displaying that the hyaluronidase test was likely effective within the device.

Table 4. Contingency table for hyaluronidase test, used in the computation of the Fisher's exact test statistic.

	Non-Pathogenic S. aureus	Non-Pathogenic S. epidermidis
Hyaluronidase Positive	9 samples	0 samples
Hyaluronidase Negative	1 sample	10 samples

Table 5. Contingency table for catalase test, used in the computation of the Fisher's exact test statistic.

	Non-Pathogenic S. aureus	Non-Pathogenic E. faecalis
Catalase Positive	8 samples	0 samples
Catalase Negative	2 samples	10 samples

Table 3. Metrics from the catalase and hydrogen sulfide tests.

Test	Sample	Average time in seconds (across four trials)
Catalase	*E. faecalis* (culture)	No Reaction
Catalase	*S. aureus* (culture)	4.5
Hydrogen Sulfide	*S. aureus* (gas)	No Reaction

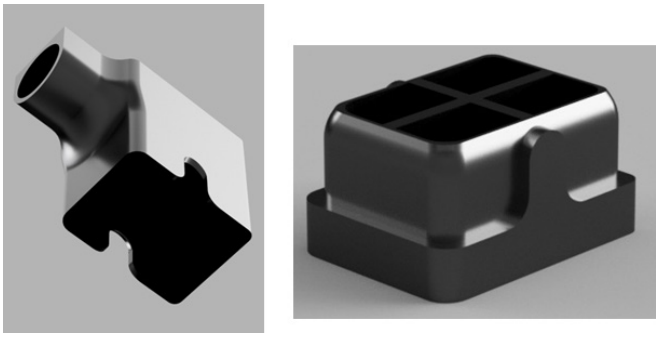

Figure 4. CAD design created to 3D-print the physical device. The main features include a straw-like design to streamline the breath, an airtight lid, and four compartments for test liquids.

For the catalase test, the null hypothesis was that there is no significant difference in a catalase test results between *S. aureus* and *E. faecalis* within the device. The alternate hypothesis was that there is a significant difference in catalase test results between *S. aureus* and *E. faecalis.* The color sensor detected a white color for eight of the *S. aureus* trials and detected no color (transparent) for two of the trials (**Table 5**). The color sensor detected no color (transparent)

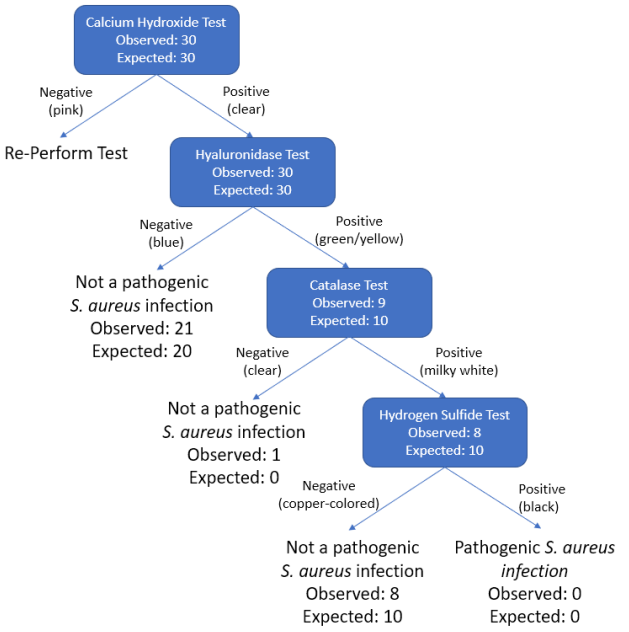

Figure 5. Flow chart of possible end results based on combinations of test results. The observed and expected counts for the final 30 trials conducted within the device are also shown.

for all 10 of the *E. faecalis* trials. The Fisher's exact statistic value was 0.0007, showing that the result is significant at $p < 0.01$. The null hypothesis can be rejected in support of the alternate hypothesis, showing the catalase test's efficacy within the device.

DISCUSSION

The aim of this work was to determine the plausibility of using enzyme biomarkers and volatile compounds released by bacteria to enable early detection and engineer a device to detect *S. aureus* in a patient's respiratory tract. These approaches were then compared to existing approaches based on time-efficiency. This study provides preliminary confirmation that gaseous metabolites and enzymes can be used to identify certain bacterial infections.

The change in pressure demonstrates the accumulation of gas that is released by *S. aureus,* containing the molecules necessary to detect the infection. The stark color change in the calcium hydroxide test indicates that the test could easily identify if a patient were breathing into the device correctly and if the necessary amount of breath were blown into the device. The average time for a distinct color change was 5.1 seconds for a 2 mL trial, making this the optimal volume of liquid to be administered in the compartment for a rapid diagnosis.

The hyaluronidase enzymes present in the *S. aureus* reacted with hyaluronic acid to form the oligosaccharide that turned Benedict's solution from blue to green. Future studies could explore how color change could be maximized - for example, if there was a heating coil in the device to heat Benedict's solution - which may provide a more noticeable color difference. Hyaluronic acid solutions of higher concentration could also provide more easily detectable changes during tests. Evaluation of the hyaluronidase test was conducted using *S. aureus* and *S. epidermidis* cultures, and it is important to note that in these trials, the number of bacterial cells transferred to the test solution likely outnumbered those in a human patient. While evaluation in this study was conducted using pure cultures, in the future, the device could be tested with healthy and infected individuals to observe its efficacy within a real human body. Before human trials can be conducted, the threshold to a positive hyaluronidase result (i.e. the number of colonies needed to trigger a color change from blue to green) could be established.

When the catalase test was performed on *S. aureus* bacteria, the result was a milk white solution. This change from a clear solution to a milky solution occurs because *S. aureus* contains catalase, which detoxifies hydrogen peroxide. *E. faecalis* displayed a negative result, and because it is genetically similar to *S. pyogenes/S. pneumoniae* in that they do not synthesize heme and therefore lack the catalase enzyme, this test serves to classify whether *S. aureus* has been identified if the user's hyaluronidase test is positive (20). If the hyaluronidase test is negative, a conclusion cannot be drawn from the catalase test, but if both the hyaluronidase and catalase tests are positive, *S. aureus* has been identified. However, pathogenicity cannot be established without the hydrogen sulfide test.

Analysis using Fisher's exact test displays the efficacy of the hyaluronidase and catalase tests within the actual device. While testing with non-pathogenic *S. aureus*, *E. faecalis,* and *S. epidermidis* shows that the hydrogen sulfide test displayed a negative result when in contact with non-pathogenic strains of bacteria, further testing is required to ensure that the proper color change occurs when in contact with pathogenic *S. aureus*. The pathogenic strains were not available in our lab for testing. Future studies could examine *S. pyogenes* or *S. pneumoniae* in comparison to *S. aureus* to certify that *S. aureus* can be differentiated from these bacteria.

After repeated testing with all four direct contact and droplet transmission approaches hosted within the device, a result was reached in under 30 seconds which is less than the time taken to perform the rapid staph test (10–20 minutes) and the *S. aureus* culture test (24–48 hours). This supports our initial hypothesis that a test based on enzymatic and volatile compound-based approaches will perform more quickly than existing techniques and provides evidence supporting the plausibility of these approaches for the accurate diagnosis of *S. aureus* infections in the respiratory tract.

METHODS

Mannitol salt agar was prepared and poured into petri dishes as the base for bacterial growth. Samples of non-pathogenic *S. aureus*, *S. epidermidis* (negative control for hyaluronidase test), and *E. faecalis* (negative control for catalase test) were each swabbed onto dishes using an inoculating loop. These plates were incubated for five days at 37°C and were used in testing of the direct-contact tests (hyaluronidase and catalase). Incubation of *S. pyogenes* or *S. pneumoniae* was not permitted in our laboratory environment and hence alternative comparison species were used. In addition, to ensure the production of gaseous metabolites by *S. aureus,* three Erlenmeyer flasks each holding 50 mL of *S. aureus* broth were closed with rubber stoppers to collect gas released by the bacteria. These liquid cultures were grown at 35°C. In 24-hour increments, the pressure inside the flask was measured using an air pressure sensor. This process was repeated over the course of five days to track the production of gas by *S. aureus*. Five days were chosen as supposed to a shorter time frame to observe any change in the rate of gas production over a longer period.

To begin the calcium hydroxide test, limewater was prepared by adding 3 grams of $Ca(OH)_2$ to 150 mL of distilled water. The limewater then rested for 24 hours to dissolve into a homogenous solution. Then, twelve drops of phenolphthalein indicator solution were added to 200 mL of distilled water along with 3 mL of lime water which turned the stock solution a magenta shade. This original solution had a pH of ~13.6 (extremely basic), and phenolphthalein changes

color between 8.2 and 10.0. Among the common acid-base indicators, phenolphthalein has the most basic pH range for a color change which is why it was chosen. The carbon dioxide must cause a drop of approximately 4 pH points before the solution changes from pink to clear. The stock solution was poured into 16 beakers: 4 with 25 mL, 4 with 10 mL, 4 with 5 mL, and 4 with 2 mL of stock solution.

The test was then administered in 16 trials between 2 subjects (the two researchers). A trial comprised of each subject blowing on to the solution, and each subject completed two trials for each volume. The subject would blow onto the solution until the solution changed from a magenta color to clear. These trials were then analyzed to find the average time in seconds to reach a color change depending on the volume of test solution to find the optimal volume that would be used in the detection device. Because accuracy did not decrease with smaller volumes, the optimal volume was chosen as 2 mL because it was the most time efficient. The color change from the calcium hydroxide is easy to detect and interpret for a user in a developing country with little medical knowledge, so the calcium hydroxide test was identified as the best positive control.

The next test developed was for the hyaluronidase enzyme. The components of the hyaluronidase test solution are hyaluronic acid and Benedict's solution. We measured 5 mL of 5.0 M hyaluronic acid into 24 different beakers, and for each set of 8 beakers, a different acid-indicator ratio was tested. The tested hyaluronic acid to Benedict's solution ratios were 5:1, 3:1, and 1:1. Benedict's solution, which is composed of sodium citrate, sodium carbonate, and copper (II) sulfate pentahydrate, changes color when in contact with simple sugars. This indicator was chosen as opposed to the Fehling's test or Tollens' test due to availability in our lab, although these solutions would all display a colorimetric indication of an oligosaccharide. Each set of 8 beakers was then divided into two groups, one group to test *S. aureus* bacteria and one group to test *S. epidermidis* bacteria. *S. epidermidis* was used as a negative control for the hyaluronidase test because its genome does not encode the hyaluronidase enzyme (21). The beakers in each group of four were labeled and corresponded to four petri dishes of *S. aureus* and four petri dishes of *S. epidermidis*. A sterile swab was used to take samples of the bacterial culture and insert it into the solution. Five swabs were taken from each petri dish and inserted into one beaker of each ratio. Using this method, every combination of ratio and bacteria type was tested four times, and time taken to reach a color change was measured for each ratio. While this is not an established method for determining the presence of hyaluronidase, the Fisher's exact test results show promise for the described approach.

The catalase test involved comparison of results from swabs of *E. faecalis* to swabs of *S. aureus*. To begin, a 3% concentration hydrogen peroxide solution was poured into eight beakers. The beakers were separated into two groups of four, one to test *S. aureus* and one to test *E. faecalis*. The beakers corresponded to four petri dishes of *S. aureus* and four petri dishes of *E. faecalis*. *E. faecalis* was used as a negative control for the catalase test because it is a genetically close relative to *S. pyogenes* and *S. pneumoniae* (*S. pyogenes* and *S. pneumoniae* were not available at our lab to us) and cannot synthesize catalase without the presence of heme (22). A sterile swab was used to take a sample from each Petri dish, and each sample was inserted into a different beaker. Similar to the hyaluronidase test, the time taken to reach an observable change from transparent to translucent (milky white) was recorded and analyzed. The catalase test works because catalyze enzymes catalyze the decomposition of hydrogen peroxide into oxygen and water. The oxygen creates bubbles in the solution, making it a translucent color. If both the hyaluronidase and catalase tests are positive, S. aureus has been identified.

The final test, the hydrogen sulfide test, required four copper sheets, each cut to 1 cm by 0.75 cm. The sheets were then scrubbed with sandpaper and dusted off to remove any impurities that may lay on the copper's surface. The sheets were wiped and sprayed with acetone to be ready for the test. Much like the calcium hydroxide test, the effectiveness of breath-based administration was evaluated. Because hydrogen sulfide-based gases are denser than air, the gas released by non-pathogenic *S. aureus* was collected by inserting a gas syringe into an Erlenmeyer flask, ensuring that it was airtight. This gas retrieval process was repeated four times, and the gas produced by *S. aureus* bacteria was released onto the prepared copper sheet. Time taken for a potential color change was recorded. The gas syringe was used to mimic the force of a human breathing into the device. While a color change was not observed because non-pathogenic bacterial strains were unavailable, the presence of hydrogen sulfides are likely the only cause of a potential change in color of copper sheets in this use case because when in contact with regular air, copper takes years to exhibit a significant color change (23). Future experiments must be conducted to ensure that a color change to black occurs in the presence of gas released by pathogenic *S. aureus*.

The following steps were taken to create the physical device. A CAD design was created in TinkerCAD, and the design allows room for four solutions needed for the chemical tests, a water-proof compartment for the color sensor and Bluetooth module, a cylindrical apparatus through which the patient can easily breathe into the device, an airtight lid which can be easily removed to interpret LED results, clean compartments for solutions, and refill the device for reuse. A TCS230 Arduino-based color recognition system, HC-05 Bluetooth module, an Arduino Nano board, and LED lights were used to configure the electronic system embedded into the device. A color sensor emits a white light and monitors the red, green, and blue components of the light reflected by a substance using three receivers. The intensity of red, green, and blue light reflected enables the sensor to determine the color of the substance. In this way, potential color changes

from each test are detected. When a user receives the device, these electronic components will be integrated into the 3D-printed casing, costing less than 30 dollars for a device that can sustain an entire community. Based on the color of each of the test solutions, appropriate LED lights are activated, telling the patient their results for each test. The integration of a sensor and LED-based result interpretation removes potential human reading errors.

After the device creation process was complete, the final stock solutions as refined in the individual chemical test trials were poured into the appropriate compartments. We conducted 30 final trials to assess the overall functionality of the device. These trials consisted of 10 *S. aureus* trials, 10 *S. epidermidis* trials, and 10 *E. faecalis* trials. The direct contact tests (hyaluronidase and catalase) were conducted by taking a small sample of the respective culture from a petri dish using a sterile inoculating loop and placing it in the test solution hosted within a compartment in the device. The breath-based tests (calcium hydroxide and hydrogen sulfide) were conducted by collecting gas in Erlenmeyer flasks, following the same methods described initially to measure the pressure of gas released by *S. aureus,* and a sterile syringe was used to collect gas from the flask after 24 hours of incubation. The syringe was used to release the gas through the straw-like blow hole of the device to mimic a person breathing through the tube as designed.

ACKNOWLEDGEMENTS

We would like to thank Ms. Vaillancourt for her helpful feedback on the manuscript. Thank you to Mr. Lowry for his guidance and the Georgia Governor's Honors Program for materials.

Received: January 9, 2020
Accepted: October 24, 2020
Published: February 20, 2021

REFERENCES

1. Revelas Angela. "Healthcare-associated infections: A public health problem." *Nigerian Medical Journal*, vol. 53, no. 2, 2012, pp. 59-64. doi: 10.4103/0300-1652.103543.
2. Tong, Steven, *et al*. "Staphylococcus aureus infections: Epidemiology, pathophysiology, clinical manifestations, and management." *Clinical Microbiology Reviews*, vol. 28, no. 3, 2015, pp. 603-661. doi: 10.1128/CMR.00134-14.
3. Burnham, Jason, and Marin Kollef. "Prevention of Staphylococcus aureus ventilator-associated pneumonia: conventional antibiotics won't cut it." *Clinical Infectious Diseases*, vol. 64, no. 8, 2017, pp. 1089-1091. doi: 10.1093/cid/cix060.
4. Paul, Suzanne, *et al*. "Direct Detection of Staphylococcus aureus from Adult and Neonate Nasal Swab Specimens Using Real-Time Polymerase Chain Reaction." *The Journal of Molecular Diagnostics*, vol. 6, no. 3, 2004, pp. 191-196. doi: 10.1016/S1525-1578(10)60509-0.
5. Conterno, L.O., *et al*. "Real-time polymerase chain reaction detection of methicillin-resistant Staphylococcus aureus: impact on nosocomial transmission and costs." *Infection Control and Hospital Epidemiology*, vol. 28, no. 10, 2007, pp. 1134-1141. doi: 10.1086/520099.
6. Tauyoun, Ahmad, *et al*. "Democratizing Molecular Diagnostics for the Developing World." *American Journal of Clinical Pathology*, vol. 141, no. 1, 2014, pp. 17-24. doi: 10.1309/AJCPA1L4KPXBJNPG.
7. Koczula, Katarzyna, and Andrea Gallotta. "Lateral flow assays." *Essays in Biochemistry*, vol. 60, no. 1, 2016, pp. 111-120. doi: 10.1042/EBC20150012.
8. Ejaimi, Gamal, and Sittelnissa Saeed. "An Introduction to Airway Assessment and Management." *Annals of International Medical and Dental Research*, vol. 3, no. 1, 2017, pp. 1-7. doi: 10.21276/aimdr.2017.3.1.AN1.
9. Hynes, Wayne, and Sheryl Walton. "Hyaluronidases of Gram-positive bacteria." *FEMS Microbiology Letters*, vol. 183, no. 2, 2000, pp. 201-207. doi: 10.1111/j.1574-6968.2000.tb08958.x.
10. Payan, Elizabeth, *et al*. "Hyaluronidase degradation of hyaluronic acid from different sources: Influence of the hydrolysis conditions on the production and the relative proportions of tetra- and hexasaccharide produced." *International Journal of Biochemistry*, vol. 25, no. 3, 1993, pp. 325-329. doi: 10.1016/0020-711X(93)90620-T.
11. Torok, Estee, and Nick Day. "Staphylococcal and streptococcal infections." *Medicine*, vol. 33, no. 5, 2005, pp. 97-100. doi: 10.1383/medc.33.5.97.64964.
12. King, Katherine, *et al*. "Aerotolerance and Peroxide Resistance in Peroxidase and PerR Mutants of Streptococcus pyogenes." *Journal of Bacteriology*, vol. 182, no. 19, 2000, pp. 5290-5299. doi: 10.1128/jb.182.19.5290-5299.2000.
13. Ibberson, Carolyn, *et al*. "Staphylococcus aureus hyaluronidase is a CodY-regulated virulence factor." *Infection and Immunity*, vol. 82, no. 10, 2014, pp. 4253-4264. doi: 10.1128/IAI.01710-14.
14. Chao, Kinlin, *et al*. "Structure of human hyaluronidase-1, a hyaluronan hydrolyzing enzyme involved in tumor growth and angiogenesis." *Biochemistry*, vol. 46, no. 21, 2007, pp. 6911-6920. doi: 10.1021/bi700382g.
15. Man, Wing, *et al*. "The microbiota of the respiratory tract: gatekeeper to respiratory health." *Nature Reviews Microbiology*, vol. 15, no. 5, 2017, pp. 259-270. doi: 10.1038/nrmicro.2017.14
16. Filipak, Wojciech, *et al*. "Molecular analysis of volatile metabolites released specifically by Staphylococcus aureus and Pseudomonas aeruginosa." *BMC Microbiology*, vol. 12, no. 113, 2012. doi: 10.1186/1471-2180-12-113.
17. Peng, Hui, *et al*. "Hydrogen Sulfide and Reactive Sulfur Species Impact Proteome S-Sulfhydration and Global

Virulence Regulation in Staphylococcus aureus." *ACS Infectious Diseases*, vol. 3, no. 10, 2017, pp. 744-755. doi: 10.1021/acsinfecdis.7b00090

18. Meldau, Dorothea, *et al*. "Dimethyl disulfide produced by the naturally associated bacterium bacillus sp B55 promotes Nicotiana attenuata growth by enhancing sulfur nutrition." *The Plant Cell*, vol. 25, no. 7, 2013, pp. 2731-2747. doi: 10.1105/tpc.113.114744
19. Tran, Thi, *et al*. "The atmospheric corrosion of copper by hydrogen sulphide in underground conditions." *Corrosion Science*, vol. 45, no. 12, 2003, pp. 2787-2802. doi: 10.1016/S0010-938X(03)00112-4.
20. Yother, Janet, *et al*. "Genetics of Streptococci, Lactococci, and Enterococci: Review of the Sixth International Conference." *Journal of Bacteriology*, vol. 184, no. 22, 2002, pp. 6085-6092. doi: 10.1128/JB.184.22.6085-6092.2002.
21. Post, Virgina, *et al*. "Comparative Genomics Study of Staphylococcus epidermidis Isolates from Orthopedic-Device-Related Infections Correlated with Patient Outcome." *Journal of Clinical Microbiology*, vol. 55, no. 10, 2017, pp. 3089-3103. doi: 10.1128/JCM.00881-17.
22. Baureder, Michael, and Lars Hederstedt. "Genes Important for Catalase Activity in Enterococcus Faecalis." *PLOS One*, vol. 7, no. 5, 2012, pp. 6351-6356. doi: 10.1128/JB.184.22.6351-6356.2002.
23. Leygraf, Christofer, *et al*. "The origin and evolution of copper patina colour." *Corrosion Science*, vol. 157, no. 2, 2019, pp. 337-346. doi: 10.1016/j.corsci.2019.05.025.

JOURNAL OF
EMERGING INVESTIGATORS

Article

The effect of wind mitigation devices on gabled roofs

Sara Kaufman, Nadine Leonard
North Broward Preparatory School, Coconut Creek, Florida

SUMMARY

Hurricanes are dangerous storms that can cost both lives and millions of dollars' worth of damages each year. Much of the damage from hurricanes comes from winds that cause pressure differences and uplift forces that can make roofs blow off. Methods in place today to mitigate these forces primarily involve the strength and type of attachments of the roof to the walls of the house, but previous studies have shown how mitigation devices can redirect the airflow on a roof to reduce the uplift forces. The purpose of this study was to test devices installed on a gabled roof to see which reduced the actual uplift forces best. A wind tunnel made of PVC pipe, an acrylic sheet, and a leaf blower on a wooden base, simulated the hurricane winds. Three gabled birdhouse roofs were each modified with different mitigation devices: a rounded edge, a barrier shape, or an airfoil. The barrier edge had no significant effect on the time for the roof to blow off. The rounded edge and the airfoil had significant effects, with the airfoil taking the longest time for the roof to blow off. This suggests that the addition of airfoil devices on roofs, specifically in areas that are prone to hurricanes such as Florida, could keep roofs in place during hurricanes, thus reducing insurance bills, overall damage costs, and the loss of lives.

INTRODUCTION

Hurricanes are very large and extremely powerful storms that move around a central point called an eye. They can occur all over the world, although they go by different names in various regions. The word "hurricane" is used for storms in the north Atlantic or eastern Pacific Oceans, while the north Pacific and Philippines use the word "typhoon". Storms that develop in the south Pacific and Indian Oceans use the term "cyclone" (1). These storms cause a lot of damage. They can destroy homes, unroot trees, and even cause major damage or death to people and animals (1). Most hurricanes hit the United States in the South, along both the Gulf and Atlantic coasts. From 1900 to 2018, 206 hurricanes hit U.S. territory (2). Hurricane Katrina in 2005 was the single most expensive U.S. hurricane to date, costing $116.9 billion in damages, although that annual amount was passed in 2017 by back-to-back Hurricanes Harvey and Irma, which cost over $125 billion worth of combined damages in Texas and Florida (2-3).

Hurricanes can be classified into five different categories based on the average sustained wind speed over a period of one minute, excluding gusts. This scale of five categories is known as the Saffir-Simpson Hurricane Wind Scale (4). **Table 1** summarizes the classification of the scale based on wind speed and the roof damage in each of the categories (4).

Approximately forty-one hurricanes have been analyzed with the scale between 1960 and 2006 (5), although an earlier version of the scale included information about storm surge and central pressure of the storm (4). The current scale is based only on sustained winds and is used to prepare communities in the United States that are in the path of a hurricane by providing examples of the type of damage that can be expected from the winds in each category. Hurricane Katrina was recorded as a Category 3 hurricane at landfall, Hurricane Harvey was a Category 4 hurricane, and Hurricane Irma hit the Florida Keys as a Category 4 hurricane before being downgraded to a Category 3 as it hit the mainland coast of Florida (2). It is often the same regions that get hit with hurricanes of varying strengths repeatedly, causing people to lose their homes, and sometimes their lives. For this reason, it is important to try to find a solution to lessen the damage these storms cause.

The average house is very vulnerable during a strong hurricane, especially at the roof because of the uplift forces from the wind. Uplift forces are one of three types of wind load forces that affect buildings and need to be taken into consideration in their design. The three types of wind load forces are shear loads, which are horizontal forces produced by winds that would make the building tilt; lateral loads, which are the pushing and pulling forces that would cause a building to move off of its foundation; and upload forces, which are created from pressure differences of the wind flowing over the roof (pulling the roof up from above) and under the roof overhangs (pushing the roof up from below) (6). Wind uplift force is a function of the wind pressure (P), the surface area (A), and the drag coefficient for the shape of the roof (C_d):

$$\textit{Wind Uplift Force} = P*A*C_d$$

Wind pressure, in the formula above, is a function of the air density (ρ) and the square of the velocity of the wind (v) (7):

$$P = 1/2\ \rho v^2$$

In a hurricane, a slightly higher wind means a lot more

Table 1. Saffir-Simpson Hurricane Wind Scale.

Category	Wind Speeds	Types of Roof Damage Due to Hurricane Winds
1	119-153 km/h	Very dangerous winds can result in damage to roof, shingles, vinyl siding and gutters. Mobile homes can be destroyed.
2	154-177 km/h	Extremely dangerous winds can cause major roof and siding damage or can cause roofs to fly off poorly built and older homes.
3 (major)	178-208 km/h	Major damage or removal of roof decking and the gable ends (the vertical triangular wall between the sloping ends of a gabled roof).
4 (major)	209-251 km/h	Catastrophic damage including loss of most of the roof structure and/or some exterior walls, even on solidly built framed houses.
5 (major)	252 km/h or higher	Catastrophic damage, with a high percentage of framed homes being destroyed from wall collapse and complete failure of the roof.

force (8). Most damage to roofs during a hurricane is caused by spiraling winds that form when the oncoming wind from the hurricane hits a bulky structure with sharply defined sides. This spiraling wind is known as a vortex. The vortices change the pressure distribution across the roof, causing the suction that results in damaging uplift forces on the roof (9). Certain house and roof types could improve the durability of the house during a hurricane. For example, very large overhangs on a roof could cause the entire roof to fly off, so reducing or eliminating overhangs is a good design for hurricane-prone areas. Overall, hurricanes cause significant damage to roofs because of uplift forces.

If the roof of a house or the house itself is slanted in the direction of the wind, then the house can have more stability. Circular roofs cause the wind to simply curve around the house. Holes in a wall allow the wind to pass through and lessens the amount of wind passing through, whilst acting like a regular wall. Raised houses let a lot of wind go under, not up against the house, and they allow water to accumulate under the house, preventing floods (10).

Previous experiments with mitigation devices have been conducted to try to lesson vortices on roofs, but they have been primarily on high- and low-rise buildings with flat roofs. In one experiment, the mitigation devices used were a barrier, a circular-out, a circular-in, a slope-out, a slope-in and an airfoil edge. Of these, the airfoil edge produced the smallest uplift loads (8). In another experiment, researchers examined vortex reduction using different roof attachment methods and a modified rounded edge design on a flat roof. The modified edge was useful in reducing vortices (11). In yet another experiment, different types of parapets successfully mitigated the effects of high winds on flat roofs (12). In researching the type of wind mitigation devices used in previous tests, parapets seemed to be the most effective in displacing or disrupting the formation of vortices, although rounded devices were also effective in reducing uplift forces, as they eliminate vortex-forming sharp edges (9). However, little research has been done on a gabled roof. Only one previous experiment was found in the research using a gabled roof, in which researchers tested trellises (pergolas), roof extensions of gable ends, ridgeline extensions, and sideways extensions of walls as the mitigation devices. The results demonstrated a reduction in peak suction with all these devices (13). In the current study, we used a gabled roof because it has been shown that the high rising feature of a gabled roof makes it more resistant to vortex formation during a hurricane than a flat roof and because it is a more common design in modern day residential buildings (8).

After examining the literature and previous research done on this subject, the hypothesis for this experiment stated that if a barrier, a rounded shape, or an airfoil mitigation device were put on a gabled roof and tested against simulated hurricane winds, then the roof with the airfoil shape mitigation device would take the longest amount of time to blow off. The hypothesis was based primarily on the research done by Aly (8), in which an airfoil edge was the most effective device to mitigate winds, and Suaris and Irwin (12), in which different parapets proved effective in mitigating the effects of wind on flat roofs. The perpendicular airfoil in this experiment is a unique design that combines Aly's airfoil edge with Suaris and Irwin's raised parapets.

We simulated Category 2 winds on three different mitigation device designs and found that the upright airfoil design performed best in keeping the roof attached for the longest amount of time. The results from this experiment suggest that the aerodynamics of an upright airfoil could present a solution for the problem of roofs flying off houses when subjected to hurricane wind forces and should be in studied further detail.

RESULTS

We tested three different types of wind mitigation devices against simulated hurricane winds to see which device reduces the uplift forces the most compared to a common gabled roof. We tested gabled roofs on small birdhouses with winds simulated by a homemade open wind tunnel, constructed using a leaf blower and PVC pipe (**Figure 1**). This design was an inexpensive but effective way of testing the effects of strong winds, using a birdhouse that was approximately a 1:200 scale model of the size of a real gabled roof house. The mitigation devices were a rounded shape, a barrier, and a

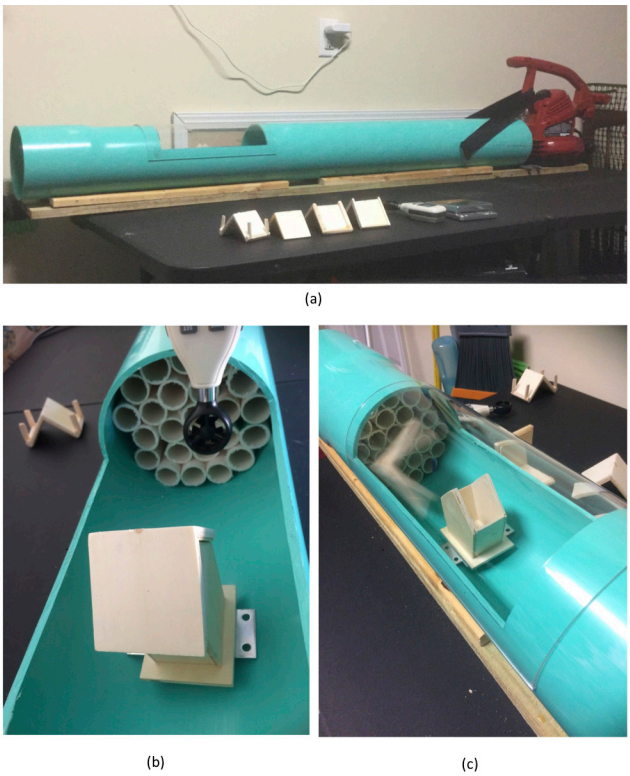

Figure 1. Wind tunnel. a) The experiment was conducted in a homemade open wind tunnel made of PVC pipes, acrylic, a leaf blower, and a wooden base. **b)** A roofless birdhouse was bolted onto a metal plate in the tunnel and each roof was placed on top for testing. The wind speed was measured prior to testing the control roof. **c)** An acrylic cover was placed over the test section and the leaf blower was turned on as the timer was started. The wind hit the roof against one of the slanted sides until the roof completely flew off the birdhouse and the timer was stopped.

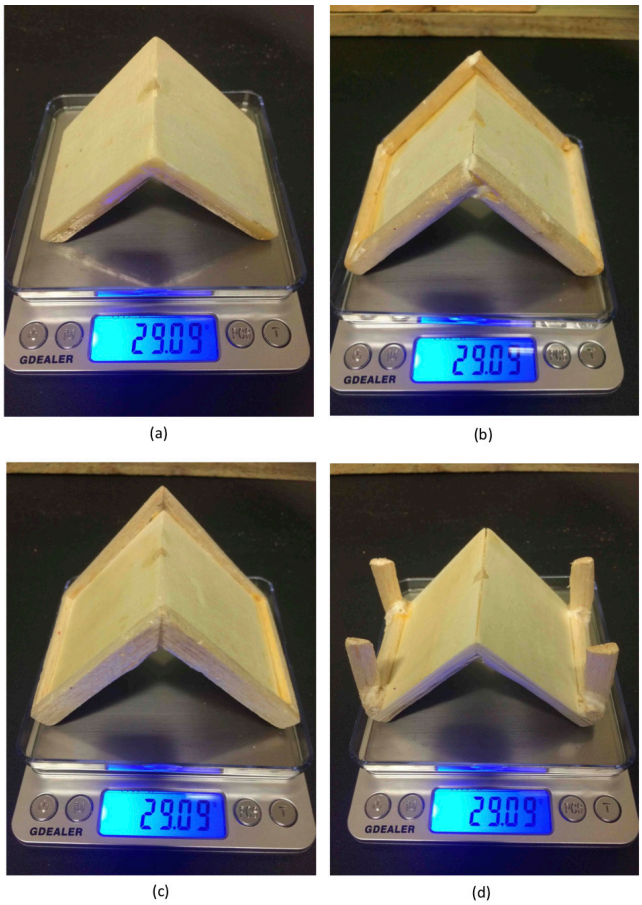

Figure 2. Control and modified roofs. Craft store birdhouse roofs were modified with different mitigation devices. **a)** Control roof with no mitigation device. **b)** Rounded edge mitigation device. **c)** Barrier edge mitigation device. **d)** Upright airfoil mitigation device.

perpendicular airfoil shape. We chose a rounded edge (**Figure 2b**) because domed houses have been found to survive hurricanes (14); a flat edge barrier mitigation device (**Figure 2c**) because of the previous study with a barrier edge on a flat roof (15); and an upright airfoil design (**Figure 2d**) because of the research mentioned earlier showing evidence that airfoil edges and parapets are effective at mitigating uplift forces on flat roofs. By combining the design of an airfoil edge and a parapet, the resulting mitigation device was an upright airfoil, which resembles a winglet on an airplane. Further research into winglets showed that their main purpose is to redirect vortices on airplane wings, thus reducing drag and providing fuel savings to airlines (16). Since the rationale behind this experiment was to find a mitigation device that could reduce the vortices that cause uplift forces on a roof, an upright airfoil was a promising design to test on the roof.

The airfoil significantly outperformed the other roof wind mitigation devices in all ten trials, with the time from when the blower was turned on to when the roof completely flew off the house ranging from 9.12 to 21.05 seconds (**Figure 3**). The rounded edge also took a large amount of time to fly off, more than the other two devices, over a range of 5.78-9.45 seconds. However, the airfoil did a substantially better job than the rounded edge. There was little difference between the control roof (2.97-5.84 seconds) and the roof with the barrier edge mitigation device (3.61-7.29 seconds, **Figure 3**). The averages of the control and barrier roof, 4.19 seconds and 4.31 seconds respectively, were each less than one-third of the average time for the airfoil, at 13.77 seconds. All of the results are within three standard deviations, except for the airfoil, which was slightly above (σ = 3.11), due to an outlier on the first trial.

P-values for this experiment were calculated on an Excel spreadsheet, using a default alpha of 0.05, and those independent results were validated through a Holm-Bonfferoni correction. With a p-value of 0.40, the barrier edge did not significantly impact the amount of time it took for the roof to fly off when compared to the control roof with no mitigation device. However, the rounded edge and the airfoil configurations both had *p*-values of $p < 0.01$ (**Figure 3**), meaning that those devices significantly increased the time it took for the roofs to fly off when compared to the control roof.

DISCUSSION

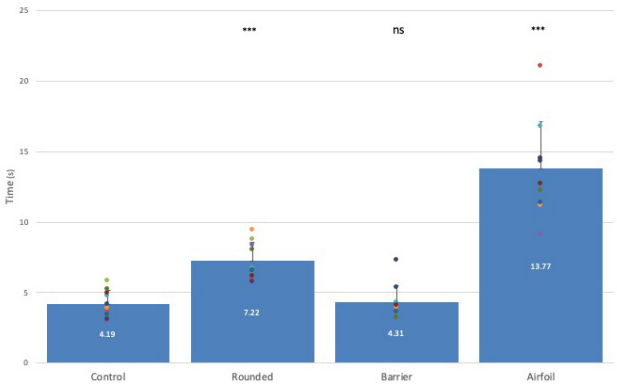

Figure 3. Time for roof to blow off using different mitigation devices on a gabled roof. The control roof and each roof with a mitigation device were tested 10 times, with the timer starting as soon as the leaf blower was turned on to full power and ending when the roof completely blew off the house. The blue bars indicate the average time it took each roof to fly off over ten trials, represented by the scattered dots. The error bars show standard deviation. On average, all roofs with mitigation devices stayed on longer than the control roof, although the improvement with the barrier roof was nonsignificant (ns, p = 0.40). The roof with the rounded edge performed much better than the control roof, staying on the house almost twice as long, and the roof with the airfoil mitigation device performed the best, staying on the house over three times as long as the control roof. Both the rounded edge and airfoil roofs had p-values < 0.01 (***), indicating that they contribute significantly to the reduction of uplift forces on a gabled roof when compared to the roof with no mitigation device.

Of the three mitigation devices tested in this experiment, the airfoil design had the greatest effect on mitigating the winds on the gabled roof from the simulated hurricane. The roof with the upright airfoil configuration stayed on the roof more than three times longer than both the control roof and the roof with the barrier edge. The barrier edge produced a non-significant improvement over the control roof, but the other two devices showed significant increases in the time the roofs stayed attached to the house before flying off when compared to the control. The experiment supported our hypothesis that if the same three mitigation devices were tested against simulated hurricane winds on a gabled roof, then the roof with the airfoil shape mitigation device would take the longest amount of time to blow off. This hypothesis was based on previous research that used an airfoil edge and another that used parapets to mitigate the uplift forces, but an upright airfoil design had never been tested before. By adding modifications to the edge of a gabled roof, the experiment showed that the destructive airflow patterns caused by high winds can be easily changed. The roof with the airfoil design stayed on almost twice as long as the rounded edge by redirecting the vortices that create the uplift forces, making it the most promising device for mitigating those damaging forces on gabled roofs.

This experiment may lead to the addition of certain mitigation devices on roofs, specifically in areas that are prone to hurricanes such as Florida. This would decrease the number of roofs being blown off during hurricanes, saving thousands of dollars in insurance claims and roof repair. The mitigation device is cost effective because it would not mean putting a new roof on houses, just adding the device to existing roofs. The airfoil mitigation device on the roof would redirect and reduce the formation of vortices, increasing the time taken for roofs to blow off and lessening insurance bills.

The wind measured at the beginning of the wind tunnel was 7.7 meters per second (m/s), or 27.7 km per hour, and the birdhouse was approximately a 1:200 scale model of the size of a real home. Although the leaf blower was rated at approximately 67 m/s, the air expands quickly after exiting the leaf blower nozzle and slows even more as it travels through the smaller PVC pipes. This considerably slows the output air down before reaching the test window. Because the wind created enough uplift forces to lift the roof off the house in all trials, the equivalent wind could have been comparable to at least a Category 2 hurricane (based on the Saffir-Simpson Hurricane Wind Scale descriptions of damage possible for each category). However, it is hard to make an accurate estimate of the hurricane category of the winds simulated in this experiment because the roofs used in this experiment were those of birdhouses, not of real houses, and the because the wind came from a homemade wind tunnel, not an actual hurricane. Also, these roofs were made from unfinished craft wood and the mitigation devices were made from balsa wood; not solid construction-grade wooden frames with metal, asphalt, shingles, or tiles to protect and weigh them down. Finally, the roofs were not attached in any way to the birdhouse as a real roof would be attached to the structure of the house. This was another factor that differentiated this experiment from a real hurricane situation but did not detract from the results of this experiment, because the lack of attachment was consistent for all roofs being tested, including the control. This experiment was not testing construction strength or materials. Instead, it tested aerodynamic forces acting on the roof during high winds.

Before testing, a trial run with the wind tunnel was performed. During that initial trial run, the roof did not fly off at all because the airflow straighteners were lined up with the beginning of the test window, making the air coming out too laminar when it hit the roof and not allowing the formation of vortices. By moving the straighteners back toward the leaf blower by about an inch, vortices were able to form on the roof edges. The straighteners stayed in this new position for all testing, which allowed the straighteners to serve their function of keeping the angle the wind hit the roof to be constant throughout all trials, yet still allow vortices to form.

A systematic error in this experiment was that most wind tunnels are used for looking at wind patterns, not for simulating hurricanes. This may have made the wind flow differently from wind in a hurricane. Some random errors in this experiment were that the stopwatch and knob on the wind tunnel turn on at different speeds. The knob takes longer to reach full power (the amount used for testing), while the stopwatch is instantaneous.

This may lead the results to be a few milliseconds off.

Additionally, wind vortices change the pressure distribution on the roof. If the roofs fly off because of pressure differences, an idea to consider would be inserting a PVC pipe through the house. The pipe would have small holes, allowing air to pass through, but not rain or strong wind gusts. This or some other pressure release valve/system combined with the airfoil roof could eliminate roofs flying off all together.

In addition, it would be interesting to contrast between the constant wind used in this experiment and simulated gusts of wind. In this experiment, a constant wind was used because the Saffir-Simpson Scale uses sustained wind speed to determine a hurricane's category. However, gusts could be utilized to show how the same roof design may hold up to other types of natural disasters or during the eye of the hurricane when the wind stops temporarily before increasing rapidly again. The gusts could be simulated by making a mechanical device, such as a metal plate attached to a lever, that would block the output from the leaf blower that could be moved to different positions without taking the acrylic top off the wind tunnel. The design of the roofs themselves can also be altered. For example, it would be interesting to see if there is a direct relationship between the weight of the roof and the time it takes before it blows off, or if combining both the rounded edge and the airfoil mitigation device onto one roof significantly changes the results. Finally, the roof's aerodynamic properties could be simulated in a Computational Fluid Dynamics (CFD) analysis, which would make it easier to manipulate and understand all the forces acting upon them. CFD has been used more and more since the 1970's as a way of studying airflow around buildings because it is more practical, faster, and cheaper than using wind tunnels, and it allows them better control of the data being studied (17). The results from this experiment could be validated and expanded using computational tools.

The next step in testing the airfoil design would be to test different configurations of airfoils, including airfoils of different heights and multiple airfoils spread across the edge of the roof. Several roofs with the same devices should be made for experimental replication, and the wind should be tested hitting the house from different directions other than just directly onto the broad side. This would allow a study of how the wind vortices can form on different parts of the roof, as winds typically shift during hurricanes. The house could also be mounted on a rotating platform to see how the wind affects it from multiple directions with only a quick period of time in each direction. Another way of achieving this same purpose would be to make the house stationary but attached to a point outside of the wind tunnel via a cutout in the wind tunnel, and then have the wind tunnel on a rotating disk so it would circle around the house. If the results of either of these methods for variable wind direction are the same as the results from this experiment, that would strengthen the support for the airfoil shape as the most favorable mitigation device for keeping the roof on the house as stated in the hypothesis of this experiment (if a barrier, a rounded shape, or an airfoil mitigation device were put on a gabled roof and tested against simulated hurricane winds, then the roof with the airfoil shape mitigation device would take the longest amount of time to blow off). Ideally, this could lead to a full-scale test. Florida International University's Wall of Wind Experimental Facility is one example of a full-scale wind tunnel specifically designed to study the effects of wind on infrastructure and to find possible solutions to mitigate the problem. Full-scale testing of a model with a roof that is physically attached to the house in actual hurricane winds would validate the results presented in this paper.

In this experiment, a total of three modified roofs were tested against uplift forces on a gabled roof. The roofs were modified with the following types of mitigation devices: a rounded edge, a flat edge barrier device, and four upright airfoils. The roof with the flat barrier edge showed a non-significant change in the amount of time it took for the roof to fly off when compared to the control roof, but the roofs with the rounded edge device and the airfoil device stayed on significantly longer than the control roof. T-test results showed p-values < 0.01 for each of those two roofs. The mitigation device that made the roof stay on the longest in simulated hurricane winds and the roof with the lowest p-value was the airfoil. Staying on almost twice as long as the roof with the rounded edge and over three times longer than both the control roof with no mitigation device and the roof with the barrier edge, this last design has the best potential of all of the designs studied in this paper to minimize the potential of roofs flying off in hurricanes, thus possibly saving lives and millions of dollars' worth of property damage.

MATERIALS AND METHODS

Wind Tunnel Construction

The homemade wind tunnel was built using a 152.4 cm length, 15.24 cm diameter Schedule 40 PVC pipe and a Toro Ultra Electric Leaf Blower with a high-speed nozzle, rated at 0.702 air horsepower. A viewing window approximately one-third of the way from the edge of the pipe was made by cutting a 29.0 cm opening with a depth midway through the pipe. A window, using a cut sheet of acrylic that was heated in an oven and molded over a slightly smaller pipe until cool, was placed over the viewing window to prevent air from escaping. Two sets of twenty-five 20-cm sections of 1.9 cm diameter PVC pipe were joined together separately and gently tapped into the large pipe on either side of the viewing window with a rubber mallet. These small pipes straightened the airflow that came out of the leaf blower. A test bed was made and attached to the inside bottom of the large pipe in the center of the viewing window, and then the wind tunnel was bolted onto a plank of wood to keep it from rolling. A plastic kitchen funnel with approximately the same inside diameter as the large PVC pipe was taped onto the leaf blower high-speed nozzle to diffuse the air coming out of the leaf blower, and the leaf blower nozzle was then inserted into large PVC pipe on the side farthest from the viewing window. Using Velcro, the leaf blower motor was then attached to the wooden plank to keep it from shifting from vibration when turned on. **Figure 1a**

shows a photo of the completed wind tunnel. **Figure 1b** shows the placement of the birdhouse inside, and **Figure 1c** shows the operating tunnel with the acrylic window in place. **Figure 4** shows a CAD drawing of the wind tunnel with dimensions and includes an expanded view of the birdhouse in the tunnel with its dimensions and position relative to the wind from the leaf blower.

House and Mitigation Device Construction

Four natural unfinished wood birdhouses (Birdhouse by ArtMinds, Model 308374) were purchased from a local craft store for testing. The roofs were removed and all but one roofless birdhouse wall discarded. The trim and hanging string were removed from the roofs and the perch was removed from the house. All holes were completely sealed with wood or glue to prevent air from entering the house while testing. The roofless birdhouse was then bolted onto the test bed of the wind tunnel. The mitigation devices were made using a 1 cm x 0.5 cm x 91.44 cm balsa wood stick, an Exacto knife, and sandpaper. Each mitigation device was designed so the barrier and rounded edges matched the edge length of the roof. The remaining wood from the stick was cut into 4 equal pieces that would become the airfoil designs. Each piece of the balsa wood stick was then sanded into the desired shape. The mitigation devices were then each attached to a roof using wood glue, ensuring that each of the roofs weighed the same when completed so that just the aerodynamic effects of the devices were observed (**Figure 2**). The weight of each roof was adjusted by either sanding any excess weight off or adding wood glue to the bottom side as needed.

Mitigation Device Testing

Before testing, the wind was measured by holding a JRLGD Model 816A-EN-00 digital anemometer at the beginning of the test window and turning on the leaf blower to full power (**Figure 1b**). For this experiment, the wind was recorded at 7.7 m/s. The roofs were then positioned onto the birdhouse bolted inside the wind tunnel and were not attached in any way - allowing just the geometry to hold it in place. Next, the acrylic window was placed over the test section and the leaf blower was turned on to full speed. An iPhone stopwatch was used to measure the amount of time it took for the roof to fly off the birdhouse, starting the timer immediately as the blower dial began to be turned on to full speed and stopping it when the roof detached from the roof (**Figure 1c**). The results of each of the 10 trials per roof were recorded, starting with 10 sequential trials of the control roof, followed by 10 trials of the rounded edge roof, then 10 trials of the barrier edge roof, and finally 10 trials of the roof with the airfoil mitigation device. The roofs were inspected for damage and reweighed after each trial before being positioned back on to the birdhouse. Wind speed, weight of the house, the weight of each roof being tested (including mitigation devices), the angle the wind hit the roof (angle of incidence), the placement of the roof on the house without using attachments, and the orientation of the house in the tunnel were constant across groups.

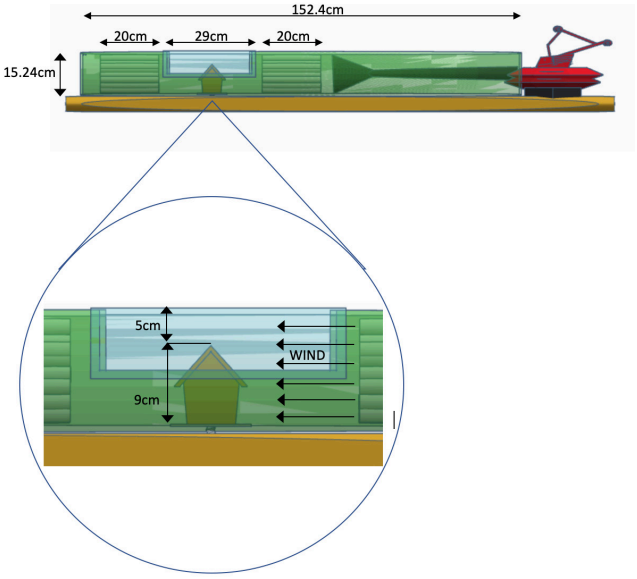

Figure 4. Wind tunnel dimensions and birdhouse placement. A wind tunnel was built using a 152.4 cm length 15.24 cm diameter PVC pipe and a leaf blower. A funnel was duct taped onto the end of the leaf blower nozzle to control the expansion of air exiting the blower. The air then passed through twenty-five 20 cm length pipes (1.90 cm diameter) to reduce random turbulence that would skew the results before hitting the side of a 9 cm tall birdhouse with the gabled roof placed on top. A gap of 5 cm between the top of the roof and the acrylic viewing window allowed room for the roof to lift off the house, as observed from the 29 cm test window cutout in the large pipe.

Statistical Analysis

The data from this experiment was recorded in a table which was put into an Excel spreadsheet. From the table, the data was analyzed in Excel by calculating averages and standard deviation and by performing a two-sample t-test assuming equal variances to calculate the p-values. This allowed a determination of the probability that none of the devices would make a difference as to how long each roof stayed on, when compared to the control roof. For the *p*-value calculation, the Excel default alpha of 0.05 was used, and then a Holm-Bonferroni correction was performed to correct for the three independent comparisons and confirm the experiment's results.

ACKNOWLEDGEMENTS

I would like to begin by thanking Mrs. Leya Joykutty of American Heritage School for helping me get this project started, and Mr. Howard York of North Broward Preparatory School for helping me get this paper finished. Mr. York has enabled me to improve my skills as a researcher and inspired me to pursue scientific research in the future. I would also like to express my gratitude to each of the five amazing scientific reviewers, the editors, and the entire JEI staff for their patience and support.

Received: August 18, 2020
Accepted: February 10, 2021
Published: February 20, 2021

REFERENCES

1. Morsink, Kalila. "Hurricanes, Typhoons, and Cyclones". Smithsonian Institute, 2018, www.ocean.si.edu/planet-ocean/waves-storms-tsunamis/hurricanes-typhoons-and-cyclones. Accessed October 22, 2020.
2. Weinkle, J., Landsea, C., Collins, D. et al. "Normalized hurricane damage in the continental United States 1900–2017." *Nat. Sustain.,* Vol. 1, 2018, pp. 808–813.
3. Klotzbach, P. J., S. G. Bowen, R. Pielke, and M. Bell. "Continental U.S. Hurricane Landfall Frequency and Associated Damage: Observations and Future Risks." *Bull. Amer. Meteor. Soc.*, Vol. 99, 2018, pp. 1359–1376.
4. "Saffir-Simpson hurricane wind scale." NOAA. www.nhc.noaa.gov/aboutsshws.php. Accessed September 22, 2016.
5. Senkbeil, J. C., & Sheridan, S. C. "A post landfall hurricane classification system for the United States." *Journal of Coastal Research*, *22*(5), 2006, 1025-1034.
6. Reichel, Claudette. "What's a Wind Load?" LSU, 2018, www.lsuagcenter.com. Accessed October 4, 2020.
7. Baer, Bryon. "How to Convert Wind Speed to Roof Uplift", HomeSteady, Updated 2017, www.homesteady.com/how-12008762-convert-wind-speed-roof-uplift.html . Accessed October 4, 2020.
8. Aly, A.-M. "Aerodynamic mitigation of wind uplift loads on low-rise buildings." The 2014 World Congress on Advances in Civil, Environmental, and Materials Research (ACEM14), August 24-28, 2014, Busan, Korea. Conference Presentation.
9. Surry, D. and Lin, J.X. "The effect of surroundings and corner geometric modifications on roof pressure on low-rise buildings." *Journal of Wind Engineering and Industrial Aerodynamics*, Vol. 58, Issues 1-2, 1995, pp 113-138.
10. Schellenbaum, A. "19 examples of stunning hurricane-resistant architecture." October 30, 2012, www.curbed.com/2012/10/30/10312068/19-examples-of-stunning-hurricane-resistant-architecture. Accessed on September 18, 2016.
11. Blessing, Collette & Chowdhury, Arindam & Lin, Jason & Huang, Peng. "Full-scale validation of vortex suppression techniques for mitigation of roof uplift." *Engineering Structures*, Vol. 31, Issue 12, 2009, pp 2936-2946.
12. Suaris, W. & Irwin, P. "Effect of roof-edge parapets on mitigating extreme roof suctions." *Journal of Wind Engineering and Industrial Aerodynamics*. Vol. 98, Issues 10-11, 2010, pp. 483-491.
13. Bitsuamlak, G., Warsido, W., Ledesma, E., and Chowdhury, A.G. "Aerodynamic Mitigation of Roof and Wall Corner Suctions Using Simple Architectural Elements." *Journal of Engineering Mechanics*, Vol. 139, Issue 3, 2013, pp 396-408.
14. "Advantages of Domes", Dome of a Home, 2013, www.domeofahome.com/dome-information/advantages-of-domes/. Accessed August 15, 2018.
15. "Spoilers". www.grc.nasa.gov/WWW/K-12/airplane/spoil.html. Accessed on August 30, 2018.
16. Larson, George C. "How things work: Winglets." Air & Space Magazine, 2001, www.airspacemag.com/flight-today/how-things-work-winglets-2468375/. Accessed August 27, 2018.
17. Phillips, Duncan A. and Soligo, Michael J. "Will CFD Ever Replace Wind Tunnels for Building Wind Simulations?" *International Journal of High-Rise Buildings*, 2019, Vol. 8, No. 2, 107-116.

JOURNAL OF
EMERGING INVESTIGATORS

Article

Exploring unconventional growing methods to promote healthy growth in common household plants: *Tagetes patula* L. and *Lepidium sativum*

Andrew Nguyen, Ryan Nguyen, Erika Williams
Fountain Valley High School, Fountain Valley, California

SUMMARY

Chemical fertilizers have been used in increasing quantities for household gardening and commercial agriculture worldwide since their advent during the Green Revolution. Such fertilizers have detrimental impacts on the environment, contributing to nutrient runoff and aquatic dead zones. At the same time, water consumption for agricultural needs has skyrocketed. Alternative growing methods are urgently needed to reduce the impacts of plant cultivation. This study focused on finding more sustainable growing methods that reduce chemical fertilizer or water usage and can be used at the household level for garden plants. We hypothesized that the alternative growing methods would better encourage healthy plant growth as compared to a control. Several marigold (*Tagetes patula* L.) and garden cress (*Lepidium sativum*) plants were observed over a 13-week period. Metrics for healthy plant growth were height at first bloom, growing time, and survival rate. The results indicated that the treatments did not have a statistically significant effect on marigold and garden cress growth times in addition to marigold heights. However, the Deep Water Culture (DWC) treatment for garden cress plants significantly increased the height at first bloom compared to the control group. For rates of surviving plants, the treatments had little effect on garden cress, but the Eggshell Grounds, Wick System, and DWC system groups outperformed the control group for marigolds.

INTRODUCTION

During the late 20th century, a series of technological and agricultural innovations revolutionized commercial agriculture (1). Known as the Green Revolution, the era intended to increase crop productivity for higher yields and featured the application of chemical fertilizers and pesticides (1). Such chemical products have repercussions for the environment, namely increased phosphorous and nitrate concentrations from runoff (2). Excess nutrients enter bodies of water to create large algal blooms that can clog waterways and create "dead-zones," where aquatic species cannot thrive, due to the oxygen-consuming decomposition of dead algae (3).

In addition to affecting animal ecosystems, fertilizers also have the potential to directly harm humans. Chemical runoff in waterways can make its way into fish, poisoning them and the humans that consume them (3). Nitrates from fertilizers may also easily enter the groundwater, poisoning surrounding communities, and causing life-threatening diseases and conditions in humans due to the toxicity of elevated nitrate levels in the body (4). With approximately one-third of the world not having access to clean drinking water, the continued heavy application of chemical fertilizers presents an issue to human society (5).

At the same time, global water usage for agricultural purposes such as crop irrigation has skyrocketed (6). To reduce the environmental impacts of plant cultivation, alternative growing methods that reduce chemical fertilizer use and water consumption are desperately required. One alternative growing method is recycling common household wastes to provide nutrients to plants. Another alternative involves hydroponics, where plants are grown in a non-soil substrate and a nutrient reservoir system that recirculates and reuses water. A study conducted by Blok, Jackson, et al. demonstrates higher growth yields from substrate-based growing, such as hydroponics, compared to soil-based growing due to superior transport rates of water, nutrients, and oxygen (6). These alternatives lessen the demands for water and chemically produced fertilizer.

We hypothesized that the application of alternative growing methods on the common garden plants dwarf French marigolds (*Tagetes patula* L.) and garden cress (*Lepidium sativum*) would better improve plant health, as determined by plant height at first bloom, plant survival rate, and growth time, in comparison to the controls. We used common household items as sources of nutrients required by plants, which include nitrogen, phosphorus, potassium, calcium, and magnesium (7). Human urine was used as a natural fertilizer for its accessibility and high nitrogen content from its chief component, urea (8). Eggshells were another natural fertilizer used due to their calcium content via calcium carbonate. Another selected fertilizer was wood ash, which is produced from slash-and-burn agriculture and contains partially water-soluble calcium, potassium, and magnesium (9). We also selected two common hydroponic systems for this project:

Table 1. Sample size for marigolds and garden cress for the six experimental treatments.

	Control (Group 1)	*Urea Solution* (Group 2)	*Burnt Foliage* (Group 3)	*Eggshell Grounds* (Group 4)	*Wick System* (Group 5)	*DWC System* (Group 6)
Marigold	5	6	4	5	6	5
Garden Cress	6	6	6	4	6	6

Note: Sample size considers only the plants that sprouted, even if they died. Plants that were seeded but never sprouted were not counted. A maximum of six seeds for each plant and treatment were observed for this study. Seeds that sprouted after the sixth sprout were removed.

Table 2. Descriptive statistics for marigolds and garden cress for three plant health metrics.

Marigold	**Average Plant Height (cm)**				**Average Growth Time (days)**		
Treatment	**Mean**	**Standard Deviation**	**Standard Error**	**Survival Rate**	**Mean**	**Standard Deviation**	**Standard Error**
Control	8.10	12.67	5.67	0.40	68.50	20.51	14.50
Urea Solution	19.37	11.89	4.85	0.83	56.00	6.20	2.77
Burnt Foliage	17.95	12.56	6.28	0.75	53.00	17.32	8.66
Eggshell Grounds	26.76	4.78	2.14	1.0	57.00	10.68	4.78
Wick System	20.68	6.11	2.49	1.0	49.33	3.61	1.47
DWC System	24.60	2.82	1.26	1.0	53.00	8.00	3.58

Garden Cress	**Average Plant Height (cm)**				**Average Growth Time (days)**		
Treatment	**Mean**	**Standard Deviation**	**Standard Error**	**Survival Rate**	**Mean**	**Standard Deviation**	**Standard Error**
Control	10.77	2.00	0.82	1.0	33.33	2.07	0.85
Urea Solution	5.98	3.55	1.45	0.83	34.00	2.65	1.19
Burnt Foliage	8.15	4.37	1.78	0.83	41.20	15.96	7.14
Eggshell Grounds	10.28	1.29	0.65	1.0	40.25	2.63	1.32
Wick System	11.75	6.67	2.72	0.83	32.80	4.92	2.20
DWC System	25.50	4.59	1.87	1.0	26.67	5.13	2.09

Note: Height at first bloom was measured from base of stem to tallest point of plant once the first bud opened completely. Growth time was measured as time taken for the plant to bloom from sprouting. Survival rate was calculated as number of plants continuing to grow after the first bloom divided by number of plants that sprouted.

wick and deep water culture (DWC). Wick systems use a wick to deliver the nutrient solution to the substrate while DWC systems partially submerge plant roots directly into the nutrient solution.

The DWC system was found to significantly increase plant height at first bloom while the Eggshell Grounds, Wick System, and DWC System treatments improved the survival rate of marigolds. This experiment demonstrated how certain alternative growing methods can have beneficial effects on plant growth in terms of increasing plant height at first bloom, increasing plant survival rates, and decreasing plant growth time.

RESULTS

To understand how recycled household wastes can be applied to plants to improve plant health, we applied a urine-based urea solution (Group 2), wood ashes from burnt lawn clipping and foliage (Group 3), and finely-ground eggshells (Group 4) to seeds planted in plain soil weekly. One set of seeds had no treatments applied to serve as the control (Group 1). Similarly, to examine the effectiveness of hydroponics systems compared to plain soil, we also grew marigold and garden cress seeds in a wick-style hydroponics system (Group 5) and a Deep Water Culture system (Group 6). The plants were grown and observed to create sample sizes of at most 6 (**Table 1**). Plant growth was monitored over a 13-week period.

First, we examined the average plant height at first bloom, which was the height at which the first flower bud opened completely, measured from the base of the stem to the tallest point of the plant. For the marigolds, there was variation in average plant height, but no statistical significance between the six treatments (p = 0.058) (**Table 2, Figure 1**). For the garden cress, there was variation in average plant height at first bloom as well. Plant height was significantly higher in Group 6 (20.25 cm ± 1.87 cm) while lowest in Group 2 (5.98 cm ± 1.45 cm) (p-value < 0.05, one-way ANOVA) (**Table 2, Figure 1**). A post hoc Tukey-Kramer test with treated garden cress groups compared to the control revealed statistical significance only for the DWC treatment.

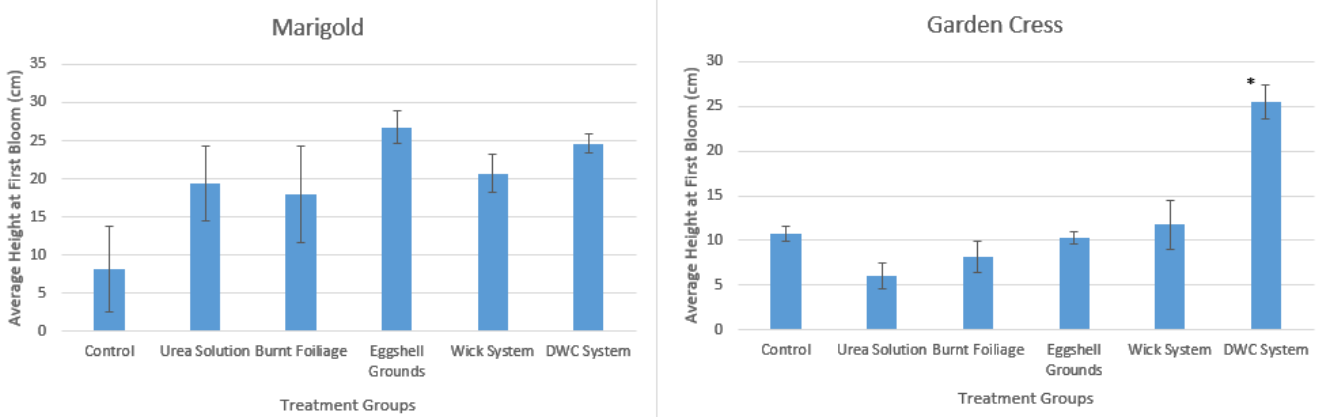

Figure 1. Average height (cm) at first bloom for marigolds (left) and garden cress (right). Plant heights were measured for six experimental groups: Control, Urea Solution, Burnt Foliage, Eggshell Grounds, Wick System, and DWC System. Error bars represent one standard error above and below the mean. An asterisk (*) represents statistical significance p < 0.05, one-way ANOVA with post hoc Tukey-Kramer test.

The effect of each treatment on the survival of each plant was also assessed. At the end of the 13-week experiment, the plant survival rate was calculated by dividing the number of plants continuing to grow after the first bloom by the number of plants that sprouted. The control group for marigolds had the lowest proportion of surviving plants, 0.4 growing/sprouted (2 plants), while the Eggshell Grounds, Wick System, and DWC System groups had the highest proportion of plant survival, 1.0 growing/sprouted (5 or 6 plants) (**Table 2, Figure 2**). For garden cress, every treatment group had roughly equal ratios of plant survival. The Urea Solution, Burnt Foliage, and Wick System groups had a survival ratio of 0.83 growing/sprouted (5 plants) while the Control, Eggshell Grounds, and DWC System groups had a ratio of 1.0 growing/sprouted (6 plants) (**Table 2, Figure 2**).

The average growth time, defined as the number of days the average plant took to bloom from the time of sprouting, was also assessed for each treatment. For the marigolds, there were no statistically significant differences between the average growth times for all six treatments ($p = 0.077$) (**Table 2, Figure 3**). For the garden cress, there was a statistically significant difference in average growth time between treatments (p-value < 0.05, one-way ANOVA) (**Table 2, Figure 3**). However, follow-up post hoc Tukey-Kramer tests between the control and other treatments revealed no statistical significance.

We also evaluated qualitative observations in both plant varieties. Starting on day 82 of experimentation, marigolds in the Urea Solution, Burnt Foliage, and Eggshell Grounds Groups developed a purple color around the edges and tips of their lower leaves (**Figure 4**). There were no significant qualitative changes in any treatment groups of the garden cress plants.

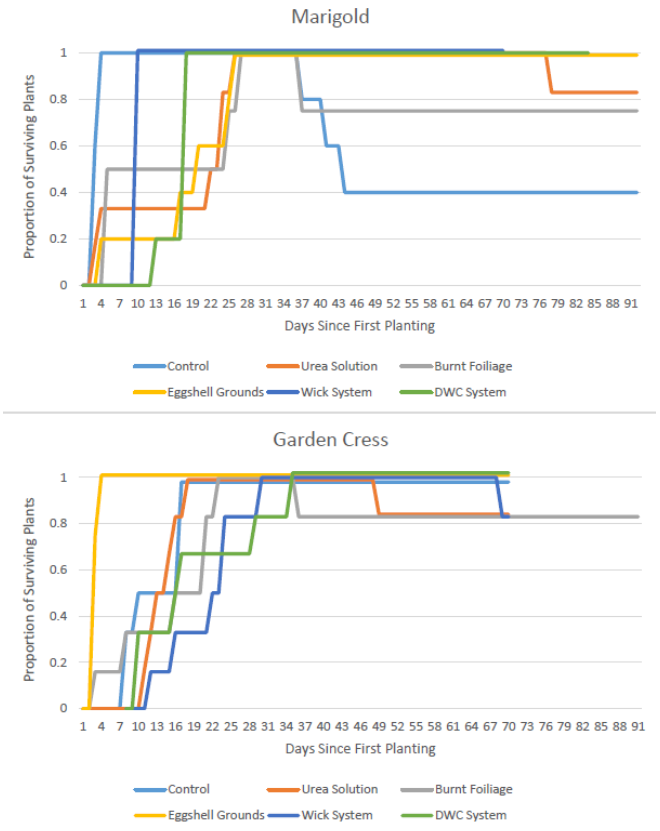

Figure 2. Plant survival rates. Survival rate of marigolds (top) and garden cress (bottom). The survival rate (growing/sprouted) was calculated for six experimental groups: Control (light blue), Urea Solution (orange), Burnt Foliage (gray), Eggshell Grounds (yellow), Wick System (dark blue), and DWC System (green). Lines that stop abruptly indicate the point at which only qualitative observations on the group were made.

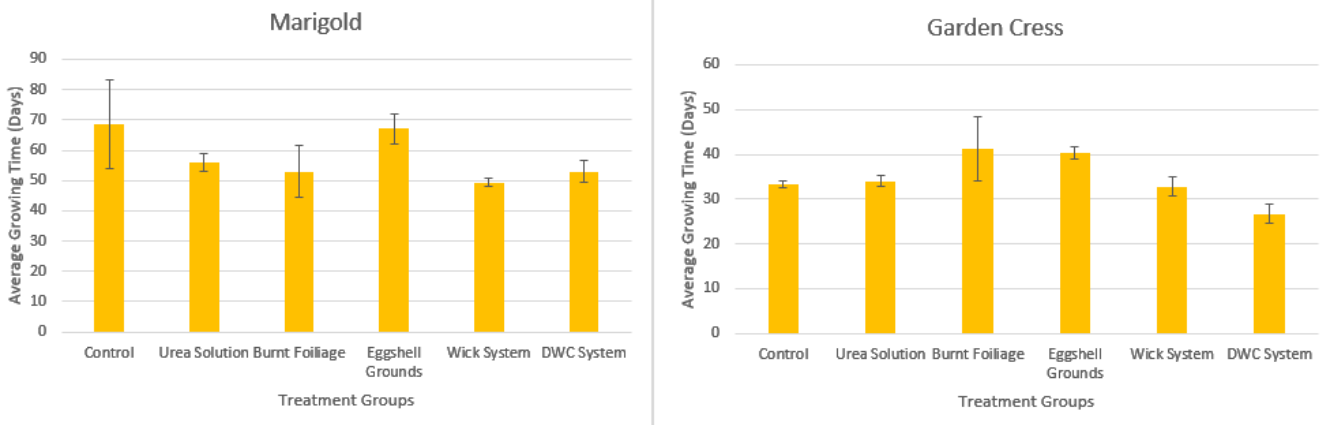

Figure 3. Average growth time (days) for marigolds (left) and garden cress (right). Growth times were measured for six experimental groups: Control, Urea Solution, Burnt Foliage, Eggshell Grounds, Wick System, and DWC System. Plants that died during the experiment or never bloomed were not included. Error bars represent one standard error above and below the mean. There was no statistical significance between groups, finding $p > 0.05$, one-way ANOVA with post hoc Tukey-Kramer test.

Figure 4. Representative photographs of the marigold plants with lower leaves that acquired a purple color. Certain marigold plants in the Urea Solution, Burnt Foliage, and Eggshell Grounds groups developed a purple hue around the edges and tips of leaves lowest on their stems. Marigolds in the Urea Solution (left) and Burnt Foliage (right) groups are shown.

DISCUSSION

Select growing methods from this study encouraged healthy plant growth, as shown by them yielding taller plants at first bloom, increasing survival rates, and decreasing growth times. The initial hypothesis was correct in some respects. This study demonstrated that simple, more environmentally conscious growing methods can be applied to household gardens, using common objects often overlooked in the house to reduce chemical fertilizer usage as well as using water-efficient hydroponic systems to reduce water consumption.

This study revealed that growing garden cress with a DWC hydroponics system increased garden cress height at first bloom at a statistically significant level compared to the control group, indicating its success in encouraging healthy plant growth. Taller plants, as compared to short plants, indicate the presence of critical nutrients and minerals required for healthy plant growth. However, the selected growing methods applied to marigolds did not result in significantly different plant heights at first bloom. This is despite the Eggshell Grounds group having the highest average plant height at first bloom, implying a possible lack in statistical power. Had there been more marigolds grown and observed, the results for marigold plant height at first bloom might have been significant as power can be increased with a greater sample size.

The experiment also indicated that plant growth time was affected for only garden cress, though there was no significant difference between the control and other treatments. Longer growth times would indicate slower growth due to a lack of nutrients, which is consistent with the findings (10). The lowest average growth time for garden cress came from the DWC treatment while the higher average growth times came from the in-ground treatments and control, which had fewer supplied nutrients. Shorter growth times would indicate heathy plant growth due to the presence of necessary nutrients. For marigolds, there was no meaningful difference between average growth times for all the treatments, demonstrating a difference in treatment efficacy based on plant types.

The discrepancy between the ANOVA results, which found statistical significance between the garden cress groups for growth time, and the post hoc Tukey-Kramer test, which found no statistical significance between the control and other treatments, is likely due to a lack of statistical power. Due to the small sample sizes, statistical power was low, thus reducing the chance a post hoc test would be able to detect a difference between treatments.

The study additionally demonstrates the impact each treatment has on the survival rate of both types of plants. While the survival rate for garden cress plants were roughly similar, the rates for marigolds varied. Group 1 marigolds (the control) had the lowest survival rate while Groups 4, 5, and 6 (Eggshell Grounds, Wick System, and DWC System) had the highest survival rates. A higher survival rate indicates healthy plant growth as the soil contains the necessary nutrients. For the marigolds, the reason for a lower survival rate for the control group is obvious, as no nutrient-bearing treatment was applied. However, the higher survival rates for the Eggshell Grounds, Wick System, and DWC System treatments demonstrate their contribution to healthy plant growth since all were successful in sustaining every marigold that sprouted. For the cress, similar survival rates, where up to one plant died for each treatment, reveal the limited impact each treatment had in sustaining the garden cress plants.

Notably, across all the plant health metrics (height, survival rate, and time to bloom), DWC System groups consistently outperformed or were equal to other growing methods. This may point to the DWC System's overall high capability of providing nutrients to plants. A similar case may be made for the Eggshell Grounds and Wick System groups for marigolds. However, in the case of the Burnt Foliage groups, this does not apply. In both marigolds and the garden cress, the plant survival rate remained the same, at a rate of approximately 0.8 growing/survived with a similar rate of decline (dying off around the 40-day mark). This suggests that the Burnt Foliage treatment may not be a very effective natural fertilizer. Similarly, Urea Solution groups across both plants had a similar survival rate; however, there was a greater disparity between when plant sprouts started to die off.

The development of a purple color in the leaves of marigolds in Groups 2, 3, and 4 indicate a phosphorus deficiency in the soil (11). As none of the treatments applied to the in-ground plants supplied phosphorus, this is not surprising. Further research may consider other unconventional growing methods to supplement the lack of phosphorus or repeating this study with phosphorus applied to each in-ground treatment.

There are multiple limitations within this study. Only a maximum of six plants for each treatment were tracked over the 13-week period. Additionally, only two types of plants were taken into consideration for this experiment. Future studies should include a greater number of individual plants for each treatment to create a larger sample size. Though marigolds and garden cress (a flower and an herb) were selected to represent an average garden, a greater variety of garden plants such as fruits, vegetables, and legumes, which have

different growing requirements, could be experimented on in further research. The narrow range of plant types also raises the question of whether these treatments would be practical on the wide-scale commercial agricultural level.

Other limitations of this study involve the manner in which it was conducted and the way the data was collected. This study was conducted for only 13 weeks. Further research may track these plants over months or years across different annual seasons and multiple growing seasons to evaluate the long-term effects of each treatment on the plants. Furthermore, this experiment only considered height at first bloom, survival rate, and growing time as metrics for plant health. Additional studies may consider more indicators of plant health such as plant weight and root condition. Moreover, plant height may be a slightly biased indicator due to natural variations in height that occur due to changing leaf positions at the time of daily data collection. Likewise, we only tracked height until the plant first bloomed. Changes in overall plant height may have occurred after data collection stopped and may have therefore been missed.

This study demonstrates more sustainable growing methods a household can employ to yield greater, healthier, and more sustainable plant growth and highlights the potential common items and wastes that can be utilized for agricultural purposes. Similarly, our findings confirm the superiority of substrate-based systems for growing plants over the traditional in-ground soil method, which may be useful as the global supply of arable soil decreases (12). Future researchers may aim to extract other minerals and nutrients from household wastes or experiment with different non-soil growing mediums to examine their effects on plant growth.

METHODS

Germination and planting

To germinate the marigold and garden cress seeds, seeds were placed between moistened paper towels in an airtight plastic bag for 1 – 2 days at room temperature (70°F), until the seeds were hydrated. Once roots or sprouts began emerging, the seeds were transferred into the soil or growing medium at a depth of 0.25 inches (6 mm). Two marigold seeds and six garden cress seeds were planted in separate soil pots. The soil used to plant marigold and garden cress seeds was obtained from the same location. Two marigold seeds were planted in a 1:1 ratio of vermiculite and perlite for the Wick System treatment while only one seed was planted in perlite alone for the DWC treatment. Six garden cress seeds were planted in a 1:1 ratio of vermiculite and perlite for the Wick System treatment while only one seed was planted in perlite for the DWC treatment.

Plant maintenance

Plants grown in dirt were watered daily. Each watering session thoroughly moistened the top of the soil. The plants were watered between two and six times daily, depending on the time of year and weather conditions. Watering was sufficient to keep plants from wilting. The marigold and garden cress pots and hydroponic systems were placed in an area with full sun. Any plants that died and all weeds were removed upon detection.

In-ground treatment preparation and application

To create the Urea Solution treatment, samples of urine and tap water were combined into a 1:1 ratio. The solution was applied directly to the soil, enough to saturate the surface. To create the Burnt Foliage treatment, dried lawn clippings and woodchips were burnt. About one teaspoon of ashes were spread on the surface of the soil. To create the Eggshell Grounds treatment, several eggshells were washed and then ground into fine shards using a mortar and pestle. About 1 teaspoon of grounds was spread on the surface of the soil.

Hydroponics systems construction

To create the Wick System treatment, a plastic juice bottle was rinsed and cleaned before being cut along its neck. The top of the bottle was inverted to serve as a pot. The bottom of the bottle was filled with the nutrient solution (detailed below). The wicks were created from recycled socks cut and plugged tightly into the bottle opening. Each wick clearly extended into the nutrient solution. The growing medium was a 1:1 mixture of perlite and vermiculite filling the pot to approximately 80% capacity (**Figure 5**).

To create the DWC System treatment, 6 oz. yogurt containers were recycled into nest pots. Four slits longitudinally were cut in each container and four openings were made at the bottom corners (**Figure 6**). Twelve holes the size of a nest pot were cut into a block of Styrofoam large enough to fit into the top of the container. Each fashioned nest pot was filled with perlite to about 75% capacity. The block was made to float on top of the nutrient solution. At the bottom of the container, two air stones were attached on each side. Both air stones were attached to an air pump by plastic tubing and connectors (**Figure 7**).

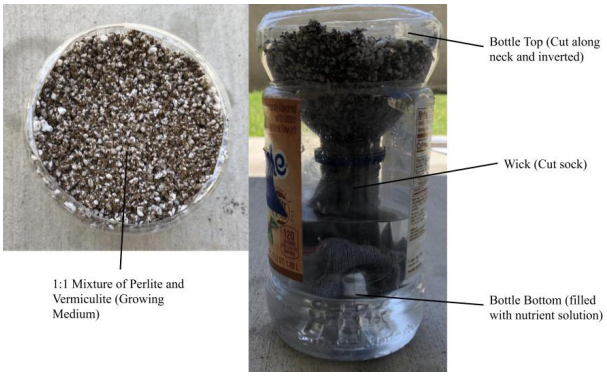

Figure 5. Wick system set-up. No plants are in the system for photographic purposes. A cleaned juice bottle was cut with the top inverted to use as a pot and the bottom as the nutrient reservoir. The growing medium is composed of a 1:1 ratio of perlite and vermiculite, which filled each pot to about 80% capacity.

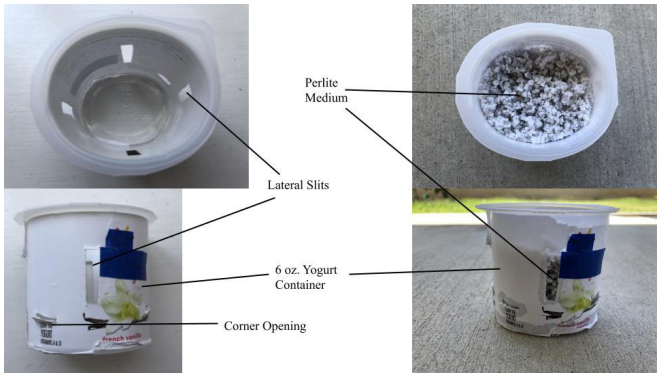

Figure 6. Nest pot construction and DWC system set-up. No plants are in the nest pot for photographic purposes. A 6 oz. yogurt cup was recycled into a net pot by cutting slits and holes into the sides. Perlite filled each nest pot to about 75% capacity.

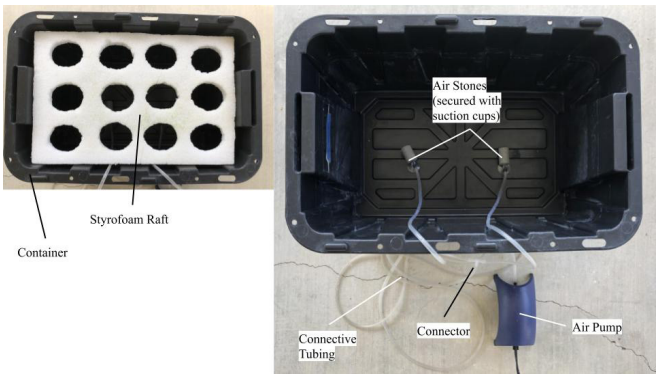

Figure 7. DWC system set-up. No plants are in the system for photographic purposes. The DWC treatments for both plants were housed in a 7-gallon container. Twelve nest pots were placed into a block of Styrofoam and floated atop the nutrient solution.

Hydroponics maintenance

All hydroponically grown plants were given a nutrient solution composed of water and plant food. The plant food was water-soluble and contained 10% nitrogen, 5% phosphate, and 14% potash (a soluble potassium compound). The Wick System plants were grown in a solution composed of 0.25 gallons of water and 0.5 teaspoons of plant food. The DWC system plants were grown in a solution composed of 5 gallons of water and 7 teaspoons of plant food. Each week, the nutrient solutions were drained and replaced. Any occurrences of algae were removed with a 3% hydrogen peroxide solution and thorough rinse with water.

Data collection

Each day in the early evening, the height of every plant was measured, from base of stem to the highest point of the plant (bud, flower, or leaf) using a length of string and ruler. The height at first bloom (when a bud opened into a flower) was used for statistical analysis. The plants were allowed to grow in a Southern California climate during the months of May to August for up to 13 weeks. Once a plant bloomed, we stopped tracking its plant height and observed only qualitative changes.

ACKNOWLEDGEMENTS

We would like to thank our parents for providing us with the funds to perform this project as well as Andrew's family members for assisting with the draining and cleaning of the hydroponics systems each week.

Received: October 13, 2020
Accepted: February 5, 2021
Published: February 25, 2021

REFERENCES

1. Ameen, Ayesha, and Shahid Raza. "Green Revolution: A Review." *International Journal of Advances in Scientific Research*, 2018, vol. 3, no. 12, pp. 129–137., doi:10.7439/ijasr.v3i12.4410.
2. Eghball, B., *et al*. "Long-Term Manure and Fertilizer Application Effects on Phosphorus and Nitrogen in Runoff." *Transactions of the ASAE*, 2002, vol. 45, no. 3, doi:10.13031/2013.8850.
3. "How Fertilizers Harm Earth More Than Help Your Lawn." *Scientific American*, Scientific American, 20 July 2009, www.scientificamerican.com/article/how-fertilizers-harm-earth/.
4. Ward, M., Jones, *et al*. "Drinking Water Nitrate and Human Health: An Updated Review." *International Journal of Environmental Research and Public Health,* 2018, vol. 15, no. 7, doi:10.3390/ijerph15071557.
5. Boano, Fulvio, *et al*. "A Review of Nature-Based Solutions for Greywater Treatment: Applications, Hydraulic Design, and Environmental Benefits." *Science of The Total Environment*, 2019, vol. 711, doi:10.1016/j.scitotenv.2019.134731.
6. Blok, Chris, *et al*. "Maximum Plant Uptakes for Water, Nutrients, and Oxygen Are Not Always Met by Irrigation Rate and Distribution in Water-Based Cultivation Systems." *Frontiers in Plant Science*, 2017, vol. 8, doi:10.3389/fpls.2017.00562.
7. White, P. J., and P. H. Brown. "Plant Nutrition for Sustainable Development and Global Health." *Annals of Botany*, 2010, vol. 105, no. 7, pp. 1073–1080. doi:10.1093/aob/mcq085.
8. Marieb, Elaine, and Katja Hoehn. *Human Anatomy & Physiology*. 8th ed., Benjamin Cummings, 2010.
9. Hauser, Stefan, and Lindsey Norgrove. "Slash-and-Burn Agriculture, Effects Of." *Encyclopedia of Biodiversity*, 2013, vol. 2, pp. 551–562., doi:10.1016/b978-0-12-384719-5.00125-8.
10. Silva, James, and Uchida, Raymond. *Plant Nutrient*

Management in Hawaii's Soils: Approaches for Tropical and Subtropical Agriculture. College of Tropical Agriculture & Human Resources, 2000.
11. Raese, J. Thomas. "Phosphorus Deficiency Symptoms in Leaves of Apple and Pear Trees as Influenced by Available Soil Phosphorus." *Communications in Soil Science and Plant Analysis*, 2002, vol. 33, no. 3-4, pp. 461–477., doi:10.1081/css-120002757.
12. Benke, Kurt, and Bruce Tomkins. "Future Food-Production Systems: Vertical Farming and Controlled-Environment Agriculture." *Sustainability: Science, Practice and Policy*, 2017, vol. 13, no. 1, pp. 13–26., doi:10.1080/15487733.2017.1394054.

JOURNAL OF
EMERGING INVESTIGATORS

Article

The effect of poverty on mosquito-borne illness across the United States

[1]Kavita Kar, [2]Russanne Low
[1]Wheeler High School, Marietta, Georgia
[2]Institute for Global Environmental Strategies (IGES), Arlington, Virginia

SUMMARY

Mosquito-borne diseases are a major issue across the world, and the objective for this project was to determine the characteristics that make some communities more susceptible to these diseases than others. We hypothesized that low-income communities are more susceptible to mosquito-borne diseases. To test this hypothesis, we identified and studied characteristics that make communities susceptible to mosquito-borne diseases, including water in square miles, average temperature, population, population density, and poverty rates per county. We used regression analysis to understand the relationship between the above variables and the total number of mosquito-borne disease cases. We found that the population of a county is the best indicator of the prevalence of mosquito-borne diseases. Rate of poverty in the county was not found to be a significant indicator of mosquito-borne diseases. This may be because poverty aggregated at county level does not describe income level variation within the county. In this research, both rural and urban counties were analyzed. Although rural counties have high rates of poverty, the population of rural counties are spread out, so they are at a lower risk of disease. Therefore, we conclude that population data needs to be studied in conjunction with poverty levels to truly understand the relationship between poverty and mosquito-borne diseases.

INTRODUCTION

Mosquitoes are deadly creatures because they are effective vectors of an array of diseases. Each year, 700 million people worldwide contract mosquito-borne diseases and 1 million die due to these diseases. Mosquitoes are an issue in both developed and developing countries (1). Mosquito-borne disease rates in the United States are on the rise and could spike if active prevention is not practiced. In 2016 alone, there were 47,461 reported cases of mosquito-borne diseases in the U.S. (2).

There are several established factors that affect the presence of mosquitoes, including climate (humidity, temperature, rainfall, etc.), freshwater availability, and the presence of blood sources (3). Climate is a large predictor of mosquito abundance; mosquitoes are drawn to warmer places and places with more rainfall (4). Mosquitoes also breed in areas where there is stagnant freshwater, such as near lakes and ponds (3). These environmental concerns are more pressing for certain parts of the U.S., like the southeast region, which has hospitable environments for mosquitoes (4).

Aedes albopictus, a species of mosquito that can carry many diseases such as dengue, chikungunya, yellow fever, and zika, has been noted to travel only up to 300 feet in search of a blood meal, and other species have a maximum flight range of 1–3 miles. This short flight range of mosquitoes creates the situation where mosquitoes are only able to exist within a certain community (5). This also means that mosquitoes do not travel between communities, and mosquitoes born in a community will only stay in that community. It has even been noted that in Baltimore, there are three times as many mosquitoes in low-income neighborhoods than in high-income neighborhoods (6). An emerging field of research describes the effect of poverty on the mosquito population in a region and the characteristics of poverty that make communities most susceptible to increased mosquito populations.

The city of Baltimore, Maryland has been a model city to study poverty in conjunction with mosquito populations. In Baltimore, the largest contributor to the disparity in mosquito populations is the land cover that surrounds the neighborhoods studied. Land cover describes the surface of the earth and what potential habitats can exist in these neighborhoods. Since Baltimore itself has a homogenous climate and the sample sites were not near freshwater sources, it is likely that the neighborhood and the fauna were the biggest influences on the number of mosquitoes in the region (7). Characteristics of low-income communities like poor waste management, high building abandonment, many rodent blood sources, and poor pest control lead to an increased population of mosquitoes (7).

Historically, low-income communities suffer with poor waste management. Rainwater collects in small pieces of trash and debris and creates a breeding ground for mosquitoes (7). The median household income was also negatively associated with the quantity of garbage (7). Lower income communities are more likely to have large numbers

of abandoned buildings, which often collect rainwater in stagnant pools that offer another breeding ground for mosquitoes (6). While wealthy communities have on average one abandoned structure per 100 buildings, median income communities have five abandoned structures per 100, and low-income communities have 26 abandoned structures per 100 (7). Additionally, people in lower income communities may not have resources to eliminate mosquito habitats and are likely to have disused containers near them. A study found that *Ae. albopictus* were 83% more abundant in disused containers and could potentially contribute to the spread of diseases (8).

In low-income communities, rats are common, and mosquitoes often feed on rats in addition to humans. This diversity of blood sources increases the total amount of sustenance for mosquitoes and can potentially support a larger mosquito population (6). There is also a disparity between the amount of money spent on mosquito control in low-income neighborhoods versus wealthy neighborhoods. The average mosquito treatment costs several hundred dollars, which may not be feasible for most low-income families to implement. Prices start around $325 and can go as high as $1,900 for seasonal control for typical pest control programs (3).

The effects of these issues include increased numbers of mosquitoes, which creates a higher number of potential vectors for mosquito-borne diseases to spread. We investigated the hypothesis that low-income communities experience mosquito-related illnesses at a higher rate than high income communities. The model created in this research includes explanatory variables aggregated at a county level: area in square miles, average temperature, population, population density, and the poverty rate per county. The dependent variable is the number of cases of neuroinvasive (most severe) mosquito-borne diseases in a county. Neuroinvasive cases of diseases are more deadly, and they constitute approximately one-third of all cases of West Nile Virus, the most common mosquito-borne disease in the US (9). This distinction was created as the reported cases of neuroinvasive disease are thought to be the most accurate indicator of arboviral activity in humans. In contrast, reported cases of non-neuroinvasive arboviral disease are more likely to be impacted by the disease awareness and healthcare seeking behavior in different communities, and by the availability and specificity of laboratory testing that is performed. The diseases included in the study are chikungunya, dengue, eastern equine encephalitis (EEE), Jamestown Canyon, La Crosse, St. Louis encephalitis, and West Nile virus. There are other mosquito-borne diseases present in the U.S., but data is consistent for only these diseases.

The scope of this research includes every county in the continental U.S. We chose Cobb and Dekalb counties to be studied in further detail because the similarities and differences between these counties may offer insights into why low-income communities experience mosquito-related illnesses at a higher rate than other communities. In addition to other variables, we investigated land cover elements in both counties. Any relationships identified in this research will add to our knowledge about social factors that influence rates of mosquito-borne diseases. Our findings could inform why and how governments and communities should allocate resources to minimize the spread of these diseases in vulnerable communities.

RESULTS

To determine whether low-income communities experience mosquito related illnesses at a higher rate than high income communities, a multiple regression analysis was performed with the total cases of mosquito-borne diseases in the U.S. as the dependent variable. This data was collected from CDC ArboNet (9).

The model tested the following explanatory variables: poverty rate, population, population density, square miles of water, and average temperature. This data was collected from the 2010 U.S. Census at the county level. The multiple R^2 values of the data and estimates were analyzed to understand how well the independent variables explained the number of cases of mosquito-borne diseases.

Rate of poverty was the primary variable we investigated with this model. Population and population density were chosen to model the spread of diseases because densely populated areas provide many more hosts and hence mosquito-borne diseases are likely to spread quickly. Square miles of water, as well as average temperature, were included to understand if climatic differences across the U.S. contributed to the number of mosquito-borne diseases. Because the U.S. has several different climate zones, we conducted further regional analysis to account for the impact of climate on mosquito populations.

A multiple linear regression model was used to predict the number of cases of mosquito-borne diseases (DV) based on the variables mentioned above. A significant regression equation was found ($F(5, 1301) = 705.12$, $\boldsymbol{p < 0.00}$), with an R^2 of 0.73000. This model predicts that cases of mosquito-borne diseases are equal to -0.00810 + 0.00055 (POPULATION) - 0.00680 (WATER) - 0.00310 (POPULATION DENSITY) + 0.33550 (POVERTY) - 0.13670 (AVG. TEMP), where cases are counted as number per county, population is counted as number of residents per county, water is counted as the square miles of water in a county, population density is counted as the population divided by the square miles of land in a county, poverty is counted as the percentage of people in a county that live below the poverty line, and the average temperature is counted as the average year-round temperature in a county in degrees Fahrenheit. The number of mosquito-borne diseases increased by 0.00055 for each additional person, increased 0.00680 for each square mile of water, decreased by 0.00310 for each person per square mile, increased 0.33550 for each percent increase in poverty rate, and decreased 0.13670 for each degree Fahrenheit. These results were analyzed beyond the national level.

To ensure climate consistency, the data was further analyzed for each climatic region of the country: Southeast, Northeast, West, Southwest, and Midwest (**Table 1**). The R^2 values were consistent across all regions, except in the Southeast region where the R^2 was extremely low. A low R^2

Table 1. R^2 values across United States regions.

Region	R^2
Southeast	0.14420
Northeast	0.67489
West	0.82290
Southwest	0.84658
Midwest	0.856970
All	0.73045

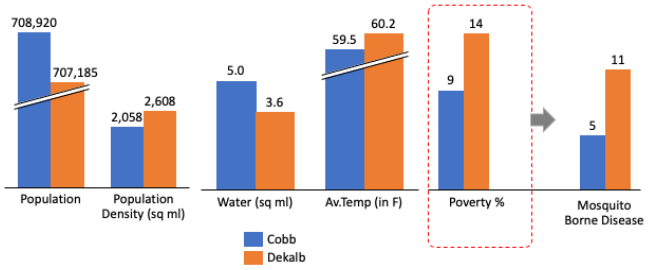

Figure 1. Comparison of social characteristics of Cobb and Dekalb counties where Dekalb has a higher poverty rate and more mosquito-borne disease cases. These characteristics establish similarity in these counties in all respects except poverty.

value means that the model did not describe the cases of mosquito-borne diseases at all, and that there was either a data consistency issue, or another variable that was not analyzed. The data chosen for the number of cases was collected by CDC ArboNET, obtained as part of a voluntary program. One irregularity identified was the number of cases in Miami-Dade County. There were no reported cases recorded for the past 5 years in the ArboNET database for this county, when in fact there have been several confirmed cases (10).

Cobb and Dekalb

Further analysis was conducted on the poverty rates of Cobb and Dekalb counties. Cobb and Dekalb counties were studied in further detail because they have many common elements. They are adjacent counties in Georgia and have similar populations, population densities, average temperatures, and square miles of water; however, the poverty rate is different between these two counties. The poverty rate in Dekalb county is 14% whereas Cobb is at 9% (**Figure 2**), however the number of mosquito-borne disease cases in Dekalb is more than double that of Cobb. The land cover in both Cobb and Dekalb was analyzed to identify elements including canopy cover, buildings, and roads (**Figures 1-2, 4**). These elements create easily identifiable mosquito breeding grounds. The land cover distribution in both Cobb and Dekalb counties were found to be similar. Both Cobb and Dekalb counties had a high percentage of buildings because they are suburban areas. The map of poverty rates was superimposed on the county maps (**Figure 3**). There were a greater number of poor areas in Dekalb than in Cobb (11).

DISCUSSION

A multiple regression model was run with the total cases of mosquito-borne diseases as the dependent variable and poverty rate, the square miles of water, the population of a county, the population density of a county, and the average temperature of a county as explanatory variables. Each explanatory variable contributed to the model, and each had certain nuances.

Population

The population variable contributed to the greatest change in R^2. Urbanization creates suitable habitats for vector mosquitoes in which there are a reduced number

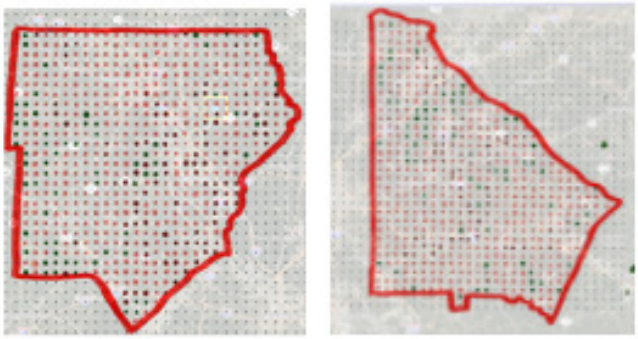

Figure 2. Depiction of the land cover of Dekalb and Cobb counties overlaid on satellite imagery of the county. The satellite imagery is from Collect Earth Online. The land cover elements described are buildings (light red), roads (dark red), and canopy cover (dark green). This comparison of land cover elements in the counties helps identify the habitats of the county.

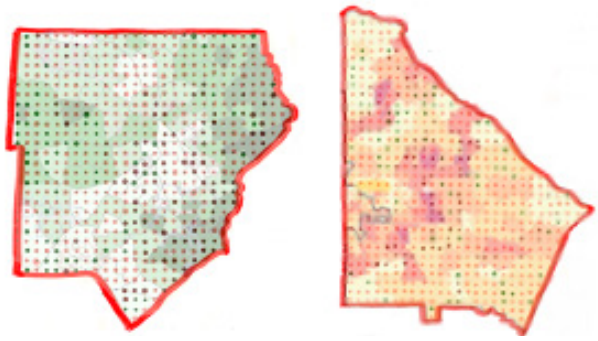

Figure 3. Depiction of the land cover of Dekalb and Cobb counties overlaid on a map of poverty in the county. The maps come from community surveys (11, 15). The darkest green indicates the wealthiest areas of the county, and the lightest green indicates the poorest areas. With the land cover elements mapped over poverty, it may be possible to understand what socioeconomic factors lead to certain land cover elements.

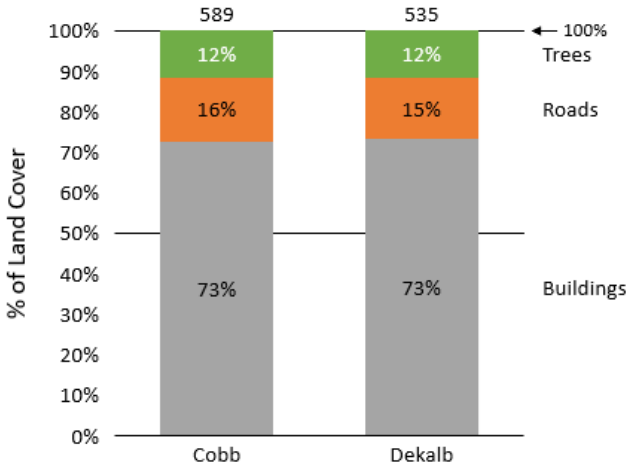

Figure 4. Cobb and Dekalb counties have similar land cover elements. Three land cover elements (canopy cover, buildings, and roads) are compared by sample sites in Cobb and Dekalb county.

of predators and human hosts are widely available (8). An alternate explanation to this is that there are simply more people for mosquitoes to infect in large cities, which leads to more mosquito-borne disease cases. Counties with high populations include metropolitan areas. Among the 10.6 million low-income working families in America, racial and ethnic minorities constitute 58%, despite only making up 40% of all working families nationwide (12). Ethnic minorities are also overrepresented in urban areas. Among urban residents, 56% are not white, compared with 32% in suburban and small metro counties and 21% in rural counties (13). In addition to this, minorities are less likely to receive adequate medical care, which puts them at a greater risk of complications from mosquito-borne diseases (13). Thus, incidence of mosquito-borne diseases across socioeconomic levels disproportionately affects ethnic minority communities. Understanding this issue is crucial when allocating city expenditure on public health measures. It will allow the government the ability to make public health decisions on a community-by-community basis.

Population density

Population density by county was not a significant contributor to the variance of R2. This is counterintuitive because a high population density is conducive to the spread in the mosquito-borne illnesses. However, county level may not be the best way to analyze population density because it relies heavily on total land area in a county, some of which may be uninhabited, and the majority of the population may be concentrated in a few urban areas. Density should therefore be studied on a granular level, potentially by Census Block Group. The most granular level of data available on ArboNET is at the county level, which may not be enough to understand the issues related to mosquito-borne illnesses. Because the distance that mosquitoes travel is small, mosquitoes only spread at a neighborhood level (5). Metropolitan areas are observed to be at a high risk of mosquito-borne diseases; thus, it is important to study the effects of mosquitoes in a more granular level here to implement preventative measures.

Poverty

Average poverty rate per county was not a significant contributor to variance. A possible reason for this is that county level aggregation is not indicative of large variation of incomes in different neighborhoods within a county. For example, in Cobb county, for the zip code 30068, the median household income is $117,475, and for the zip code 30168, the median household income is $44,911. Another example is in Dekalb county; in the zip code 30093, the median household income is $41,043, and in the zip code 30338, the median household income is $101,982 (16). These are large variations, and they affect the representation of poverty rate across a county. When this data is aggregated on a county level, these variations are lost. In prior studies about income and the effects of mosquitoes in Baltimore, data was collected and measured by street, and each part of the city was divided based on income block. This detailed separation allowed for better analysis of the effect of poverty on counts of mosquito-borne diseases. Rural communities need to be studied separately from urban communities. Rural counties have higher rates of poverty, but as the population is spread out, they may be at a lower risk of disease (3).

Temperature

The average annual temperature was not found to be a significant indicator of mosquito-borne disease in a county. The average annual temperature in the county may not be a good predictor because much of the United States has a temperate climate, where there are hot summers and cold winters (10). This may restrict preconditions needed for mosquitoes to thrive in certain regions and certain periods of time. Mosquitoes thrive year-round in tropical climates because temperatures are extremely consistent and warm. In the U.S. where there is a large band of temperate areas, averaging the temperature over a year hides the unsuitable conditions in many areas. For example, in Chicago, there are cold winters and hot summers, whereas in a coastal city, the temperature is consistent year-round. These cities could both average to the same temperature, but their climates and the opportunity that they afford mosquitoes are different. Therefore, an additional analysis was conducted by region.

Square Miles of Water

The square mileage of water in a county was not found to be a significant contributor to the number of cases of mosquito-borne diseases. This may have to do with the distribution of water sources in a county, as mosquitoes lay eggs in shallow parts of water bodies. This impacts the number of mosquitoes in a county because there may be counties with some marshy areas with multiple shallow water

bodies and in other counties there may be one large lake. For example, a county with a high square mileage of water may include a large lake, which mosquitoes would not breed in.

Cobb and Dekalb

Based on the information provided by the Baltimore studies, it is possible that many of the buildings in the low-income areas in Dekalb may be ripe for mosquito-borne diseases. Dekalb as a county has many urban, poor areas. This observation needs to be further substantiated with mosquito surveillance programs to better inform disease models. This may provide an avenue for future research to find the connections between land cover and poverty rates.

Future overall program implementations

Overall, we created a model that described mosquito-borne disease cases across the United States and have found that that it is extremely likely that counties with a high population, such as counties with large cities are further at risk of mosquito-borne diseases. Additionally, while the data is not granular enough to determine whether poverty is correlated with mosquito-borne diseases, this model sets a framework from which future research can be conducted.

The current model can be developed further by adding more descriptive data such as humidity and rainfall, and by building it on a more granular level. This will help predict the occurrence of mosquito-borne diseases more accurately. The current impediment is that the ArboNET data is limited to a county level aggregation. It is not reported at a more granular level. Also, the data may not be accurately reported because it is a voluntary program; in impoverished areas, many cases go undiagnosed and unreported (5).

Disease data only reflects past outbreaks, which are not an effective predictor for future outbreaks. For an outbreak to occur, the population must have at least one infected person. This may mean an area with a high population of mosquitoes has not yet had an infected individual yet, but if an infected individual is introduced, the disease will spread quickly. This stresses the importance of mosquito surveillance data to track the mosquitoes rather than using past disease data.

As the Baltimore studies show, understanding the effects of poverty on mosquito-borne illness requires a more local level of analysis than the county data used in this study. The next step for this research would be to expand the surveillance of mosquitoes in other cities using the GLOBE Observer program. The GLOBE Observer program is a NASA citizen science initiative to track mosquito habitats and movement patterns. This program could be used to map mosquito habitat data to the average income in the census tract the collection point lies in. One recommendation is to immediately promote this program in highly populated cities to begin analysis and prevention.

METHODS

Datasets Used

Data analysis was performed at a county level in the U.S. and by different regions, as there are several climate zones that span the United States. The analysis was conducted by comparing the neuroinvasive cases of mosquito-borne illnesses to other factors including poverty rate, square miles of water area in the county, population, population density, and average annual temperature.

The data source for arboviral diseases was ArboNET, a voluntary national arboviral surveillance system (9). This is a CDC program and data are reported by healthcare providers. Since 2003, ArboNET has collected data for all notifiable arboviral diseases. The viruses studied are Chikungunya, Dengue, Eastern equine encephalitis (EEE), Jamestown Canyon, La Crosse, St. Louis encephalitis, and West Nile. This data includes only the neuroinvasive cases of all these diseases. This measure was taken to ensure that there was not a severe disparity between wealthy and poor communities in diagnosis, given that non-neuroinvasive cases are harder to diagnose and these individuals are less likely to seek treatment. The total cases of mosquito-borne disease were aggregated for the years 2014–2019, to create a set period where yearly climate variations would not affect the total number of cases.

Poverty rate per county was collected from the U.S. Census Bureau which describes the poverty rates across all counties in the country. The data represents a five-year average of poverty rates in each county. The measure of poverty adopted by this study is the percentage of individuals in a county that earn below the poverty line. County level poverty data allowed the same level of specificity as the disease data. The water data measures the square miles of water in a county and is sourced from USA.com created from the 2010–2014 U.S. Census. The source for population, temperature, and population density per county were also sourced from USA.com, which uses U.S. Census data (17–19).

The in-depth analysis of Cobb and Dekalb counties was done using data from Collect Earth Online (20). Collect Earth characterizes and classifies land cover data from satellite imagery. Collect Earth works with GeoDash, which uses information from Google Earth Engine. The data that Google Earth uses is from Landsat imagery.

Data Collection Procedure

The disease data was requested from the CDC. The Census data was first downloaded from USA.com in csv files. The data elements that were analyzed were not in a consistent format, so Microsoft Excel functions were used to clean and merge the datasets together.

Statistical modeling

Multiple regression analysis was used to understand the relationship between the explanatory variables and the total number of mosquito-borne disease cases, and then to understand how each explanatory variable was related to the

response variable. This step was crucial in testing the guiding hypothesis because it provided insight into which explanatory variable was the most connected to the total cases of mosquito-borne diseases. This allowed us to understand the variable poverty level in a county in comparison to other factors. The multiple regression analysis was conducted in Microsoft Excel. The total number of cases of mosquito-borne disease was set as the dependent variable. Poverty rate by county, square miles of water in a county, population of a county, population density of a county, and the average temperature of a county were all used as explanatory variables. The multiple R^2 values of the data and estimates were analyzed to understand how well the data fits the regression line. This analysis was conducted at a national level first. Because this analysis was performed over a broad region with several different climate zones, we identified that climate may impact each region's interpretation. For further analysis, the data was divided by the five regions (Northeast, Southeast, Southwest, West, and the Midwest).

Cobb and Dekalb

To conduct a deeper analysis for Cobb and Dekalb counties in Georgia, satellite images of the land encompassed by the counties were selected, and the outline of each county was superimposed onto the satellite data to identify land cover characteristics: canopy cover, buildings, and roads. This is significant in determining what a county's physical features are, and the potential habitats it provides. A grid was placed over each county to simulate random sampling points for land cover data. At the location of each grid point, the land cover element was identified. After this initial land cover analysis, the land cover elements were compared, and the numbers of elements and their distributions were graphed to identify whether Cobb and Dekalb have the same land features. The land cover analysis was mapped to the regions of Cobb and Dekalb counties that had high rates of poverty. This was done to understand whether there are particular land features that arise in areas with high poverty rates.

Received: August 31, 2020
Accepted: February 15, 2021
Published: February 25, 2021

REFERENCES

1. Sowards, Will. "Why Mosquitos are the Most Dangerous Creature." *Passport Health*, 10 August 2016. https://www.passporthealthusa.com/2016/08/why-mosquitoes-are-the-most-dangerous-creature/. Accessed 21 December 2020.
2. Elflein, John. "Mosquito-borne disease cases number U.S. 2004-2018." *Statista*, 5 November 2020. https://www.statista.com/statistics/856988/reported-mosquito-borne-disease-cases-total-number/. Accessed 21 December 2020.
3. MosquitoNix Austin: Mosquito Treatment. Georgetown, TX Mosquito Control. 3 January 2019. https://mosquitonixaustin.com/georgetown-tx-mosquito-control/. Accessed 28 July 2020.
4. MacMillan, Heath. "Why your summer might be full of mosquitoes, according to a scientist." *The Conversation,* 27 January 2020. https://theconversation.com/why-your-summer-might-be-full-of-mosquitoes-according-to-a-scientist-98369. Accessed 28 July 2020.
5. Dowling, Zara, Ladeau, Shannon L., Armbruster, Peter, Biehler, Dawn, & Leisnham, Paul T. "Socioeconomic Status Affects Mosquito (Diptera: Culicidae) Larval Habitat Type Availability and Infestation Level." *Journal of Medical Entomology,* vol. 50, no. 4, 2013. doi: 10.1603/me12250
6. Goodman, Heather, *et al*. "Primary Blood-Hosts of Mosquitoes Are Influenced by Social and Ecological Conditions in a Complex Urban Landscape." *Parasites & Vectors*, vol. 11, no. 1, 2018, doi:10.1186/s13071-018-2779-7.
7. Little, E., *et al*. "Socio-Ecological Mechanisms Supporting High Densities of Aedes Albopictus (Diptera: Culicidae) in Baltimore, MD." *Journal of Medical Entomology*, vol. 54, no. 5, 2017, pp. 1183–1192., doi:10.1093/jme/tjx103.
8. Wilke, André B. B., *et al*. "Urbanization Creates Diverse Aquatic Habitats for Immature Mosquitoes in Urban Areas." *Scientific Reports*, vol. 9, no. 1, 2019, doi:10.1038/s41598-019-51787-5.
9. ArboNET. "Humanbycounty [Data File]." *CDC ArboNET*, 2020.
10. Arnfield, John. "Köppen Climate Classification." *Encyclopædia Britannica*, Encyclopædia Britannica, Inc., www.britannica.com/science/Koppen-climate-classification.
11. Neighborhood Nexus. "Dekalb Poverty Map." *Neighborhood Nexus*, opendata.atlantaregional.com/datasets/fc4bef43341346cbaa3b14d28f0e11fe
12. "DOH-Miami-Dade Health Officials Confirm Three Cases of West Nile Virus." *Florida Department of Health in Miami-Dade County*, 2020, miamidade.floridahealth.gov/newsroom/2020/10/2020-10-19-DOH-Miami-Dade-Health-Officials-Confirm-Three-Cases-of-West-Nile-Virus.html.
13. Povich, Deborah, and Brandon Roberts. Winter 2014-2015, The Working Poor Families Project, 2014, *Low-Income Working Families: The Racial/Ethnic Divide*.
14. Bridges, Khiara. "Implicit Bias and Racial Disparities in Health Care." *American Bar Association*, www.americanbar.org/groups/crsj/publications/human_rights_magazine_home/the-state-of-healthcare-in-the-united-states/racial-disparities-in-health-care/.
15. Community Profile Appendix 1. (2018). Retrieved from https://s3.us-west-2.amazonaws.com/cobbcounty.org.if-us-west-2/prod/2018-07/APPENDIX12040COMMUNITYPROFILEFINAL.pdf.
16. "30338 Income Statistics." *30338 Income Statistics - Current Census Data for Zip Codes*, 2020, www.incomebyzipcode.com/georgia/30338.

17. "U.S. Average Temperature State Rank." *USA.com*, 2020, www.usa.com/rank/us--average-temperature--state-rank.htm.
18. "U.S. Population Density County Rank." *USA.com*, 2020, www.usa.com/rank/us--population-density--county-rank.htm?yr=9000.
19. "U.S. Total Population State Rank." *USA.com*, 2020, www.usa.com/rank/us--total-population--state-rank.htm?yr=9000.
20. Collect Earth Online. (n.d.). Retrieved January 18, 2021, from https://collect.earth/.

Sponsorship

Editor's Circle $10,000+

ALLOY THERAPEUTICS

Patron $5,000+

NEW ENGLAND BioLabs® Inc.
enabling technologies in the life sciences

PORTFOLIOS WITH PURPOSE®

Institutional Supporters

HARVARD UNIVERSITY

HARVARD MEDICAL SCHOOL

Tufts UNIVERSITY

Charitable Contributions

We need your help to provide mentorship to young scientists everywhere.

JEI is supported by an entirely volunteer staff, and over 90% of our funds go towards providing educational experiences for students. Our costs include manuscript management fees, web hosting, creation of STEM education resources for teachers, and local outreach programs at our affiliate universities. We provide these services to students and teachers entirely free of any cost, and rely on generous benefactors to support our programs.

A donation of $30 will sponsor one student's scientific mentorship, peer review and publication, a six month scientific experience that in one student's words, 're-energized my curiosity towards science', and 'gave me confidence that I could take an idea I had and turn it into something that I could put out into the world'. **If you would like to donate to JEI, please visit https://emerginginvestigators.org/support, or contact us at questions@emerginginvestigators.org.** Thank you for supporting the next generation of scientists!

'Journal of Emerging Investigators, Inc. is a Section 501(c)(3) public charity organization (EIN: 45-2206379). Your donation to JEI is tax-deductible. '

emerginginvestigators.org